Host cell invasion by influenza A virus - Studies at the single-virus level

Identification and evaluation of potential antiviral targets

D I S S E R T A T I O N

zur Erlangung des akademischen Grades

Dr. rer. nat.
im Fach Biologie

eingereicht an der
Mathematisch-Naturwissenschaftlichen Fakultät I
Humboldt-Universität zu Berlin

von
Diplom-Biologe Christian Sieben

Präsident der Humboldt-Universität zu Berlin:
Prof. Dr. Jan-Hendrik Olbertz

Dekan der Mathematisch-Naturwissenschaftlichen Fakultät I:
Prof. Stefan Hecht, PhD

Gutachter:
1. Prof. Dr. Andreas Herrmann
2. PD Dr. Michael Veit
3. Prof. Dr. Richard Lucius

eingereicht am: 20.12.12
Tag der mündlichen Prüfung: 23.04.13

There is nothing permanent except change.

Heraclitus

Abstract

Influenzaviren müssen in die Wirtszelle aufgenommen werden, um dort ihr Genom freizusetzen und ihre Replikation mit Hilfe des Reproduktionsapparats der Zelle einzuleiten. Der komplexe Replikationszyklus der Influenza A Viren ist noch nicht vollständig verstanden. Er beginnt mit der Bindung des viralen Hämagglutinins (HA) an Sialinsäure (SA) auf der Zelloberfläche der Wirtszelle. Diese Bindung besitzt eine Dissoziationskonstante im unteren millimolaren Bereich (Sauter et al., 1992). In dieser Arbeit wurde die Bindungskraft zwischen Influenza A Viren und Zellen auf der Ebene einzelner Moleküle untersucht. Die Messung der Bindung von Viren an lebende Zellen mittels Einzelviruskraftspektroskopie ist dabei der natürlichen Situation sehr ähnlich.

In dieser Arbeit wurde die Bindung an Zellen mit unterschiedlicher Rezeptorkomposition verglichen. Dabei konnte gezeigt werden, dass für die zelluläre Spezifität die Präsentation des Rezeptors innerhalb der Plasmamembran der Zelle eine größere Rolle spielt als die Struktur des Rezeptorglykans selbst. Des Weiteren deuten die Beobachtung sehr kleiner Kräfte und ein stufenweises Öffnen von Bindungen auf eine multivalente Interaktion hin. Multivalenz wird oft in biologischen Bindungsprozessen beobachtet und kann Bindungskräfte enorm verstärken. Die hier durchgeführten Kraftmessungen beschreiben eine sehr dynamische Interaktion, die maßgeblich von der terminalen Sialinsäure bestimmt wird. Basierend auf diesen Ergebnissen wurden inhibitorische Nanopartikel entwickelt, die die natürliche Zelloberfläche als hochaffine Bindungsalternative imitieren. Verschiedenartige Nanopartikel wurden evaluiert und konnten die Virusaktivität um mehr als 80 % hemmen. Da über die Details multivalenter Interaktionen wenig bekannt ist, wurden Parameter wie Abstand und Präsentation der Liganden variiert. Es konnte gezeigt werden, dass die Virusinhibition durch Nanopartikel entscheidend von der Dichte der Liganden und der Partikelgröße abhängt.

Nach der Bindung wird das Virus durch Endozytose in die Zelle aufgenommen. Durch spezifische Virusmarkierung und gleichzeitiger Expression von zellulären Markerproteinen wurde der Transport einzelner Viren in lebenden Zellen verfolgt. Dabei konnte gezeigt werden, dass das Virus sowohl durch frühe, als auch durch späte Endosomen wandern muss, um sein Genom erfolgreich in das Zytoplasma zu entlassen. Außerdem verzögert das Virus die endosomale Ansäuerung um eine optimale Aufenthaltsdauer im Endosom und die lokalisierte Fusion in der Nähe des Zellkerns zu gewährleisten. Pharmakologisches Eingreifen in diese Prozesse konnte zudem weitere kritische Faktoren identifizieren, die die Effizienz der Virusinfektion stark beeinflussen.

Zusammengenommen zeichnen die Ergebnisse dieser Arbeit ein detailliertes Bild der initialen Phase der Virusinfektion. Aufbauend auf den initialen Ergebnissen, konnten inhibitorische Nanopartikel konstruiert werden, die spezifisch die Aktivität des Influenza A Virus hemmen. Diese Arbeit kann damit als Basis für gezielte antivirale Strategien dienen und dazu beitragen, die Virusinfektion bereits in der initialen Phase zu blockieren.

Abstract

Influenza virus must enter a host cell to deliver its genome, use the cells reproductive machinery and eventually initiate its replication. The replication cycle of influenza A virus is very complex and still not fully understood. It generally starts with binding of the viral protein hemagglutinin (HA) to its cellular receptor sialic acid (SA), a process that was shown to have dissociation constants in the millimolar range (Sauter et al., 1992). However, virus-cell binding is much more complex.
In this work, virus-cell attachment forces were investigated at the single molecule level using intact virus binding to living cells, a set-up that closely mimics the *in vivo* situation. Cells of different surface SA composition were compared. It could be shown that the unique presentation of the ligand within the cells plasma membrane, rather than the structure of the receptor-glycan itself, strongly affects cellular specificity. The low binding force as well as the observation of stepwise unbinding events suggest a multivalent interaction type.

Multivalency is ubiquitous in biological processes and can enormously enhance binding strength. Force measurements revealed this interaction as very dynamic and mostly depends on a terminal sialic acid moiety. Based on this finding, inhibitory nanoparticles mimicking the cell surface were constructed. Those particles serve as a high-affinity alternative for the virus to bind. Different particles were evaluated and shown to efficiently inhibit virus infection by 80 %. However, many of the molecular details of multivalent interactions remain poorly understood. Hence, parameters such as ligand spacing and presentation were varied and revealed that the density of ligands as well as the interacting surface play critical roles for virus inhibition.

Upon attachment, the virus enters the cell by endocytosis. Virus trafficking was followed at the single-virus level in living cells. The kinetics of virus transport were visualized using fluorescent marker proteins in combination with specific virus labeling. It was found that the virus needs to progress through early and late endosomal compartments in order to efficiently uncoat and release its genome. Further, the virus delays the endosomal acidification to ensure optimal residence time and fusion in the region close to the host cell nucleus. Drug treatment furthermore unraveled critical factors influencing viral infection efficiency.

Taken together, the presented results provide a detailed picture of the initial phase of influenza A virus infection. These were used to construct inhibitory nanoparticles, that can specifically inhibit virus activity. The results of this thesis further serve as the basis for targeted antiviral strategies that can block the virus during the initial steps of infection.

Contents

The following manuscripts were prepared during this thesis. A full list of publications is listed in the bibliography section.

Inhibition of influenza virus infection by multivalent sialic-acid-functionalized gold nanoparticles
Ilona Papp, Christian Sieben, Kai Ludwig, Meike Roskamp, Christoph Böttcher, Sabine Schlecht, Andreas Herrmann, and Rainer Haag
Small, 2010 Dec; 6(24)

Inhibition of influenza virus activity by multivalent glycoarchitectures with matched sizes.
Ilona Papp , Christian Sieben , Adam L. Sisson, Johanna Kostka, Christoph Böttcher, Kai Ludwig, Andreas Herrmann, and Rainer Haag
ChemBioChem, 2011 April; 12(6)
equal contribution

Bending and puncturing the influenza lipid envelope.
Sai Li, Frederic Eghiaian, Christian Sieben, Andreas Herrmann, Iwan A. T. Schaap
Biophys J, 2011 Feb; 100(3)

Influenza virus binds its host cell using multiple dynamic interactions.
Christian Sieben , Christian Kappel , Rong Zhu, Anna Wozniak, Christian Rankl, Peter Hinterdorfer, Helmut Grubmüller, Andreas Herrmann
Proc Natl Acad Sci U S A, 2012 Aug; 109(34)
equal contribution

Heterogeneity of AMPA receptor trafficking and molecular interactions revealed by super-resolution analysis of live cell imaging.
Nathanael Hozea, Deepak Nair, Eric Hosy, Christian Sieben, Suliana Manley, Andreas Herrmann, Jean-Baptiste Sibarita, Daniel Choquet, and David Holcman
Proc Natl Acad Sci U S A, 2012 Oct; 109(42)

pH-controlled two-step uncoating of influenza virus
Sai Li , Christian Sieben , Kai Ludwig, Andreas Herrmann, Frederic Eghiaian, Iwan A.T. Schaap
submitted
equal contribution

1 Introduction

1.1 The biology of *influenza A virus*

The spread and evolution of influenza viruses worldwide is monitored by the Global Influenza Surveillance and Response System (GISRS) created by the World Health Organization (WHO). The backbone of GISRS is formed by a worldwide network of national influenza centers. In Germany, the Robert Koch-Institute (RKI) is the national reference center for influenza and other respiratory diseases.
As the RKI reported, in the season of 2011/2012 influenza A viruses were detected in 9.500 patients in Germany (RKI, Saisonbericht 2011/12). For comparison, in the preceding season of 2010/11, 41.000 diagnosed infections were recorded due to the pandemic "swine flu" virus (RKI, Saisonbericht 2010/11). On average, influenza and accompanying infections can cause up to 11.000 fatalities per year in Germany (RKI, Saisonbericht 2009/10). In 2011, a study coordinated by the RKI introduced a priority ranking of human pathogens according to their importance for national surveillance and epidemiological research (Balabanova et al., 2011). Here, the case fatality rate was the most important criterion and influenza virus was ranked within the highest priority group.
Influenza A viruses have been circulating in the human population since at least 96 years, when the so far most devastating pandemic spread around the world. Between what is now known as the Spanish flu in 1918 and the most recent swine flu pandemic from 2009, another three major influenza pandemics circulated among the human population. Only two years after the appearance of the pandemic influenza virus in Mexico, another new influenza variant appeared in July 2011 in the United States (WHO). This virus has a new genetic composition: most of its genes derived from viruses circulating in pigs while one originated from the 2009 pandemic virus. Interestingly, this virus spreads from pigs into humans but only rarely between humans.
The bird flu (H5N1) appeared in 1996 and since then received a lot of public attention due to its high pandemic potential (Watanabe et al., 2012). The virus does not readily transmit from human to human and can directly infect humans only through close contact with contaminated birds. Two highly controversial studies experimentally achieved direct transmission after adapting the virus in ferrets (Imai et al., 2012; Herfst et al., 2012). However, publication of these data

sparked a worldwide discussion about biosafety laws and led to an agreed moratorium on H5N1 research (Fouchier et al., 2012).

These examples highlight the significance of influenza virus as a human pathogen. Since its discovery in 1933, the virus has lost nothing of its fascination and despite decades of scientific investigations only recently, state-of-the-art methods permit studying virus biology at entirely new levels.

1.1.1 Virus structure and morphology

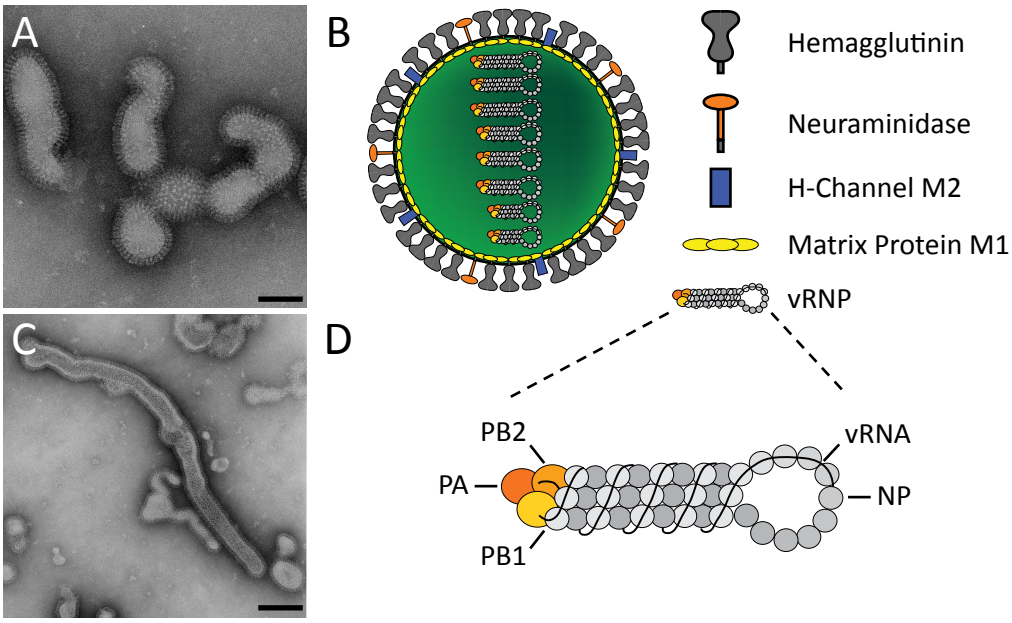

Figure 1.1: EM micrographs and schematic representation of influenza A viruses. Influenza A/X-31 viruses are very pleiomorph, but grown on chicken eggs preferentially form spherical particles that are 100-150 nm in diameter (A). Depending on the M1/M2 genes and the used propagation method, the virus can form filaments of up to several micrometer (C). Schematic representation of influenza A virus (B) and a viral ribonucleoprotein complex (vRNP) (D). PB1, PB2 and PA are subunits of the viral RNA dependent RNA polymerase complex. NP, nucleoprotein. EM micrographs were kindly provided by Dr. Kai Ludwig, Research Center of Electron Microscopy, Freie Universität Berlin. Scale bar: 100 nm.

Influenza A virus proteins

Influenza A viruses belong to the family of *Orthomyxoviridae*. They are encapsulated by a lipid bilayer and are therefore subcategorized into the group of enveloped viruses (Bouvier and Palese, 2008). The envelope harbors the two glycoproteins hemagglutinin (HA) and neuraminidase (NA) as well as the tetrameric proton channel M2 (Webster et al., 1992) (Fig. 1.1). Because of their shape, HA and NA are often referred to as spike proteins. Antigenic differences in HA and NA are used to classify influenza A viruses into 17 HA (H) and 9 NA (N) subtypes (Medina and García-Sastre, 2011; Tong et al., 2012). The most recent H17 subtype was identified in bats in 2012 (Tong et al., 2012).
Underneath the lipid bilayer is a layer of the matrix protein M1 (Fig. 1.1 B). The genome of influenza A viruses is composed of eight segments of single-stranded, negative-sense RNA (vRNA). Genomic vRNA is packed with four proteins PB1, PB2, PA and the nucleoprotein NP to form eight ribonucleoprotein complexes (vRNPs) (Fig. 1.1 D). PB1, PB2 and PA are subunits of the viral RNA dependent RNA polymerase complex. All influenza A virus proteins and their function are summarized in Table 1.1. HA is discussed in more detail in section 1.1.3.

Table 1.1: Proteins of influenza A viruses. From (Lamb and Krug, 1996) AA, amino acids; Nt, nucleotides

genome segment	protein name	length (Nt)	AA (kDa)	copies per virus	function
1	PB2	2341	759 (86)	45	viral polymerase subunit
2	PB1 PB1-F2	2341	757 (86) 87 (10)	45	viral polymerase subunit induction of apoptosis
3	PA	2233	716 (80)	45	viral polymerase subunit
4	HA	1778	566 (65)	1200	receptor binding membrane fusion
5	NP	1565	498 (56)	1000	genome packaging vRNP nuclear import
6	NA	1413	454 (55)	400	neuraminidase
7	M1 M2	1027	252 (28) 97 (15)	3000 97	matrix, assembly proton channel
8	NS1 NS2 (NEP)	890	230 (26) 121 (11)	- 160	interferon antagonist vRNP nuclear export

1.1.2 Replication cycle of influenza A virus

An overview of the influenza virus replication cycle is presented in Fig. 1.2.

Cell binding and entry

Viruses, being obligate intracellular organisms, must enter cells to replicate while using the cell s synthesis machinery. HA mediates virus-cell attachment by binding to terminal sialic acid (SA) residues on glycoproteins and -lipids within the plasma membrane. After binding, the virus enters the cell by endocytosis. Clathrin-mediated endocytosis (CME) is one of the best characterized entry pathways used by numerous viruses (Marsh and Helenius, 2006; Mercer et al., 2010). In 1981, influenza viruses were observed for the first time in coated vesicles, indicating uptake by CME (Matlin et al., 1981). However, in the same study the virus was also observed in smooth invaginations and vesicles, suggesting an alternative entry pathway. CME is often triggered by binding or clustering of specific cellular receptors (McMahon and Boucrot, 2011). In the case of influenza A virus, the actual trigger is not known. It was shown that epidermal growth factor (EGF) promotes entry (Eierhoff et al., 2010) and that the virus can use pre-existing clathrin-coated pits (CCP) or promote their *de novo* formation (Rust et al., 2004). These results suggest the requirement of post-attachment factors that trigger endocytosis after SA binding. In 2002, influenza A virus infection was also shown to occur independently of caveolin- and clathrin-mediated endocytosis (Sieczkarski and Whittaker, 2002a). In two recent papers, macropinocytosis was shown as an alternative entry pathway (Rossman et al., 2012; de Vries et al., 2011), particularly important for long filamentous viruses (Rossman et al., 2012).

Endosomal maturation and fusion

After endocytosis, the virus-containing vesicle is transported and fuses with early endosomes (EE) (Huotari and Helenius, 2011; Lozach et al., 2011) (Fig. 1.3). This transport was shown to depend on cortical actin (Lakadamyali et al., 2003). EEs function as a sorting site with specific domains. Some of these domains form recycling endosomes or vesicles maturing towards the late endosomal / lysosomal pathway. The combination of processes that lead to the formation of late endosomes / lysosomes is summarized as endosomal maturation. Important hallmarks of endosomal maturation are (1) a switch of associated small Rab GTPases and (2) an acidification of the endosomal lumen (Huotari and Helenius, 2011). Rab5 primarily associates with the EE and was shown to be a key organizer of the endocytic system which is thus extremely sensitive to Rab5 depletion (Zeigerer et al., 2012). Rab5 and its effectors are replaced by Rab7 and accompanying proteins during maturation (Huotari and Helenius, 2011). Two mechanisms were reported to facilitate the transport of cargo from early to late endosomes. One was observed

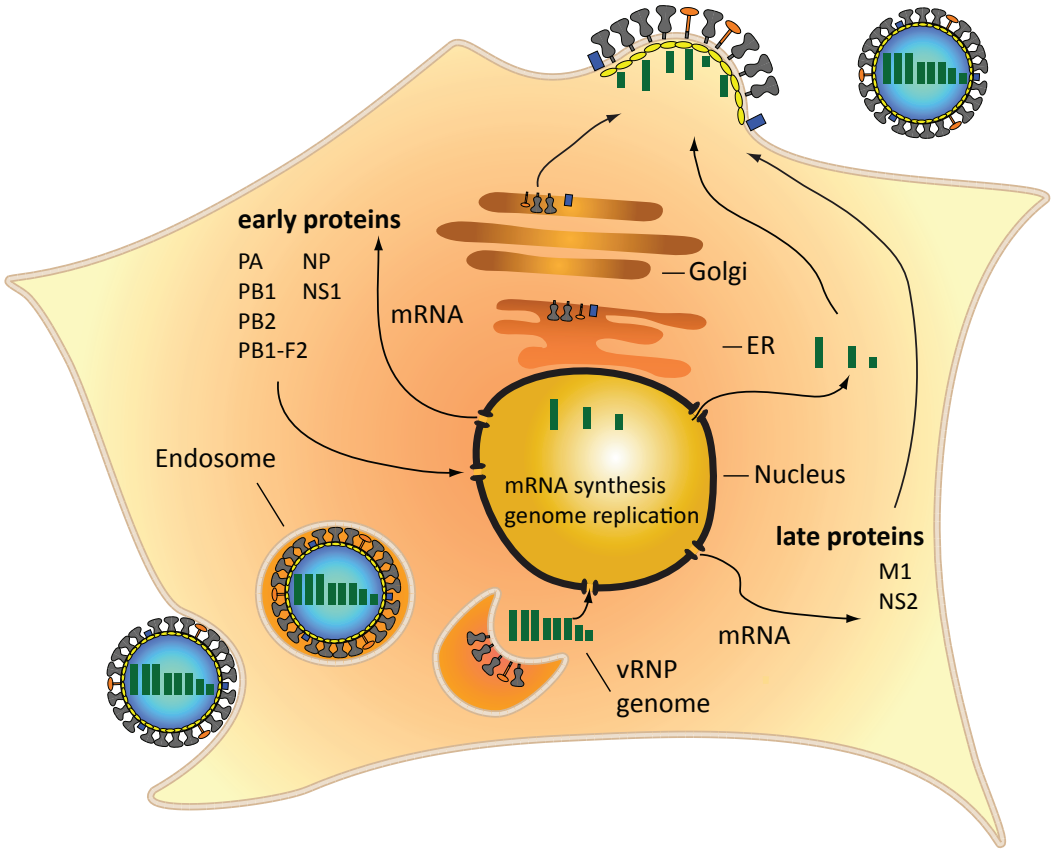

Figure 1.2: Replication cycle of influenza A virus. The virus binds to sialic acid residues on the cell surface and enters the cell by endocytosis. Clathrin-mediated endcytosis as well as macropinocytosis are described as entry pathways. The low pH in maturing or late endosomes triggers a conformational change of HA mediating fusion of viral envelope and endosomal membrane. The released genome in form of eight vRNPs translocates into the nucleus, where mRNA as well as vRNA synthesis take place. Viral proteins are translated in the cytoplasm (early proteins) or on ER-bound ribosomes (transmembrane proteins) and transported back into the nucleus or towards the plasma membrane. New viral proteins (PB1, PB2, PA, NP) assemble progeny vRNPs in the nucleus, which are exported by the help of M1 and NS2 and transferred to the budding site. The virus buds presumably by a concerted interaction of the spike proteins and M1 and is finally released by M2-mediated membrane scission.

for semliki forrest virus (SFV) and proposes that early and late endosomes are rather static and vesicles facilitate transport from one to the other (Vonderheit and Helenius, 2005). The second model proposes a conversion of Rab proteins as the trigger of maturation into LE. Specific regulators, the first SAND1/Mon1 was identified in *C.elegans*, control this process (Rink et al., 2005).

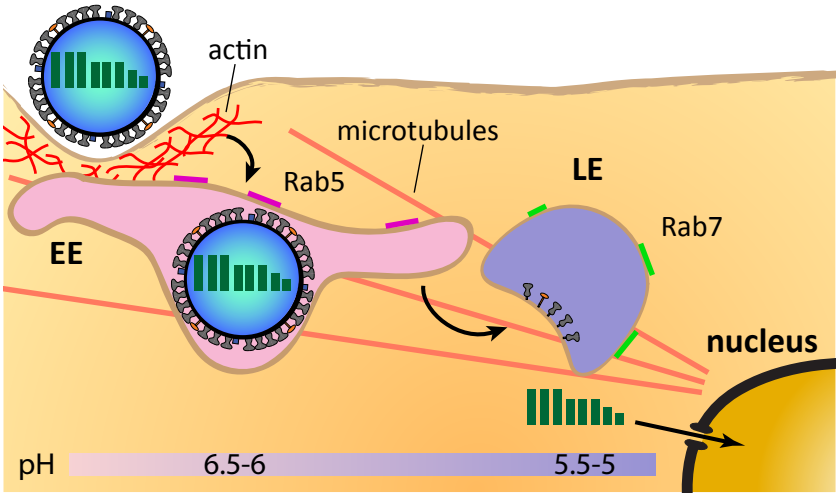

Figure 1.3: Endocytic trafficking of influenza A virus. Influenza A virus is internalized into vesicles, which are transported towards and fuse with early endosomes (EE). EE are regulated by associated Rab5 GTPases (magenta), typical markers for these compartments. In the course of maturation the endosomes are acidified by membrane bound V-type proton ATPases. In addition, Rab5 and its effectors are exchanged for Rab7 (green), which decorates late endosomes (LE). The endosomes travel along microtubules mediated by the motor protein dynein. When the pH decreases, the virus fuses and its genome is released into the cytoplasm.

A low intravesicular pH is important for protein sorting and degradation, activity of hydrolytic enzymes as well as inactivation of pathogens. It is mainly regulated by the number of V-type ATPases within the endosomal membrane. The pH values of the corresponding compartments are illustrated in Figure 1.3. Influenza viruses were shown to be transported along microtubules within endosomal vesicles (Rust et al., 2004; Lakadamyali et al., 2006, 2003) and that this transport occurs before and after virus-containing endosomes co-localize with early endosomal compartments (Lakadamyali et al., 2006, 2003). The vesicles typically travel towards the perinuclear region (PNR) similar to ligands bound for degradation. The pH decrease within the endosome triggers a conformational change of the viral HA, eventually leading to fusion of the endosomal membrane with the viral envelope.

Viral protein synthesis and virus assembly.

During endosomal maturation the viral M2 proton channel acidifies the virus lumen, which is thought to promote dissociation of M1 from vRNPs (Martin and Helenius, 1991b; Helenius, 1992a). Indeed, it was shown that import of vRNPs into the nucleus depends on the action of M2 and is sensitive to the M2 inhibitor amantadine (Martin and Helenius, 1991b). Cytosolic vRNPs quickly translocate into the nucleus (Babcock et al., 2004), a process that is mediated by a nuclear localization sequence (NLS) within NP interacting with importin (Portela and Digard, 2002). Inside the nucleus, the viral RNA polymerase (PA) initiates synthesis of viral mRNA (+ stranded) as well as replication of the viral RNA (- stranded). At first, the viral PB2 binds host mRNAs while PA cleaves 10-13 bases downstream of the 5 -cap (cap snatching). This small fragment (m^7 GpppG) is used by PB1 as a primer to synthesize viral mRNA (Steinhauer and Skehel, 2002). vRNA is produced using a copy RNA intermediate which is neither capped nor polyadenylated and corresponds to the full vRNA complement. The switch from transcription to replication is not fully understood. The accumulation of viral NP and small virus-derived RNAs (Perez et al., 2010) were previously suggested to be involved.
NS1, NP and the polymerase subunits are the first synthesized proteins (Shapiro et al., 1987). The transmembrane proteins HA, NA and M2 are later translated by membrane-bound ribosomes into the ER. Hence, the proteins enter the secretory pathway including post-translational protein modification in the Golgi apparatus and further transport to the plasma membrane (Copeland et al., 1986, 1988). The polymerase proteins NP and vRNA form new vRNP complexes which are exported from the nucleus with the help of NS2 and M1 (Portela and Digard, 2002). Recently, it was shown that newly synthesized vRNPs accumulate at the microtubule organization center (MTOC) after leaving the nucleus. They are then transported in Rab11-positive vesicles along microtubules towards the cell periphery (Amorim et al., 2011). The spike proteins NA and HA accumulate in cholesterol- and sphingolipid-enriched lipid domains (lipid rafts) (Scolari et al., 2009; Kundu et al., 1996; Engel et al., 2010). Here they bind M1 (Ali et al., 2000), which as well binds to progeny vRNPs (Ye et al., 1999) and by that forms a bridge connecting the spike proteins with the genome segments at the virus assembly site (Nayak et al., 2004). The actual budding process is likely determined by multiple factors promoting membrane curvature and budding. Local accumulation of HA and NA could induce membrane curvature (Stachowiak et al., 2012). M2, one of the latest proteins expressed, is thought to stabilize the newly formed bud and initiate scission of the fully equipped progeny virus (Rossman and Lamb, 2011; Thaa et al., 2010).

1.1.3 The influenza A virus hemagglutinin (HA)

HA is synthesized by membrane-bound ribosomes into the endoplasmic reticulum (ER) as a pre-cursor protein HA0. HA0 is later cleaved into the membrane bound subunit HA2 and the membrane distal subunit HA1 (Fig. 1.4) (Wilson et al., 1981; Skehel and Wiley, 2000). In association with chaperones, HA0 monomers form non-covalently linked homotrimers in the ER, which then travel through the Golgi apparatus to the plasma membrane (Copeland et al., 1986, 1988). For most HAs, the cleavage site between HA1 and HA2 (Fig. 1.4 A) is a single arginine residue (monobasic cleavage site) and the precursor is cleaved by extracellular enzymes. In some avian HAs (H5 and H7), the cleavage site is longer and contains multiple arginine residues (polybasic cleavage site) (Horimoto and Kawaoka, 2005). In any case, cleavage generates the highly conserved N-terminus of HA2 (residues 1-10), called the fusion peptide. The trimeric organization of the protein is preserved during this process. Since cleavage of HA0 is mandatory for HAs function, more efficient cleavage at a polybasic cleavage site correlates with higher pathogenicity.

The merger of two membranes is a thermodynamically favored process but has a high kinetic barrier (Harrison, 2008). Low pH treatment of HA leads to an irreversible conformational change (Skehel and Wiley, 2000, 2002), forming the so-called post-fusion or low-pH conformation of HA and supplying the energy needed for membrane fusion. The fusion protein HA itself needs an activation, under native conditions in the form of proton binding. The activation can also be triggered by high temperature or a strong denaturant like urea (Carr et al., 1997). This means that HA, and consequently the whole virus, is intrinsically metastable, a hallmark of all viruses.

The conformational change of HA can be divided into three steps (Fig.1.4C). (1) Protonation of HA1 leads to dissociation of intratrimeric contacts and allows water to enter the central cavity of the trimer (Böttcher et al., 1999; Huang et al., 2003). (2) The top loop of the HA2 N-terminus undergoes a loop-to-helix transition resulting in an extended coiled-coil conformation of the three monomers (extended intermediate). The coils contain hydrophobic and hydrophilic amino acids in a repetitive manner, forming a heptad pattern (heptad repeats, Carr and Kim (1993)). (3) In the C-terminal part of HA2, the extended intermediate collapses at its base and thereby draws the fusion peptide towards the transmembrane region (Harrison, 2008). The large-scale conformational change can be compared with the opening and closing of a jackknife. HA at neutral pH is in a spring-loaded conformation, which is in line with the observation that recombinant HA2 spontaneously folds into the low-pH conformation (Carr and Kim, 1993; Chen et al., 1995).

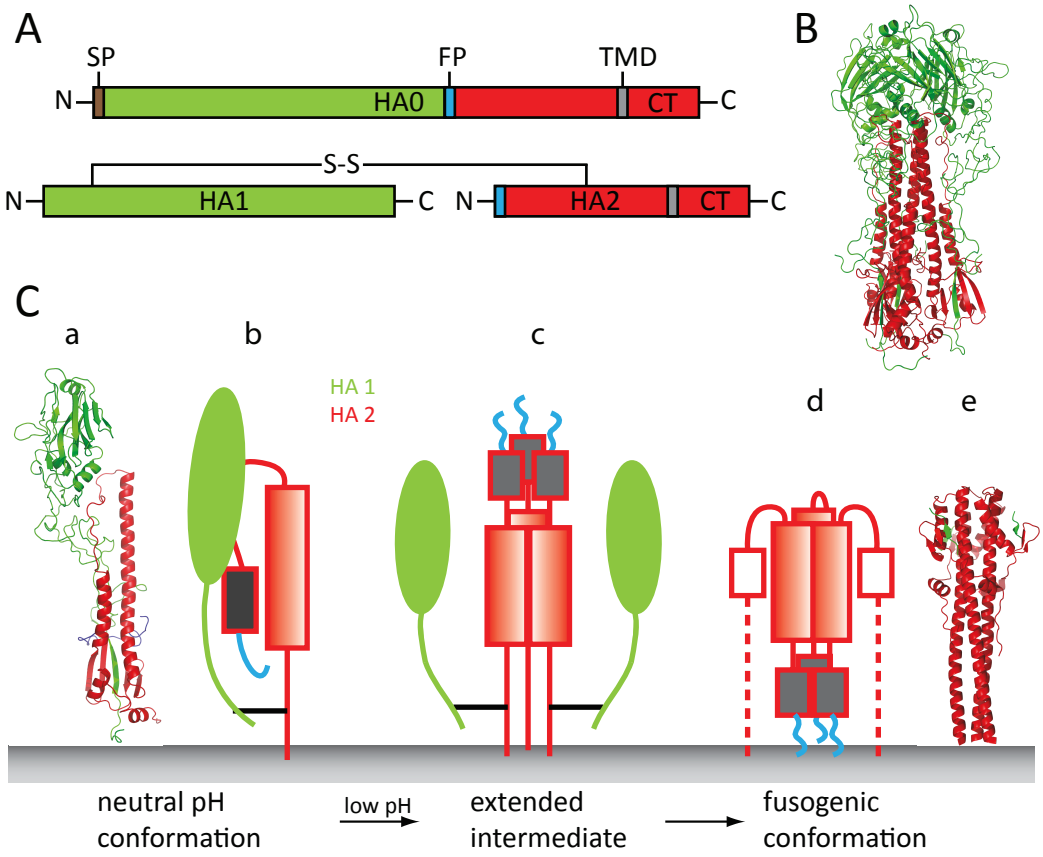

Figure 1.4: Structure, cleavage and conformational change of HA. HA is expressed as a precursor HA0 (A), which is cleaved into HA1 and HA2 by Golgi-localized or extracellular proteases. The two subunits remain connected by a disulfide linkage. The full protein assembles into a non-covalently linked homotrimer (B, from Weis et al. (1988)). Low pH triggers a conformational change of HA. The proposed sequence considering the two crystal structures of the neutral (a) and the low-pH form (e) is depicted in (C). Protonation of HA1 leads to dissociation of intratrimeric contacts, which allows water to enter the central cavity of the HA ectodomain (Böttcher et al., 1999; Huang et al., 2003). The top loop of the HA2 N-terminus undergoes a loop-to-helix transition which results in an extended coiled-coil of the three monomers (extended intermediate, c). In the C-terminal part of HA2, the extended intermediate collapses and thereby draws the fusion peptide towards the transmembrane region (d). The dotted part is not resolved in the crystal structure and corresponds to the C-terminal part of HA2 including the transmembrane region. SP signal peptide, FP fusion peptide, TMD transmembrane domain, CT cytoplasmic tail.

Receptor-binding speci city of HA

The membrane distal HA subunit (HA1) carries the receptor-binding site (RBS) recognizing 5-N-acetyl neuraminic acid (sialic acid, SA) residues on the cell surface (Fig. 1.5). The RBS is a shallow pocket on the top of the globular head of HA1 (Weis et al., 1988). It is formed by a number of conserved amino acid residues: among them amino acids at positions 98 (tyrosine), 153 (tryptophan), 183 (histidine), and 195 (tyrosine) form the base of the pocket. The edges are built by three conserved elements, namely the loops 130 and 220 as well as the helix 190 (Fig. 1.5). The two major linkages between sialic acid and adjacent carbohydrates (mainly galactose) are either of -2,3 (SA -2,3Gal) or -2,6 (SA -2,6Gal) glycosidic nature (see also 1.4.1 and Fig. 1.7). This small difference is of great importance since different HA subtypes have different recognition specificities for these SA linkages. In particular, avian influenza A viruses preferentially bind -2,3-linked SA, while human viruses prefer to bind -2,6 linked SA (Gambaryan et al., 1999; Matrosovich et al., 1997; Rogers et al., 1983).
Receptor binding is crucial for host specificity and supposed to be a major interspecies barrier (Neumann et al., 2009). The preference of avian viruses to bind SA -2,3Gal matches the occurrence of this sugar on epithelial cells in the intestinal tract of birds, the replication site of avian influenza viruses (Nicholls et al., 2008). In contrast, the human upper respiratory tract is rich in SA -2,6Gal.
The receptor-binding specificity is affected by the amino acid composition of the RBS. H2 and H3 HAs with amino acids glutamine and glycine at position 226 and 228 preferentially bind -2,3 linked SA. A change of 226 to leucine and 228 to serine was shown to switch binding preference towards the human type receptor (Gambaryan et al., 1999). For H1 HAs, position 190 and 225 were shown to be important (Gambaryan et al., 1999). Asparagine at both positions confers binding to human-type receptors. Glutamine at position 190 and glycine at 225 alters binding in favor of avian-type receptors.

1.2 Inhibition of influenza A virus infection

1.2.1 Prophylactic antiviral approach

To prevent human influenza infection, an efficient vaccine is needed. However, due to the high variability of the viral spike proteins HA and NA, which define the antigenic phenotype, it is difficult to produce neutralizing antibodies (Subbarao and Joseph, 2007). One approach to circumvent this problem is to adjust the vaccine composition after every season to include new variants. This works quite well for the seasonal influenza strains, but requires constant global influenza infection monitoring of circulating strains. Currently, one H1N1, one H3N2 and one

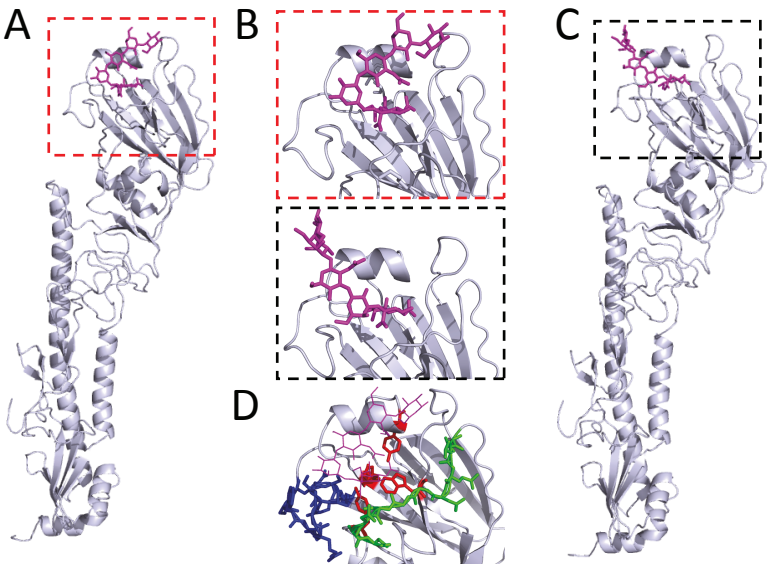

Figure 1.5: Structure of the HA receptor-binding site with bound ligands in -2,6 and -2,3 conformation (from Eisen et al. (1997)). Structure of one HA monomer from influenza A/X-31 bound to lactoseries tetrasaccharide c (LSTc, -2,6 SA) (A, B) and lactoseries tetrasaccharide a (LSTa, -2,3 SA) (C,B). The binding pocket of HA is shown in detail in (D). The main structural motifs are the base (Tyr98, Trp153, His183, Tyr195, red) as well as the loops 130 (green) and 220 (blue).

influenza B strain are used to produce annual vaccines against seasonal influenza. The big aim of influenza vaccine oriented science is finding neutralizing antibodies (nAbs) that target the more conserved stem region of HA. Some recent studies have demonstrated the progress in this area. Sui *et al.* (Sui et al., 2009) used recombinant HA to select non-immune human antibodies from a phage display library and could show that the binding site is located in the stem region. More recently, two studies have characterized broadly neutralizing antibodies (bnAb) that act on a spectrum of influenza viruses within groups 1 and 2 (Ekiert et al., 2012; Corti et al., 2011). However, despite the good characterization of these antibodies the main question is how to elicit their production to sufficient titers in humans. A problem also known in the context of prophylactic HIV vaccines (Karlsson Hedestam et al., 2008). In the following two sections therapeutic rather than prophylactic approaches will be discussed.

1.2.2 Therapeutic antiviral approaches

Currently, only four substances are approved as anti-influenza therapeutics for medical use. Two of them, amantadine and rimantadine, are within the class of adamantane derivatives known to bind and inhibit the influenza envelope proton channel M2. Amantadine was the first synthetic substance shown to inhibit influenza virus replication (Davies et al., 1964). Despite their high

effectiveness, the use of adamantan(amin)e derivatives is limited, mainly because several side effects and broadly evolved resistance have been documented (Carlescu et al., 2009), especially among H3N2 viruses (De Clercq, 2006).
The second class of influenza antiviral substances are neuraminidase inhibitors (von Itzstein, 2007). Influenza NA is critical for infection initiation (Ohuchi et al., 2006) as well as for the release of progeny viruses. Deletion of NA impairs infection and leads to virus aggregation on the cell surface (Matrosovich et al., 2004b; Beigel and Bray, 2008). Two NA inhibitors, oseltamivir (trade name Tamiflu) and zanamivir (trade name Relenza), are approved since 1999 and were shown to be highly effective against influenza A and B viruses (Beigel and Bray, 2008). Both compounds block the active sialic acid binding site of NA, of which the structure is known including the position of resistance mediating mutations (von Itzstein, 2007).
A lot of experimental inhibitors targeting other viral proteins were discussed in the recent literature. The NP binding compound Nucleozin (Kao et al., 2010) and a new class of polymerase inhibiting substances (Muratore et al., 2012) were effective against influenza virus replication *in vitro* with negligible cytotoxicity. Another promising class of broad-spectrum antivirals based on small chemical inhibitors was shown to inhibit a wide range of enveloped viruses by targeting the virus membrane and interfering with membrane fusion (Wolf et al., 2010).
An additional approach that uses multiple SA residues on a multivalent scaffold as competitive binding inhibitors is discussed in the section 1.3.2.

1.3 Multivalency

1.3.1 Mechanism of multivalent interactions

Multivalency describes the concept of multiple binding events happening at once and increasing the overall binding strength. The simplest expression of multivalency is the simultaneous interaction of multiple receptor-ligand pairs. Multivalency is ubiquitous in biology and dramatically enhances the overall avidity compared to the low single-interaction affinity. The term affinity is used in this context to describe the attempt of a single receptor-ligand pair to form a complex. If the interaction is mediated by many coexisting interactions the term avidity is often used (Mammen et al., 1998).
Its easy to imagine the effect of multivalency when thinking of a hook-and-loop fastener. One single hook and loop pair is very weak, but an ensemble of many interactions can provide a lot more resistance. Multivalency and positive cooperativity are not necessarily linked. The best characterized example of positive cooperativity in biologic systems is hemoglobin. Here, the second oxygen molecule binds to the tetrameric hemoglobin with higher affinity than the

first, which results in positive cooperativity. In contrast, most multivalent systems are rather negatively cooperative due to steric reasons.

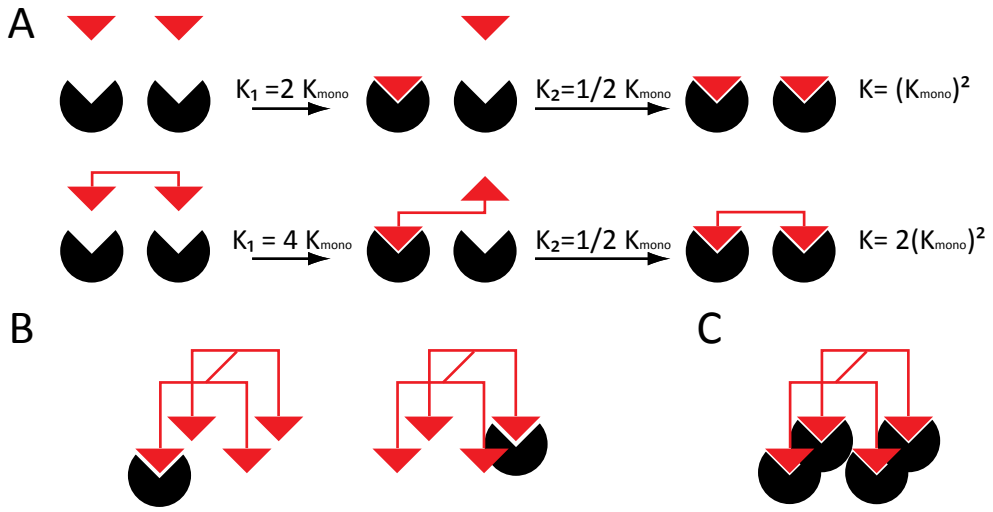

Figure 1.6: Mechanism of multivalent interactions. Mechanism of multivalent binding depicted by a bivalent example (A). Two monovalent ligands bind to two receptors and each ligand has the binding constant K_{mono}, which gives 2 K_{mono} due to the presence of 2 receptors. The probability for the second binding is reduced to 1/2 of K_{mono}. In contrast, if the two ligands are connected by a linker, the first binding constant increases to 4 K_{mono} due to 4 possible binding situations. The second binding constant strongly depends on the linker but is approximately equal to K_{mono}. The overall binding constant results from the product of the two equilibrium constants K_1 and K_2. B and C illustrate two major mechanisms that contribute to the multivalent effect. The local concentration after binding of the first ligand is strongly increased, which leads to high re-association rates and higher functional affinity even in the case of only one interaction. Multiple presented receptors allow many simultaneous interactions, which provides steric stabilization of the complex (C). Adapted from (Fasting et al., 2012; Krishnamurthy et al., 2006)

Several mechanisms can influence multivalent binding. A high local concentration of ligands promotes high re-association rates after dissociation and hence higher probability of binding for each individual ligand. In addition, the entropic penalty of the multivalent ligand to escape the bound state is reduced. The overall entropy of a system with n receptors and n free monovalent ligands depends on the solvation, rotation, and translation entropy ($\Delta S_{mono} = \Delta S_{trans} + \Delta S_{rot} + \Delta S_{sol}$). When a single ligand binds, the entire entropy will only slightly change. In contrast, when the ligands are connected by a multivalent scaffold the system loses some of its translation and rotation entropy if one individual ligand in the scaffold becomes connected to a single receptor site. Hence, the first binding is entropically more difficult than the subsequent binding events. As a direct consequence, the macroscopic dissociation is strongly reduced compared to the monovalent ligand. The simplest case of a bivalent association is shown in Fig. 1.6 (e.g an antibody with two binding sites).

1.3.2 Multivalency in biological systems

The binding between carbohydrates and carbohydrate-binding proteins (lectins) is typically very weak. Since glycans are ubiquitous on biological surfaces, the majority of multivalent binding systems are of the glycan-lectin type. Some of them are discussed below.

Host-pathogen interaction

Many enveloped viruses feature a dense layer of membrane spike proteins. These spike proteins mediate the initial virus-cell attachment for influenza virus as well as other viruses like corona viruses (e.g. severe acute respiratory syndrome (SARS) virus), rhabdoviruses (rabies virus, vesicular stomatitis virus (VSV)) or simian virus 40 (SV40). The binding principle is similar since all of them rely on multiple simultaneous interactions.
Bacteria are the second major pathogen group that interacts in a multivalent way with their host cell. For example, cell adhesion of *Escherichia coli* and *Helicobacter pylori* depends on multivalent glycan interactions (Lehmann et al., 2006; Mammen et al., 1998). Some bacteria such as *Vibrio cholerae* or the recently discussed enterohemorragic *E.coli* (EHEC) secrete toxins, which interact with cell-surface glycans in a multivalent way. Two of them, Cholera as well as Shiga toxin belong to the pentameric AB_5 class. Each monomer is composed of a cell binding B subunit that delivers the cytotoxic A subunit (Collins and Paulson, 2004). Monomeric Shiga toxin binding to its receptor has a dissociation constant in the mM range, while the multivalent attachment to the cell has a K_d of 1 nM (Kitov et al., 2000). Recently, it was shown that binding of Shiga and Cholera toxin as well as SV40 to GM1 gangliosides induces membrane curvature an this presumably triggers endocytosis (Ewers et al., 2010). This is a direct link between multivalent binding and downstream signaling caused by the provided scaffold (Ewers et al., 2010).

Cell-cell interaction

The binding of leukocytes is a well characterized example of multivalent cell-cell interaction (Ley et al., 2007). Leukocytes are very important during inflammatory processes. They circulate in the blood until they recognize special lectins, so-called selectins, on the inner surface of the vascular endothelium. L-selectins are present on leukocytes and P- and E-selectins are found in the endothelium. All selectins bind sialyl $Lewis^X$ (sLe^x) residues on the respective opposite cell membrane. sLe^x is a complex carbohydrate that contains a terminal sialic acid as well as a fucose branched from the subsequent lactose. This leads to binding and unbinding of leukocytes to the vascular endothelium (leukocyte rolling) until they reach the cite of inflammation. Here, additional integrin binding triggers extravasation of leukocytes into the inflamed tissue.

Inhibition of influenza A virus activity using multivalency

The emergence of drug-resistant virus variants hinders the search for influenza antivirals. Therefore it would be reasonable to assume that the globular head of HA due to its high variability, is an unfavorable target for anti-influenza drugs.
However, many examples of multivalency in host-pathogen binding (some are discussed in 1.3.2) inspired the idea of using this mechanism to interfere with cell adhesion. In the case of influenza A virus, those inhibitors function as binding competitors that directly target the RBS of HA. As mentioned before, the binding pocket is widely conserved to guarantee virus-host cell binding (Skehel and Wiley, 2000).
Multivalent SA presentation has been done before, using the following approaches. Polymers such as polyacrylamide (Sigal et al., 1996; Mammen et al., 1995), PAMAM (Reuter et al., 1999; Landers et al., 2002) or the polysaccharide chitosan (Umemura et al., 2008; Li et al., 2011) bear the advantage of good control of the molecule size. However, a disadvantage is that the degree of functionalization (dF), i.e. the number of SA per molecule and the position on the polymers is statistically distributed (statistical polymers). In other studies liposomes (Spevak et al., 1993), proteins (Pritchett and Paulson, 1989) or only peptides (Zevgiti et al., 2011; Totani, 2003) were successfully utilized to present multiple SA residues. The dF within the mentioned SA-carriers covers a wide range between the simplest case of a bivalent peptide (Unverzagt et al., 1994) up to several thousand SA residues on chitosan polymers (Umemura et al., 2008).

1.4 The biology of sialic acids

1.4.1 Glycosylation in mammalian cells

Sialic acid is a collective name for a group of 43 molecules, wherein the one that is N-acetylated at the fifth position is called N-acetyl neuraminic acid, the primary sialic acid (Fig. 1.7 A). The remaining nine carbon atoms within the conserved sialic acid backbone can be derivatized in many ways forming this group of glycans (Varki and Schauer, 2009). Glycans can be attached to proteins either by amide linkage (N-glycosilation) or glycosidic linkage (O-glycosylation). This type of protein modification is achieved by about 200 glycosyltransferases in mammalian cells (Moremen et al., 2012). The expression and competition of these proteins strongly influences the abundance and structure of different glycans in a certain cell or tissue (called glycome). The primary modification starts co-translationally in the ER by a protein complex, called oligosaccharyltransferase (OST) (Fig. 1.7 D) (Lizak et al., 2011). OST, which is presumably coupled to the Sec61 translocation protein, facilitates the transfer of an oligosaccharide from a lipid bound precursor to the nascent polypeptide chain appearing from Sec61 (Kelleher and

Gilmore, 2006). These early oligosaccharides mainly contain glucose (Glc), mannose (Man) and N-acetyl glucoseamine (GlcNac) and are further processed by Golgi-localized enzymes, which where shown to be spatially separated by the *cis-trans* morphology of the Golgi complex (Rabouille et al., 1995). This hierarchical organizations and the fact that glycans can be either extended or trimmed illustrates the variety of the resulting protein modification, as shown in a mass spectrometry-based glycome analysis of CHO cells (North et al., 2010). ER-originated glycans can be further extended with GlcNac, galactose (Gal) and terminal sialic acid. In addition, fucose residues can be attached to GlcNac at different positions, leading among others to the earlier discussed sLe^x glycan. Notably, the terminal sialic acid can be attached to the adjacent Gal either by a -2,3 or 2,6-glycosodic linkage (Fig. 1.7 B, C), which is mainly determined by the expression of Gal-specific sialyltransferases (Xu et al., 2011).

In addition to proteins, lipids can also be glycosylated. Glycosphingolipids are the major group of glycolipids and contain the membrane bound ceramide, which is modified in the Golgi apparatus in a hierarchical way, similar to proteins as described above. Glc and Gal are first attached in the *cis* and *medial* Golgi apparatus. The glycan is further extended by attachment of N-acetylgalactosamine (GalNac) and sialic acid. Sialylated glycosphingolipids are called gangliosides, due to their discovery in brain samples. Gangliosides can be very complex and contain multiple branches and SA moieties. As for proteins, ganglioside architecture mainly depends on the tissue and the enzyme repertoire of the cell type.

1.4.2 Functions of sialic acids

Sialic acids are involved in many cellular recognition events and further function as a biological mask in processes that were previously named as antirecognition (Schauer, 2009). A good example of SA in antirecognition was already discussed in 1.3.2. The strong sialylation of red blood cells prevents their aggregation due to the bulky electronegative surface and also supports the formation and opening of developing blood vessels (Strilić et al., 2010). Desialylation of aged RBCs leads to recognition of open Galactose-endings by hepatocytes leading to their clearance from the circulating blood (Kerfoot et al., 2008). On the other hand, oversialylation protects malignant tumor cells or pathogens from being exposed to cellular defense mechanisms (Schauer, 2009, 2000). The bacterium *Streptococcus* exposes SA and interacts with SA binding proteins on neutrophils. This leads to decreased immune response and is also called molecular mimicry (Carlin et al., 2009).

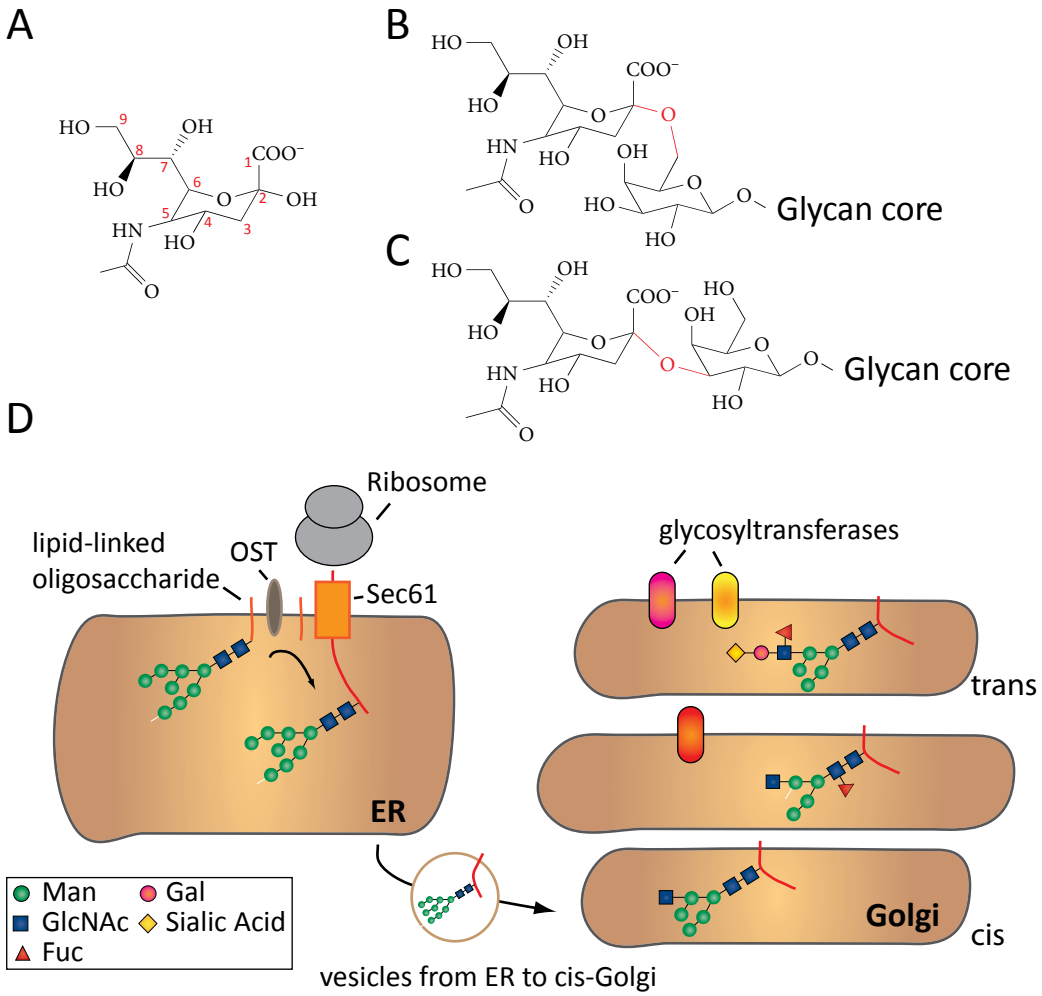

Figure 1.7: Structure of sialic acid conjugates and synthesis of complex glycans in mammalian cells. In mammalian cells, sialic acid is often modified (N-acetylated) at the fifth position (Neu5Ac). The carbon atoms are numbered in red (A). Sialic acid is commonly coupled to galactose via a α-2,3-(B) or -2,6 (C)-glycosidic linkage (shown in red). In D the glycosylation of transmembrane proteins is briefly summarized. During the co-translational protein transport in the ER via the translocon Sec61, oligosaccharyltransferases (OST) transfer oligosaccharides from lipid precursors to the nascent peptide chain. These early oligosaccharides mainly contain glucose (Glc), mannose (Man) and N-acetyl glucoseamine (GlcNac). The glycans are further modified by Golgi-localized glycosyltransferases, which are localized at specific sites to ensure hierarchical glycosylation.

Siglecs

Given the variety of SA derivatives and their terminal location, it seems obvious that SA is used by numerous SA-binding proteins in various recognition mechanisms. Selectins on leukocytes were already mentioned in 1.3.2. Another important group of proteins are SA-binding immunoglobulin-superfamily lectins (Siglecs) (O Reilly and Paulson, 2009; Crocker et al., 2007; Crocker, 2002). Siglecs are transmembrane proteins that belong to the immunoglobin superfamily. They have several external immunoglobin repeats, in which the terminal carries the SA-binding domain and a cytosolic tail where most Siglecs carry an immunoreceptor tyrosine-based inhibitory motif (ITIM). ITIMs function as inhibitory receptors and suppress activation signals that originate from receptors associated with immunoreceptor tyrosine-based activation motifs (ITAMs) (Crocker et al., 2007). Siglecs are expressed on the surface of many immune cells and specifically recognize SA and the linkage to Gal. These proteins mediate interactions in *cis*- as well as *trans* (i.e. on the same cell or between cells) (Crocker et al., 2007; Crocker, 2002). Many Siglecs are masked by *cis*-mediated SA binding due to a very high local SA concentration on immune cells.

SA in host-pathogen interactions

Haemophilus in uenzae, a bacteria that is found at high abundance in the lungs of flu patients and thus was regarded as the causative agent until the influenza virus was discovered in 1933 (Taubenberger et al., 2007), was found to posses SA-specific lectins (Lehmann et al., 2006). Today, it is known that influenza is caused by an influenza virus infection and that flu patients often suffer from secondary bacterial infections (superinfection), which presumably caused most of the fatal casualties of the 1918 flu pandemic (Taubenberger et al., 2007). As mentioned in section 1.3.2, some bacteria such as *Clostridium botulinum* and *Vibrio cholerae* secrete soluble toxic lectins. These toxins bind gangliosides and subsequently enter cells by endocytosis where in the cytoplasm they exhibit catalytical activity on cellular proteins. Another group of SA-binding pathogens are protozoic parasites. *Plasmodium falciparum* the causative pathogen of Malaria was shown to use SA for erythrocyte binding (Varki and Varki, 2007). In addition, various strains of *Leishmania* as well as *Trypanosoma* utilize SA as a host-cell interaction partner (Lehmann et al., 2006). Some pathogens have also evolved to use SA in combination with host-cell specific lectins for cell-adhesion. For Porcine Reproductive and Respiratory Syndrome virus (PRRSV) it was shown that the Siglec sialoadhesin in combination with heparan sulfate are necessary for virus attachment and uptake into pig alveolar macrophages (Delputte et al., 2005). *Neisseria meningitidis*, the causative agent of meningitis, utilizes sialoadhesin as well as Siglec-5 for attachment to macrophages.

In conclusion, the diversity and the exposed position of SA on mammalian glycans have presumably co-evolved with a great variety of pathogens that use SA as specific attachment sites. SA-synthesizing as well as SA-deficient organisms (such as plants) have developed SA-binding lectins to recognize SA residues with great specificity (Lehmann et al., 2006). Other examples for SA-mediated host-pathogen interactions are summarized in Table 1.2.

Table 1.2: Sialic acid mediated host-pathogen interaction. VP, virus protein; HN, hemagglutinin neuraminidase; EBA, erythrocyte-binding antigen; PRRSV, porcine reproductive and respiratory syndrome virus; sd, strain dependent; TS, trans sialidase

	pathogen name	pathogen factor	host factor
Viruses	Influenza A virus	HA	SA
	Simian Virus 40	VP1	GM1
	Rotavirus	VP4	GM1
	Newcastle desease virus	HN	GM1-3
	PRRSV	SA	Sialoadhesin
Bacteria	*Escherichia coli*	sd	SA
	Streptococcus	sd	SA
	Helicobacter	SabA	SA
	Haemophilus in uenzae	HifA	SA
	Vibrio cholerae	cholera toxin	SA
	Clostridium botulinum	botulinum toxin	SA
	Neisseria meningitidis	SA	Sialoadhesin, Siglec-5
Protozoic parasites	*Plasmodium falciparum*	EBA	SA
	Trypanosoma cruzi	inactive TS	SA
	Leishmania	nd	SA

1.5 Single molecule manipulation

Regarding the number of molecules that are present within a given system, there are at least two investigational approaches. The first and classical one is the ensemble or bulk approach,

where a large number of molecules in a certain reaction/experimental condition are followed. This approach is very robust, but the result is an average of a population of molecules. But probably, each molecule behaves differently and the average does not account for the biologic variability. A similar situation is valid for single cells within a population. Here the term cell-to-cell variability was introduced and investigated in several experimental approaches, with the result that cells in a population strongly differ in their response to a certain external cue (e.g endocytosis) (Snijder and Pelkmans, 2011; Snijder et al., 2009).
To look on processes or cells *in singulo* can reveal details about the mechanisms and real kinetics of a reaction. While single-cell methods (e.g. high resolution microscopy) provide information about the behavior of single cells, for the manipulation and description of single molecules, other methods are necessary. Two of these methods, optical tweezers and atomic force microscopy, will be described in the next section.

1.5.1 Optical tweezers (OT)

Optical tweezers originate from an observation made by Arthur Ashkin in 1970 (Ashkin, 1970). Ashkin observed, that the momentum transported by light can exert forces on particles with different refractive index compared to the surrounding medium. The forces that determine an optical trap are sketched in Fig. 1.8. Importantly, optical traps use high-power lasers with a gaussian beam profile, i.e. the center beam has the highest intensity. To minimize interaction with biological specimen by the high-power lasers (3W), the lasers operate with near-infrared light with a wavelength of 1064 nm (Wozniak et al., 2009). In comparison, conventional confocal microscopes use lasers at 10-20 mW.
If this laser light hits a spherical particle (e.g. a bead, Fig.1.8) the light is refracted at the edges of the bead, changing the direction of the deflected beam (Veigel and Schmidt, 2011). This causes a momentum change of the light beam and induces a momentum transfer onto the bead. The amount of the momentum transferred onto the bead depends on the intensity of the deflected light and thus on the gaussian beam profile. Hence, the total force exerted on the particle is combined of forces produced by the different rays within the beam. This is called the gradient force and represents the most important force component of optical traps.
The second component is also based on the particle characteristic of the light, which can induce radiation pressure. The so called scattering force pushes the particle in the direction of the propagating beam. The gradient force must overcome the scattering force, which is realized experimentally by using a high-numerical aperture (NA) objective and creating a steep light intensity gradient (Neuman and Nagy, 2008). As a result of both components, the particle is stabilized in the center of the beam slightly downstream of the focus (Veigel and Schmidt, 2011). The x-y position of the trapped particles can be measured by detecting the laser beam with nm-

precision on a quadrant photodiode (QPD), a light-sensitive diode that is divided into four equal segments. The total light intensity reaching the detector provides informations about the particle position in z-direction. After calibrating the optical trap, displacement of a particle from the center of the beam can be directly translated into the applied force. This allows to investigate processes at the level of single molecules.

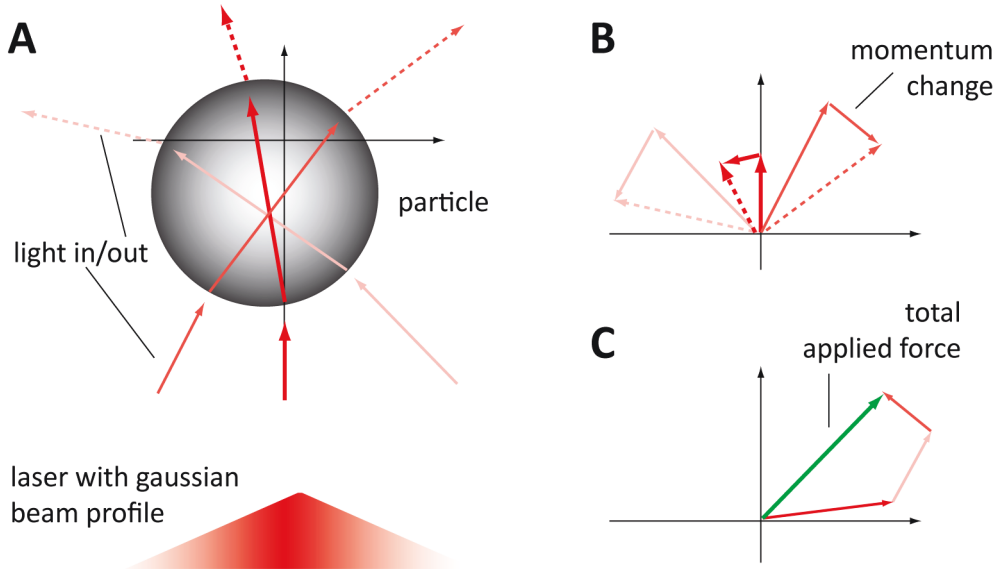

Figure 1.8: Mechanism of optical trapping. Optical tweezers operate with high power near-infrared lasers with a gaussian beam profile (i.e. the center beam has the highest intensity), which are focussed by a high NA microscopic objective (A, lower panel). In case of a spherical particle getting into proximity of the beam focus, the beam will be deflected at the edges of the particle, which leads to a changed direction of the deflected beam (A, upper part). This causes a momentum change of the light beam and a resulting momentum transfer on the bead directed in the opposite direction (B). The total force applied on the particle (green arrow) is the sum of forces produced by the different rays within the beam (C).

1.5.2 Atomic force microscopy (AFM)

In contrast to optical tweezers, the atomic force microscope is a contact tool, where a sample is probed by a mechanical sensor (scanning probe microscopy (SPM)). The sensor is a very sharp tip at the end of a cantilever arm. The tip is of pyramidal shape, with a tip diameter of only a few nm. The AFM tip scans surfaces and creates a contour image of the sample. The position of the tip is measured by pointing a laser beam at the cantilever and detecting the reflection with a photodiode. If the tip scans an uneven surface the cantilever will bend and alter the signal produced at the photodoide (Fig. 1.9A). In combination with rasterized sample scanning, the topography of a biological specimen can be determined. AFM can reach spatial resolutions of 1nm, which allows imaging of single proteins such as rhodopsin (Fotiadis et al., 2003) or

connexin 26 gap junctions (Müller et al., 2002).
The precise detection of the cantilever position enables force measurements in axial direction. The cantilever can be functionalized using highly specific and resistant attachment methods (Ebner et al., 2009) with proteins, cells or viruses (Muller, 2008). In force spectroscopy mode, the functionalized cantilever is lowered on a interacting surface (e.g. a cell) until binding occurs or the cantilever touches the surface. The cantilever is retracted and in case of a binding event will bend until the underlying bond fails and the cantilever returns into the zero-force position. The process is called a force-distance cycle and permits atomic force spectroscopy experiments as well as OT-based force spectroscopy (Fig. 1.9B).

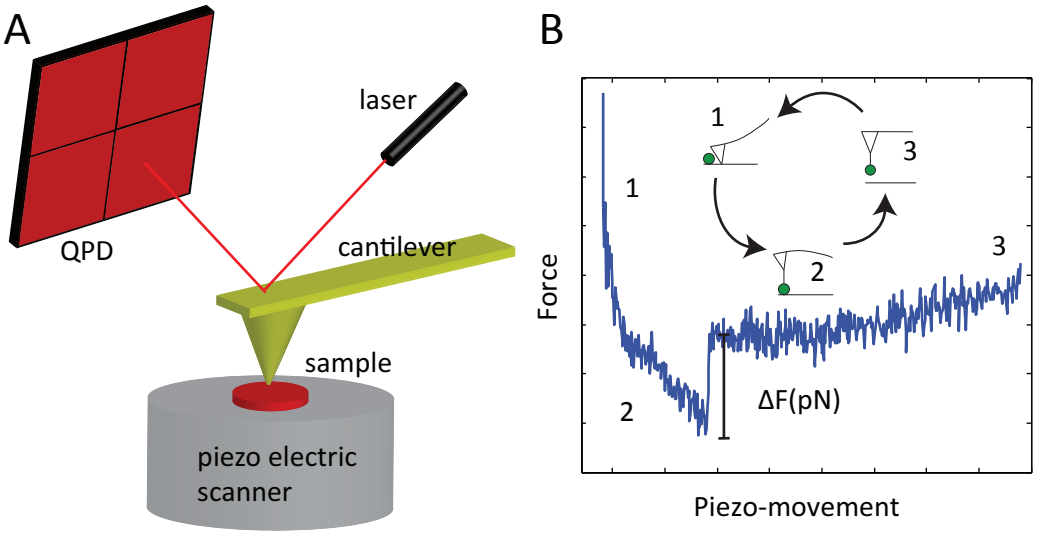

Figure 1.9: Components of an atomic force microscope and illustration of a force distance cycle. Components and the principle of atomic force microscopy (A).The sample is attached to a piezoelectric scanner that allows movement with nm-precision. The sample is scanned with a very sharp tip (tip diameter 5-10 nm) attached to a cantilever. The cantilever acts as a Hookean spring and hence bending can be translated into applied force. The deflection of the cantilever is measured by pointing a laser on the back of the cantilever and detecting the reflection on a quadrant photo diode (QPD). During a force-distance cycle (B) the cantilever is lowered until touching the surface of the sample (1). Subsequently, the cantilever is retracted at a defined velocity. In case of an interaction, the cantilever will bend towards the sample (2) until the underlying bond fails and the cantilever returns into the zero-force position (3).

1.6 Single molecule force spectroscopy (SMFS)

A variety of experimental studies at single-molecule level illustrates the versatility of AFM and OT. Well-known examples for OT-based experiments are investigations of walking motor proteins such as myosin and kinesin or of the catalytic activity of DNA-binding enzymes (Fazal

and Block, 2011). The two first studies that describe the mechanical unfolding of a single protein were conducted in parallel by AFM and OT and were published together in 1997 (Rief et al., 1997; Kellermayer et al., 1997). Thereafter, AFM was successfully used to study the unfolding of rhodopsin (Oesterhelt et al., 2000) and the unbinding of biotin from streptavidin (Yuan et al., 2000). However, except for the study of Yuan and colleagues (Yuan et al., 2000), these studies describe processes that where monitored by spatial displacement. In dynamic force spectroscopy (DFS), the resistance of a discrete molecular interaction is probed under tension in a dynamic range of force loads. This includes a repetitive scheme of force distance cycles (Fig. 1.9 B) while varying the pulling velocity (i.e. force load or loading rate) (Hinterdorfer and Dufrêne, 2006). In force spectroscopy, the AFM cantilever and the optical trap, respectively, act as a Hookean spring, which is connected to the interacting sample. When the spring constant of the cantilever (or the stiffness of the optical trap) is known, the deflection linearly scales with the applied force. During a pulling experiment, the anchor between sample and bead or cantilever must be more resistant than the interaction to be investigated. In this case, the investigated interaction will unbind first and the resulting rupture force (F) in most cases increases with the applied loading rate (r) (Müller et al., 2009). A model to describe this relation was introduced by Bell and Evans (Eq. 1.1) (Evans, 1999; Evans and Ritchie, 1997; Bell, 1978). According to the model, the most probable rupture force (F) increases with increasing loading rate (r) (Fig. 1.10), which can be controlled by the pulling velocity v leaving the force the only unknown parameter. Looking at the energy landscape of a simple ligand-receptor interaction, the bound state is separated from the unbound state by an energy barrier (Fig. 1.10). The height of the barrier determines the spontaneous unbinding rate (k_{off}) and its position is at x_u along the reaction coordinate (Rief and Grubmüller, 2002).

$$F(r) = \frac{k_B T}{x_u} ln\left(\frac{r x_u}{k_{off} k_B T}\right) \tag{1.1}$$

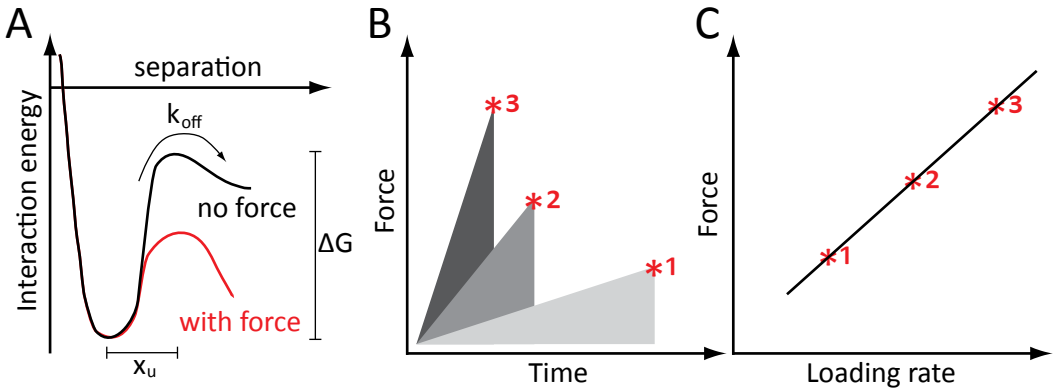

Figure 1.10: Bell-Evans model of single molecule force spectroscopy. The model describes the transition of a receptor-ligand interaction between a bound and an unbound state (A). The energy landscape of this interaction is shown in black. The interaction must overcome a single energy barrier with the height ΔG. In case a pulling potential is attached to one of the binding partners, the energy barrier is lowered and this allows unbinding. According to the model, the most probable rupture force F increases exponentially with increasing loading rate r (B). That means that the failure rate of the bond increases and the lifetime decreases. In the case depicted in A, a single energy barrier is overcome which leads to a linear dependence of F against $log\, r$ (C). The curve can be described using Eq. 1.1 and provides the dissociation rate without force k_{off} and the position of the transition state x_u.

1.7 Aims of this thesis

Influenza poses a constant threat to public health and is under continuing surveillance by several institutions worldwide. In order to develop new antiviral strategies, it is highly important to understand the details of virus replication. In the course of its complex infectious cycle, influenza A virus must deliver its genome to a host cell and hijack the cells reproductive machinery to eventually initiate its own replication. Recent studies indicate that essential parts of the replicative cycle, including the early phase of binding and invasion are still not well understood. For example, virus-cell binding might not solely depend on different conformations of sialic acid. Rather, attachment is a heterogeneous process that is affected by the virus presenting its spike protein HA as well as the cell presenting the corresponding receptors. Another example, as we reasoned, is an optimized interplay between endosome acidification and structural intermediates of viral components eventually leading to release of the virus genome into the host cell. This close correlation goes far beyond the low pH-triggered conformational change of HA as the only driving force behind genome release.

This thesis provides a detailed study about the initial phase of influenza virus infection. Virus binding was investigated using an experimental system that closely mimics the natural situation. Via modern OT- and AFM-based force spectroscopy, virus binding was studied at the single molecule level. Using this approach combined with the characterization of cell surface glycans gives an unprecedented insight into receptor binding specificity. The subsequent infection steps were investigated by high-resolution fluorescence microscopy. Virus labeling and parallel expression of cellular markers allows studying the trafficking and fusion kinetics of individual viruses. Further, pH-sensitive fluorophores were utilized to trace endosomal acidification kinetics at single vesicle- and whole cell level.

Considering known problems and drawbacks of current anti-influenza therapy (e.g. development of resistances), we demonstrate exemplarily that results from the present study can be used to develop target-directed antiviral drugs. We used our results to design and evaluate competitive binding inhibitors - a potential new class of influenza antivirals. Receptor-coated nanoparticles, which mimic the cell surface, provide a high affinity alternative for the virus to bind. Particle-based inhibitors were tested using assays to study HA-related virus activity, including virus-cell binding and fusion.

In summary, this comprehensive investigation of the first steps of influenza virus infection identifies potential targets for antiviral therapy. The study further gives an example how the detailed analysis of virus binding can directly be translated into effective antiviral approaches.

2 Materials and Methods

2.1 Materials

2.1.1 Biological Material

Cell lines

Name	Species	Origin	Source
MDCK 2	*Canis familliaris*	kidney epithel	ATCC: CCL-34
CHO K1	*Cricetulus griseus*	ovary, epithel like	ATCC: CCL-61
A549	*Homo sapiens*	epithel	ATCC: CCL-185

Virus strains

Influenza A/X-31 (H3N2) was grown in 10-day old embryonated chicken eggs as described in 2.2.3. X-31 is a reassortant influenza strain between A/Aichi/2/68 (H3N2) and A/Puerto Rico/8/34 (H1N1). HA and NA define the antigenic phenotype. X-31 carries HA and NA from influenza A/Aichi/2/68 and is thus considered a H3N2 virus. Influenza A/WSN/33 and A/Panama/99 were grown in MDCK cells and concentrated from cell supernatant by ultracentrifugation at 100.000 g for 1.5 h. The purity of the virus samples was verified by SDS-Page.

Plasmids

Name	Insert	Source
pEYFP	full HA-YFP	kindly provided by M. Veit (FU Berlin)
pCDNA3	Rab5-GFP	kindly provided by V. Haucke (FU Berlin)
pEGFP	Rab7-GFP	kindly provided by V. Haucke (FU Berlin)

2.1.2 Media and Solutions

Cell Culture Media and reagents

Application	Composition	Source
Cell growth	DMEM	PAA
	10 % fetal calf serum	PAA
	200 mM L-glutamine	PAA
	1 % Penicillin/Streptomycin	PAA
Cell passaging	PBS with/without	PAA
	100 mg/ml CaCl and MgCl	
	PBS with 0.5 mg/ml Trypsin,	PAA
	0.22 mg/ml EDTA	
Cell freezing	70 % DMEM	
medium	20 % fetal calf serum	
	10 % DMSO	
Infection	DMEM	PAA
medium	0.2 % BSA	Sigma
Transfection	Lipofectamine2000	Invitrogen
	Turbofect	Fermentas

Buffers

Buffer	Composition
PBS	137 mM NaCl, 2.7 mM KCl,
	10 mM Na_2HPO_4 + 2 H_2O, 1.76 mM KH_2PO_4
Fusion buffer	150 mM NaCl,
	10 mM Sodium acetate, pH 7.4
Cell fusion buffer	10 mM HEPES, 10 mM MES
	150 mM NaCl, pH 5
Stacking SDS-gel buffer	1 M Tris/HCl pH 6.8
Separating SDS-gel buffer	1 M Tris/HCl pH 9.0
SDS loading buffer	63 mM Tris/HCl, 10 % glycerol,
	2 % SDS, 0.0025 % Bromophenol blue
	100 mM -mercaptoethanol
SDS running buffer	25 mM Tris/HCl, 192 mM glycine, 0.1 % SDS
Fixation buffer	PBS, 2 % Paraformaldehyde
	0.02 % Glutaraldehyde
Permeabilization buffer	PBS, 0.2 % BSA, 0.2 % Triton X-100
Antibody diluent	PBS, 0.2 % BSA
Fixation buffer (FACS)	PBS, 2 % Paraformaldehyde
Permeabilization buffer (FACS)	PBS, 0.2 % Saponin
Blocking buffer (FACS)	PBS, 0.2 % Saponin, 2% BSA
Antibody diluent (FACS)	PBS, 0.2 % Saponin, 2% BSA
standard pH buffer	mixing 50 mM HEPES with 50 mM MES both con-
pH 4.5 - 7.5	taining 50 mM NaCl
	30 mM ammonium acetate, 40 mM sodium azide
	10 µM Monensin or Nigericin
hemolysis buffer	10 mM Na_2HPO_4 + 2 H_2O, 1.76 mM KH_2PO_4
	pH 7.4

2.1.3 Reagents

Chemicals

Standard chemicals were obtained from Merck, Sigma and Roth. Others are listed below.

Name	Source
Nocodazole	Sigma
Cytochalasin D	Sigma
Ammonium chloride (NH_4Cl)	Sigma
Bafilomycin A	Sigma
Monensin	Sigma
Nigerizin	Sigma
Amantadine	Sigma
Neuraminidase from *Clostridium perfringens*	Sigma
PageRuler ™ Prestained Protein Ladder	Fermentas
Mowiol	Roth
Octylglycoside	Boehringer

Fluorescent Markers

Name	Source
octadecylrhodamine B (R18)	Invitrogen
1,1 -dioctadecyl-3,3,3 ,3 - tetramethylindodicarbocyanine (DiD)	Invitrogen
4-(4-(Dihexadecylamino)styryl)-N-Methylpyridinium Iodide (DiA)	Invitrogen
1,1 -dioctadecyl-3,3,3 ,3 -tetramethylindocarbocyanine perchlorate (DiI)	Invitrogen
4,4 -Bis (1-anilinonaphthalene 8-sulfonate), bis-ANS	Invitrogen
4 ,6-diamidino-2-phenylindole, DAPI	Invitrogen
Hoechst 33342	Invitrogen
Rho-Phalloidin	Invitrogen
Lysotracker™ Red	Invitrogen
FITC-dextran (10.000 kDa)	Sigma
FITC/Rhodamine-dextran (10.000 kDa)	Invitogen
Propidium iodide	Sigma
Lectin from *Triticum vulgaris*, WGA (FITC conjugate)	Sigma
Lectin from *Maachia amurensis*, MAA (Rhodamine conjugate)	EY Laboratories
Lectin from *Sambucus nigra*, SNA (FITC conjugate)	EY Laboratories

Antibodies

Primary antibodies

Antigen	Species	Source
Influenza A nucleoprotein	mouse	Millipore
Influenza A nucleoprotein, FITC conjugate	mouse	Millipore
Influenza A H3N2 polyclonal	goat	Virostat
Influenza A H3N2 M1	goat	Virostat
-tubulin	mouse	Sigma

Secondary antibodies

Conjugate	Source
anti-mouse IgG Cy2	Amersham
anti-mouse IgG Alexa 568	Invitrogen
anti-goat IgG Cy3	Sigma

2.1.4 Kits

Name	Source
BCA Protein Assay Reagent Kit	Pierce
Total Protein Kit Lowry	Sigma
QIAprep Spin MiniPrep Kit	Qiagen
Plasmid MaxiPrep Kit	Qiagen
RNEasy Mini Kit (RNA Isolation)	Qiagen
Celltiter Blue Cell Viability Assay	Promega

2.1.5 Multivalent polyglycerol and gold nanopraticles

All multivalent polyglycerol particles (PG) were synthesized and provided by Dr. Ilona Papp and Prof. Dr. Rainer Haag (FU Berlin). Gold colloids (AuNP) were synthesized by Dr. Meike Roskamp and Prof. Dr. Sabine Schlecht (now Justus-Liebig-Universität Gießen). Final functionalization of gold colloids was performed by Dr. Ilona Papp. The particles vary in their size and degree of functionalization (dF).

Name	MW (kDa)	diameter (nm)	Df (%)	SA units
PG 1	6.6	3 0.1	15	6
PG 2	14.4	3 0.7	50	20
PG 3	23	3 1.3	90	35
sulfated PG	6.5	4 1.1	85	0
PG 4	8,000	50 5.6	12	10,000
PG 5	27,000	70 6.8	80	60,000
SA AuNP	n.d.	14	full	10.000
SA AuNP	n.d.	2	full	2.000
OH AuNP	n.d.	14	full	only OH

2.1.6 Consumables

Material	Source
Cell culture flasks (T25, T75, T175)	Nunc
Cell culture plates	Nunc, Sarstedt
96-well, µclear cell culture plate, black	Greiner
cell scraper	Sarstedt
Cryo tubes (1.5 ml)	Sarstedt
Round bottom tubes, 5 ml	Sarstedt
Glass bottom petri dishes, 35 mm	MatTek
Microscopy glass slides	Roth
Glass cover slips	Roth
Fluorescence cuvette, 10x10 mm	Hellma
Parafilm®	Pechiney
Slide-A-Lyzer dialysis casette	Pierce
Polystyrene beads 1.5 µm	Bangs Laboratories

2.1.7 Equipment

Experiments were done using standard modern laboratory equipment. Others are listed below.

Name	**Configuration**
Olympus FV-1000	IX-81 microscope 60x/1.2 Water UPlanSApo 405, 560 nm diode lasers 458, 488, 515 nm Argon laser 3 confocal PMTs climatization chamber
Olympus FV-1000MPE	IX-81 microscope 60x/1.2 Water UPlanSApo 405, 440, 560, 635 nm diode lasers (458), 488, 515 nm Argon laser 3 confocal PMTs climatization chamber
Olympus IX-81 epifluorescence microscope	HBO lamb 60x/1.35 Oil Zeiss Filter cubes: U-MWNiba, U-MWG2
BD FACScan	488 nm argon laser line Filters: 560 SP, 530 SP
BD FACSAria II	375, 488, 405, 633 nm laser line Filters: 515 - 545 nm, 564 - 606 nm, 600 - 620 nm
Horiba Jobin Yvon Fluoromax 4 steady state fluorescence spectrometer	high-power xenon light source temperature-controlled sample chamber with stirrer
Eppendorf Biophotometer Plus	equipped with a microliter sample cell (IMPLEN)
CASY ® cell counter Model TTC 45/60/150	150 µm capilary

2.1.8 Software

Name	Supplier
Olympus FV1000 3.1	Olympus
MetaMorph	Molecular Devices
CellQuest	Beckton Dickinson
FACS Diva Software	Beckton Dickinson
FlowJo	Tree Star, Inc.
ImageJ	US National Institute of Health (NIH)
Localize for IDL	kindly provided by Daniel R. Larson (NIH, USA)
Photoshop	Adobe®
Illustrator	Adobe®
Matlab	The Mathworks
Igor Pro	Wavemetrics
FluorEssence™	Horiba
Origin	OriginLab
PyMOL	DeLano Scientific LLC
Microsoft Office 2003	Microsoft
Prism	GraphPad Software, Inc.
LaTeX	

2.2 Methods

2.2.1 Cell culture

The cells were propagated in growth medium in 25, 75 or 175 cm^2 culture flasks at 37 C and 5% CO_2. The cells were passaged every 3 - 5 days before they had reached full confluency. To this end, the cells were washed twice with PBS -/- and detached using trypsin-EDTA at 37 C for 5 - 15 min. Trypsinization was stopped by addition of growth medium and approximately 1 10^6 cells were seeded in a new 75 cm^2 culture flask. For the different assays, cells were seeded into 6-, 12-well plates or petri dishes. For long term storage, the cells from one 75 cm^2 culture flask were detached, pelleted for 5 min at 2000 g and resuspended in freezing medium. The cells were kept at -80 C for 24 hours and subsequently stored in liquid nitrogen.

2.2.2 Cell viability assay

To monitor the cell viability under the used experimental conditions, two assays were used. The Celltiter Blue Cell Viability Assay uses the metabolic conversion of resazurin to resorufin by metabolically active cells. This results in a fluorescent product which can be measured at $_{ex}$ = 560 nm / $_{em}$ = 590 nm. Cells were grown in a µclear 96-well plate, washed once with PBS and incubated with 25 µl of the indicated test substance at 37 C. The volume was added up to 100 µl with DMEM and 25 µl Celltiter blue reagent was added. The cells were incubated for 1h at 37 C. The fluorescent signal was recorded on a Tecan 200 Pro microplate reader. As a flow cytometric alternative cells where detached from the cell culture plate using PBS -/- containing 2 mM EDTA. The cells were washed in PBS, peletted (2000 g, 5 min) and resuspended in PBS. Propidium iodide (PI) was added to a final concentration of 1 µg/ml, briefly vortexed and immediately analyzed by flow cytometry. PI is membrane impermeable and excluded from viable cells which show a much lower fluorescence signal.

2.2.3 Virus preparation

Influenza A virus X-31 (H3N2) was propagated in chicken eggs as follows. Embryonated chicken eggs were cultured in a home-made incubation chamber that allows constant temperature of 37 C and rotation of the eggs. After 11 days, allantoic fluid from a previous preparation (09.11.97) was diluted 1 : 500.000 and 200 µl were injected into the allantoic cavity of each egg. The virus was allowed to propagate within the cells of the allantoic cavity for 48 h before the allantoic fluid was collected. The fluid was cleared from cell debris by low speed centrifugation at 3000 g for 30 min. The virus was pelleted by ultracentrifugation at 100.000 g for 90 min. The virus pellet was resuspended in PBS and homogenized with a Teflon-coated homogenizer. At

last the total protein content was determined by BCA assay and the virus was stored in aliquots at -80 C.

2.2.4 Preparation of red blood cell ghosts.

Purified human erythrocytes (Blutbank, Charité) were washed three times in PBS (2000 g, 10 min). One volume of erythrocytes (red blood cells, RBC) was resuspended in 10 times the volume ice cold hemolysis buffer. The cells were lysed for 30 - 50 min on ice and centrifuged for 20 min at 5000 g. The lysed RBCs were incubated on ice for 10 min with occasional stirring. This lysis-washing cycles were repeated until the pellet appeared white. The cells were washed in PBS, pelleted and stored at 4 C with 0.02 % sodium azide.

2.2.5 Whole cell-virus binding assay

Influenza A virus was labeled with octadecylrhodamine B (R18) as follows. The virus was diluted to a concentration of 1 mg/ml in PBS and incubated with R18 (20 µM final conc.) for 30 min at RT. Unbound R18 was removed by centrifugation for 5 min at 50.000 g. The pellet was resuspended in PBS. Red blood cells were washed in PBS and diluted to 1%. 40 µl RBCs (10^8 cells) were mixed with 10 µl labeled virus and incubated at RT for 20 min. Unbound virus was removed by centrifugation (5 min, 1200 g). The pellet was resuspended in PBS, and the fluorescence per red blood cell was measured by flow cytometry on a BD FACScan and FACSAria II flow cytometer. The data were acquired using BD CellQuest and FACSDiva software. The data were analyzed using FlowJo. Virus binding to adherent cells was analyzed as follows. Cells were detached from the culture plate using PBS -/- supplemented with 2 mM EDTA for 20 - 40 min at 37 C. The cells were washed in PBS, the cell number was determined using a Casy cell counter and 2 10^5 cells were mixed with 10 µg labeled virus for 20 min at RT. Unbound virus was removed by centrifugation (5 min, 1200 g) and the sample was analyzed as described above.

2.2.6 Hemagglutination inhibition assay (HAI)

Influenza viruses bind to and crosslink erythrocytes due to their spike protein HA. This process is called hemagglutination and serves as a method to determine the amount of virus in a given sample. However, it can also be used to evaluate binding inhibitors. First, the minimal effective virus concentration (HA Titer) was determined. Influenza A/X-31 virus was diluted to 1 mg/ml protein concentration in PBS. In a 96-well plate 25 µl virus were serially diluted in an equal amount of PBS -/-. Purified human RBCs were washed with PBS and diluted to 1%. 50 µl RBCs were added to the virus dilution and incubated for 1 h at RT. Effective hemagglutination resulted

in a gel when viewed from the top. If the virus concentration was too low the RBCs settle and formed a pellet on the bottom of the well (Fig. 2.1). The minimal effective virus concentration was tripled and incubated with serially diluted inhibitors for 30 min at RT until RBCs were added as described above. The lowest concentration that still prevents hemagglutination is defined as the K_{HAI}.

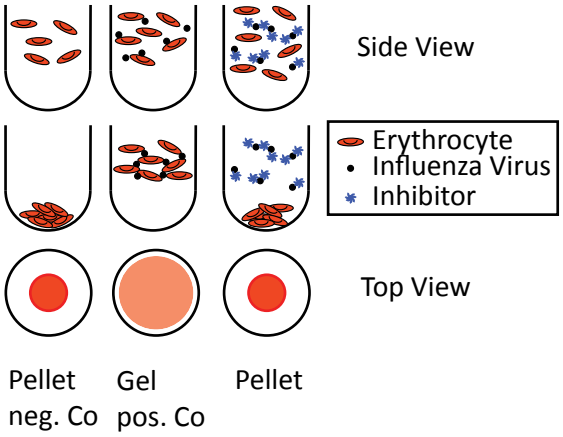

Figure 2.1: Hemagglutination inhibition assay (HAI). Influenza viruses are able to agglutinate red blood cells. The assay is performed in a 96-well plate format. Viruses are mixed with human erythrocytes which are eventually cross-linked and form a gel seen from above. This effect can be used to determine virus titers or the effect of potential competitive binding inhibitors. In this case the virus is pre-incubated with an inhibitor, which can inhibit RBC binding. The inhibitor is serially diluted and the lowest concentration that still prevents hemagglutination is defined as the K_{HAI}

2.2.7 Influenza virus fusion assay

Virus-cell fusion was measured by monitoring the fluorescence de-quenching (FDQ) of the lipid-like fluorophore R18 upon fusion of R18-labeled viruses with ghost membranes (Krumbiegel et al., 1994). To this end, 10 µl labeled virus suspension (1 mg/ml) was mixed with 40 µl ghost suspension ($\approx 2{*}10^5$ cells) and incubated for 20 min at RT. Unbound virus was removed by centrifugation (5 min, 1200 g). The virus-ghost suspension was transferred to a glass cuvette containing pre-warmed fusion buffer (pH 7.4), and the fluorescence was detected (λ_{ex} = 560 nm; λ_{em} = 590 nm) by using a Horiba Yobin Yvon FluoroMax spectrofluorometer. Fusion was triggered by the addition of citric acid (0.2 M). The suspension was stirred continuously with a 2 by 8 mm Teflon-coated magnetic stirring bar. After 600 s the fusion was stopped by adding Triton X-100 (50 µl, final concentration 0.5%) to obtain maximum R18 de-quenching. The final pH in the cuvette was measured using a standard pH meter. The percentage of FDQ was

calculated as:

$$FDQ(\%) = \frac{F(t) \quad F(0)}{(F_{max} \quad F(0))} \quad 100 \tag{2.1}$$

where F(0) and F(t) are the fluorescence intensity before starting fusion and at a given time (t), respectively.

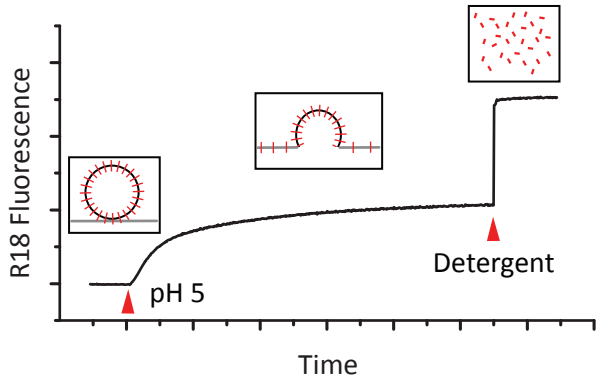

Figure 2.2: Influenza virus-cell fusion assay. Influenza virus was labeled with R18 at self-quenched concentration. The labeled virus was incubated with red blood cell ghosts for 20 min at RT. Unbound virus was removed by centrifugation (5 min, 1200 g). The virus-ghost suspension was transferred to a glass cuvette containing pre-warmed fusion buffer (pH 7.4), and the fluorescence was detected ($_{ex}$ = 560 nm; $_{em}$ = 590 nm) by using a Horiba Yobin Yvon FluoroMax spectrofluorometer. Fusion was triggered by setting the pH to 5 by adding citric acid (0.25 µM). The fusion was stopped by adding Triton X-100 (50 µl, final conc. 0.5%) to obtain maximum R18 de-quenching.

2.2.8 Infection with influenza virus

Approximately 1-5 10^6 MDCK cells were seeded 14 - 24 h prior to the experiment in 35 mm petri dishes or on 15 mm glass cover slips in a 12-well plate. Influenza A virus was diluted in PBS to a final protein concentration of 1 mg/ml. The virus was then further diluted in infection medium to a final concentration of 20 µg/ml, which corresponds to a MOI of 25 - 50. The virus was added to adherent cells and after 1 h of adhesion at 37 C, unbound virus was removed, and the cells were incubated in infection medium for 5 - 7 h.

2.2.9 Live cell microscopy

All microscopic experiments using living cells were performed in 35 mm petri dishes. The used microscope was equipped with an incubation chamber that provided constant temperature of 37 C as well as 5 % CO_2.

2.2.10 Immunostaining for microscopy and flow cytometry

For microscopy, the cells were washed twice in PBS and fixed for 30 min in fixation buffer. The cells were washed again twice in PBS and transferred into permeabilization buffer for 20 - 25 min. Primary antibodies were diluted 1:1000 and either dropped in the middle of a glass bottom petri dish or 20 µl were dropped on Parafilm and cells growing on glass slides were put upside-down on the drop. The cells were labeled for 1 h at RT, washed in PBS 3 10 min and incubated with the secondary antibody for 1 h. The cells were counterstained with DAPI in PBS at a final concentration of 0.2 µg/ml and finally washed 3 10 min. Cells in petri dishes were directly used for microscopy in PBS buffer. Glass cover slips were mounted on glass slides using mowiol and after drying were stored in the dark at 4 C. For flow cytometry, the cells were scraped from the petri dish and fixed for 20 min fixation buffer. The cells were kept on ice throughout the staining. The cells were washed, pelleted at 1000 g for 5 min and permeabilized for 20 min. The cells were incubated in blocking buffer for 20 min and labeled with the first antibody for 45 min. The cells were washed 3 5 min and labeled with the secondary antibody for 30 min. After a final washing step the cells were kept on ice until analysis. Fluorescence values per cell were measured by using a Beckton Dickinson FACScan or FACSAria II flow cytometer and data were acquired using BD CellQuest and FACSDiva software. The data were analyzed using FlowJo.

2.2.11 Transfection of expression plasmids

Cells were transfected with expression plasmids using Lipofectamine2000 or Turbofect according to the manufacturers manual. To this end, cells were seeded in 35 mm glass bottom petri dished and grown until they reached 70 - 90 % confluency. 10 µl Lipofectamine2000 and 4 µg DNA were diluted separately in 250 µl serum-free medium. After 5 min DNA and Lipofectamine2000 were mixed and further incubated for 20 min at room temperature. The cells were washed in PBS and the DNA/Lipofectamine2000 mix was added with additional 1.5 ml serum-free medium. After 4 h the medium was changed to growth medium. The protocol is essentially the same for Turbofect, but without medium change after 4 hours.

2.2.12 Intracellular pH measurement

To determine the pH inside individual endosomes, one has to introduce a pH sensitive molecule into the endocytic pathway. To this end, endocytic uptake markers labeled with pH (in)sensitive fluorophores were used. MDCK cells were seeded in glass-bottom petri dishes one day prior to the experiment. On the day of the experiment, the cells were serum-starved in DMEM for 30 min at 37 C. FITC/Rhodamine conjugated dextran was added at a concentration of 10 mg/ml in DMEM. The cells were incubated for 5 min at 37 C (Pulse), washed 3 times with PBS,

transferred into pre-warmed DMEM and the fluorescence was immediately followed using a confocal microscope (Chase). For flow cytometric pH determination, the cells were detached from the petri dish after the serum-starvation using PBS -/- supplemented with 2 mM EDTA. The cells were washed 3 times in PBS (centrifugation at 2000 g, 5 min) and incubated in 10 mg/ml FITC/Rho-Dextran for 5 min at 37 C in a pre-heated water bath. The cells were pelleted, divided into aliquots of 10^5 cells and chased for up to 60 min. Each aliquot was diluted in PBS and the fluorescence was immediately quantified by flow cytometry.
In order to measure the pH inside individual endosomes in the presence of a virus particle, the virus was diluted to 1 mg/ml and labeled with 20 µM DiD for 2 h at RT. To remove unbound dye, the virus was centrifuged at 50.000 g for 10 min, resuspended in PBS and diluted in 10 mg/ml FITC-Dextran. The suspension was added to the cells and internalized for 5 min at 37 C. The cells were washed in PBS, transferred in pre-warmed DMEM and the fluorescence was immediately followed using a confocal microscope. In the microscopic as well as in the flow cytometer approach, the mean fluorescence values of FITC and Rhodamine/DiD were measured for each sample, and the autofluorescence from unlabeled samples was subtracted. The ratio of FITC to Rhodamine/DiD was determined, and the intravesicular pH was calculated from the standard curve.

Generation of a pH-standard curve of dextran-labeled compartments

To generate a pH-standard curve for the dextran labeled compartments, the whole cell was equilibrated with a pre-determined pH and the resulting fluorescence ratio was measured by flow cytometry (Bayer et al., 1998; Baravalle et al., 2005). Cells were pulsed as described above, pelleted and divided into 7 aliquots. These were resuspended in standard pH buffers and left on ice for 10 min for ATP depletion and equilibration of intravesicular pH (pH clamped). Figure 2.3 A shows three normalized calibration curves. In the first experiment the cells were equilibrated without ionophore. For the other two either 10 µM nigerizin or monensin was present. The calibration was repeated without ionophore and the resulting curve was fitted to Eq. 2.2 (Fig. 2.3 B). The obtained parameters were used to calculate the pH from the FITC/Rho ratio.

$$R(pH) = base + \frac{max \quad base}{1 + 10^{((xhalf \quad pH) \ rate)}} \tag{2.2}$$

2.2.13 Intracellular fusion assay

Influenza A/X-31 virus was diluted to 1 mg/ml in PBS -/- and labeled with 20 µM R18 for 30 min at RT. Unbound R18 was removed by centrifugation at 50.000 g for 10 min and the virus was resuspended in PBS. The labeled virus was diluted to 20 µg/ml in DMEM containing 0.2 % BSA,

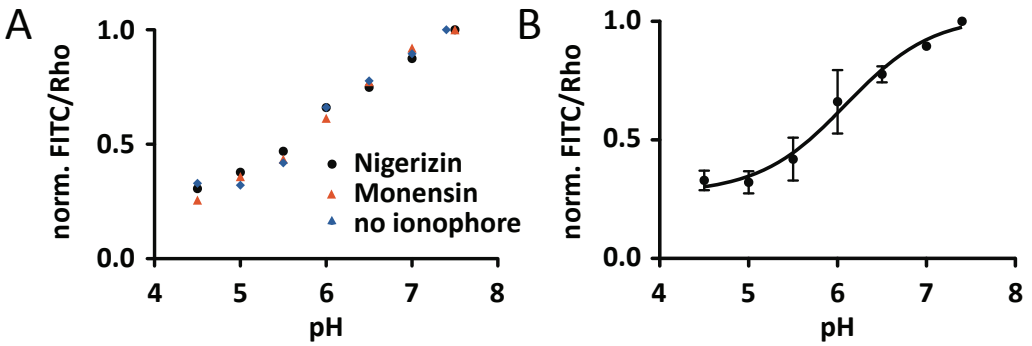

Figure 2.3: Generation of a pH-standard curve of dextran-labeled compartments. Cells were pulsed as described above, washed and divided into 7 aliquots. These were resuspended in standard pH buffers and left on ice for 10 min for ATP depletion and for equilibration of intravesicular pH (pH clamped). During this step there was either no ionophore or 10 µM nigerizin/monensin present. FITC and Rhodamine signal was quantified by flow cytometry (A). The calibration was repeated without ionophore and the resulting curve was fitted to Eq. 2.2 (B). Error bars correspond to SEM of three independent experiments.

filtered using a 0.2 µm pore size sterile filter and applied on MDCK cells in glass bottom petri dishes. The cells were incubated on ice for 10 min, washed 3 times with cold PBS, transferred in warm DMEM and the fluorescence was immediately followed using a confocal microscope. Fusion was indicated by a marked increase of the R18 signal due to de-quenching during fusion of virus envelope with the endosomal membrane. In a second assay, fusion was followed using a double-staining protocol, as described before (Sakai et al., 2006). 100 µg viruses were diluted in 1 ml PBS and transferred in a 2 ml round-bottom eppendorf tube. Under constant shaking 66 µM DiI and 33 µM DiO were added dropwise (6 µl each) to the virus suspension. Under constant inverting the virus was labeled for 1 h at RT. The virus was filtered using a 0.2 µm pore size sterile filter and applied on MDCK cells. The samples were further processed as described above.

2.2.14 Quanti cation of the nuclear NP signal

Cells were immunostained against the viral NP and the nucleus was counterstained with DAPI as described in section 2.2.10. Z-stacks spanning the whole cell were recorded at different positions of the petri dish. NP and DAPI stacks were summed using Image J. A binary mask of the nucleus was created from the DAPI image, inverted and subtracted from the NP image. The resulting image shows only signal in the nucleus leaving the rest of the cytoplasm dark. Finally, the summed pixel intensity of the calculated image was measured.

2.2.15 Lectin binding assay and neuraminidase treatment

For microscopic analysis, cells were grown in glass bottom petri dishes. The cells where washed with PBS and incubated with WGA (40 µg/ml), SNA (10 µg/ml) or MAA (50 µg/ml) for 20 min on ice (see 2.1.3 for lectin specifications). The cells were washed in PBS and either immediately used for confocal microscopy or incubated in fixation buffer for 30 min, washed in PBS and mounted for microscopy. For flow cytometry, the cells were detached from the culture plate using PBS supplemented with 2 mM EDTA for 20 - 30 min. The cells were washed in PBS and labeled with lectins as stated above. After the final washing step, the cells were immediately used for flow cytometric analysis. To cleave of sialic acid residues from the cell surface the cells were incubated with 1 U/ml neuraminidase (NA) *Clostridium perfringens* for 10 min at 37 C.

2.2.16 Preparation of virus-coated polystyrene beads

Polystyrene (PS) beads were washed in PBS. Influenza A /X-31 was labeled with R18 as described above. Unbound R18 was removed by centrifugation 5 min at 50.000 g and the pellet was resuspended in PBS. The virus was diluted to 20 µg/ml in PBS and viral aggregates were removed with a 200 nm pore size sterile filter. 5 µl beads in PBS (0.1 % solids) were added and both were incubated for 30 min at 4 C. Unbound virus was removed by centrifugation. The pellet was dissolved in PBS buffer containing 3 % BSA and again incubated for 30 min at RT. Finally, the beads were washed in PBS and stored at 4 C for maximum 2 days.

2.2.17 Single Virus force spectroscopy using optical tweezers

Optical tweezers experiments were conducted at JPK Instruments AG, Bouchestrasse 12, 12435 Berlin with the help of Dr. Anna Wozniak.

For optical tweezers force measurements we used the JPK Nanotracker (Wozniak et al., 2009). The trapping of the PS beads was performed using a 1064 nm laser at intensities between 1 - 3 W. For the calibration of the optical trap, the Brownian motion of a bead at certain laser intensities was measured. The power spectrum of a diffusing particle in a viscous liquid, held by a trap of stiffness k can be fitted to a Lorentzian curve (Wozniak et al., 2009). This provides the trap stiffness k and together with the detector sensitivity the signals can be calibrated either in nanometer displacement or piconewton forces. The value of the force of impingement, ranging between 10 to 50 pN, was selected to promote single-bond formation between host cell surface receptors and HA glycoproteins. Cells were seeded one day prior to the experiment kept in growth medium. All measurement were carried out in PBS buffer at 37 C.

2.2.18 SVFS using atomic force spectroscopy

AFM experiments were conducted in the laboratory of Prof. Peter Hinterdorfer at Johannes Kepler University Linz, Institute of Biophysics, A-4020 Linz, Austria with the help of Dr. Rong Zhu.

AFM-based force spectroscopy was performed with an Agilent 5500 AFM combined with an iMIC microscope (TILL Photonics, Germany). Cells were seeded one day prior to the experiment kept in growth medium. The glass bottom petri dish was mounted with the AFM, which was put on the optical microscope through a specially designed XY stage. Before force measurements, the cantilever with a nominal spring constant of 10 pN/nm functionalized with influenza A/X-31 was incubated in 5 mg/ml BSA for 30 min in order to minimize the non-specific interaction between the cantilever tip and the cell surface. The force measurements were performed in PBS buffer. After the cantilever tip approached to the cell surface, force distance curves were repeatedly measured with Z-scanning range of 2 µm, cycle duration of 0.5 - 8 s, 500 data points per curve, and typical force limit of about 40-70 pN.

2.2.19 Force Spectroscopy Data Analysis

Force-distance curves were analyzed using MatLab (MathWorks Inc.) and Igor Pro (Wavemetrics Inc.). The loading rates were determined by multiplying the pulling velocity with the effective spring constant k_{eff}, where k_{eff} is the slope of the force distance curve at rupture. In the single-barrier model (Evans and Ritchie, 1997), the most probable rupture force F is given as a function of the loading rate r:

$$F(r) = \frac{k_B T}{x_u} ln\left(\frac{r x_u}{k_{off} k_B T}\right) \tag{2.3}$$

Where k_B is the Boltzman constant, k_{off} is the dissociation rate constant of the complex without force and x_u marks the thermally averaged projection of the transition state along the direction of the force. The parameters x_u and k_{off} were determined by fitting the most probable rupture force F against the applied loading rate r.

3 Results

3.1 Single virus force spectroscopy (SVFS)

It was one of the main aims of this study to characterize the interaction between influenza A viruses and the cell surface at quantitative level. In order to minimally interfere with the structure of virus and cell, single molecule force spectroscopy was used as described in section 2.3. Applying this approach to single viruses provides the advantage to investigate virus-cell binding in a unique experimental set-up that mimics the situation on the cell surface very closely (single virus force spectroscopy).

3.1.1 SVFS using optical tweezers.

Preparation of virus coated beads

First, it was tried to manipulate single influenza A viruses using optical tweezers. Viruses were labeled with R18 as described in 2.2.5 and subsequently filtered using a 0.2 µm pore size filter. The virus suspension was diluted in PBS buffer and transferred to the optical tweezers device. After turning on the laser, the scattering signal was continuously recorded. As shown in Fig. 3.1 A, the lateral scattering signal indicates that successively viral particles entered the optical trap. In the following, two problems occurred. First, the viruses quickly adsorbed to the cover glass surface (Fig. 3.1 B). Second, it was not possible to control the accumulation of viruses and the calibration of the trap holding a single virus turned out to be inaccurate. Due to the mentioned difficulties the system was changed towards using spherical beads as virus carriers.
Polystyrene (PS) beads are frequently used as sample carriers in OT-based force spectroscopy experiments (Mameren et al., 2011) since proteins show fast and strong adsorption on PS surfaces (Sagvolden et al., 1999). PS beads with a diameter of 1.5 µm were prepared as described in section 2.2.16. At high concentration the virus particles adsorbed to the bead surface without visible gaps as observed by confocal microscopy (Fig. 3.1 C). To decrease the chance of multiple binding events the virus suspension was diluted before addition of the PS beads. The fluorescence per bead was visualized by confocal microscopy and quantified by flow cytometry (Fig. 3.1 D). Dilution of virus particles during the adsorption reduced the amount of bound virus

by up to 90 %. To fill the gaps between viruses, the beads were further incubated with BSA.

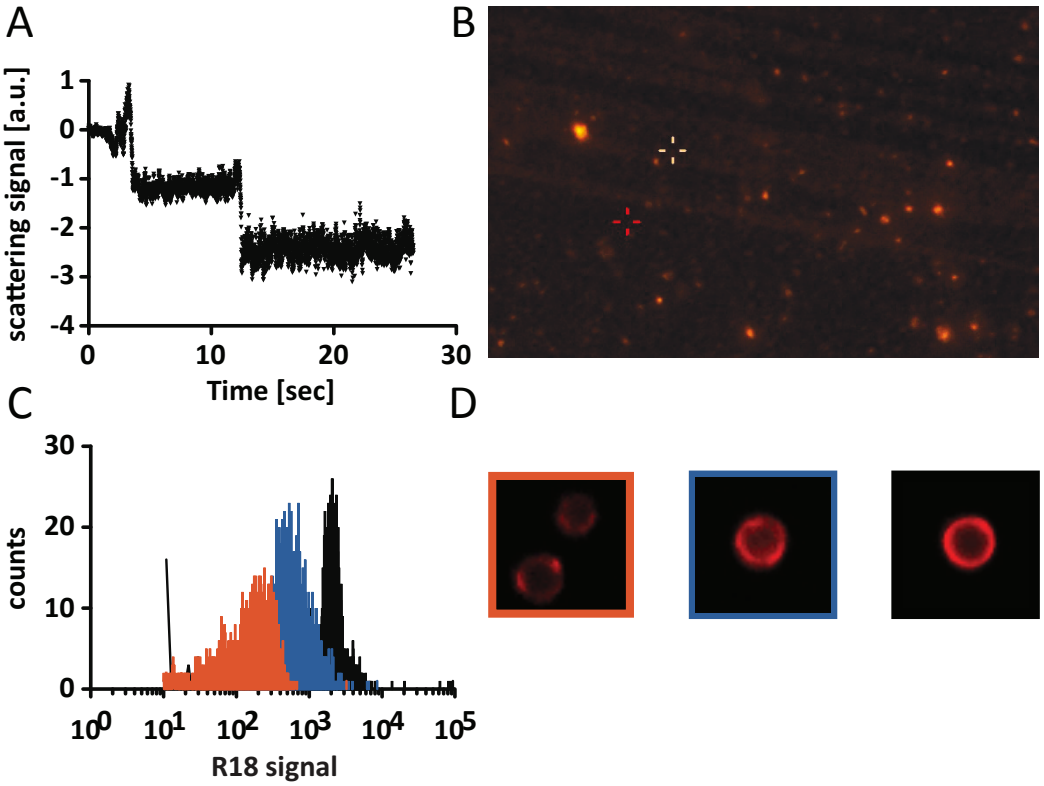

Figure 3.1: Trapping single influenza A viruses and preparation of virus-coated beads. (A) Influenza A/X-31 viruses were labeled with R18, filtered and transferred to the optical tweezers device. After turning on the laser, successively single virus particles entered the trap, which is indicated by a stepwise increase of the scattering signal. The trapped viruses could not be detected by eye or the installed CCD camera (B). The position of the first (red) and secondary (white) trap laser are marked by the corresponding crosses. In this study, only the primary laser trap was used. To improve the stability of the probe and to get an accurate trap calibration, viruses were adsorbed on PS beads at different concentrations. Beads (0.1 % solids) were incubated with 20, 5 and 0.2 µg/ml R18-labeled virus for 30 min at 4 C. The beads were pelleted and the coating was verified by confocal microscopy (D) and quantified by flow cytometry (C). The frame color corresponds to the respective histogram in C.

Single virus force measurements using optical tweezers

For force measurements, CHO and MDCK cells were seeded one day prior to the experiment at a density of 1-5 10^5 cells per petri dish. The cells were washed and kept in pre-warmed PBS at 37 C. The virus-coated beads were added directly to the buffer. By choosing a low cell density, it was assured that 80-90 % of the beads sedimented on the dish surface without direct cell attachment. In this way, the approach gave enough space to move a bead towards a target cell from each direction. Prior to the force distance cycles the beads were trapped and moved to

a position approx. 3-5 µm from the cell border. The distance and the speed were set and each force-distance cycle was repeated 1-5 times. Then the bead and the position on the cell was changed. Only very clear and sharp cell edges were selected to ensure that the bead was not in contact with filopodia or other cell extensions. The contact force was kept between 5-50 pN and the bead was retracted without delay to reduce the chance of multiple bindings.
Single and stepwise rupture events were detected which indicate unbinding of individual receptor-ligand complexes (Fig 3.2 A, B). For CHO cells in most cases rupture forces of 12 pN for a pulling velocity of 200 nm/sec were found. Very similar, for MDCK cells a maximum frequency for 10 pN at the same retraction speed was observed. In contrast to CHO cells, on MDCK cells a significant amount of rupture events at higher force values with a maximum at 23 pN where found (Fig 3.2 C). This force value likely corresponds to two simultaneously rupturing bonds. However, to increase the chance of single molecule interactions, CHO cells were used for all further optical tweezer measurements.
Virus-cell binding was further investigated after the cells were treated with neuraminidase (NA). After NA treatment, the size of the unbinding events was very similar compared to control cells while the binding probability was strongly reduced by 60 - 70 % of the control level. To obtain a force spectrum over a dynamic range, the pulling velocity v was varied between 0.5 - 10 µm/sec. Plotting the resulting loading rate against the measured most probable rupture force revealed a linear dependence (Fig 3.2 D). Considering the theory, this dependence indicates that a single energy barrier is crossed in the thermally active regime (see section 2.3). Accordingly, from the plot in Fig 3.2 D, the separation from the energy barrier x_u and the kinetic off-rate constant k_{off} can be determined by fitting the curve to Eq. 1.1. The obtained values are summarized in Table 3.1.

3.1.2 Single virus force measurements using AFM

Influenza viruses from two strains A/X-31 (H3N2) and A/WSN (H1N1) were covalently attached to AFM cantilevers using a bi-functional crosslinker as described in Rankl et al. (2008). CHO, MDCK and A549 cells were seeded in glass bottom petri dishes one day prior to the experiment. Suitable cells were localized using an inverted light microscope, the cantilever was moved above the cell and lowered until touching the plasma membrane. For all cell-virus combinations force distance curves were recorded at pulling velocities between 0.5 - 4 µm/sec to allow dynamic force spectroscopy analysis. Single and stepwise unbinding events were detected indicating the rupture of individual receptor molecules (Fig. 3.3 A, B). Increasing the pulling velocity led to an increase of the most probable rupture force with a linear loading rate dependence. Fitting the dynamic force spectrum to Eq. 1.1 revealed the kinetic off-rate constant and the separation of the bound state to the energy barrier. The obtained values are summarized in

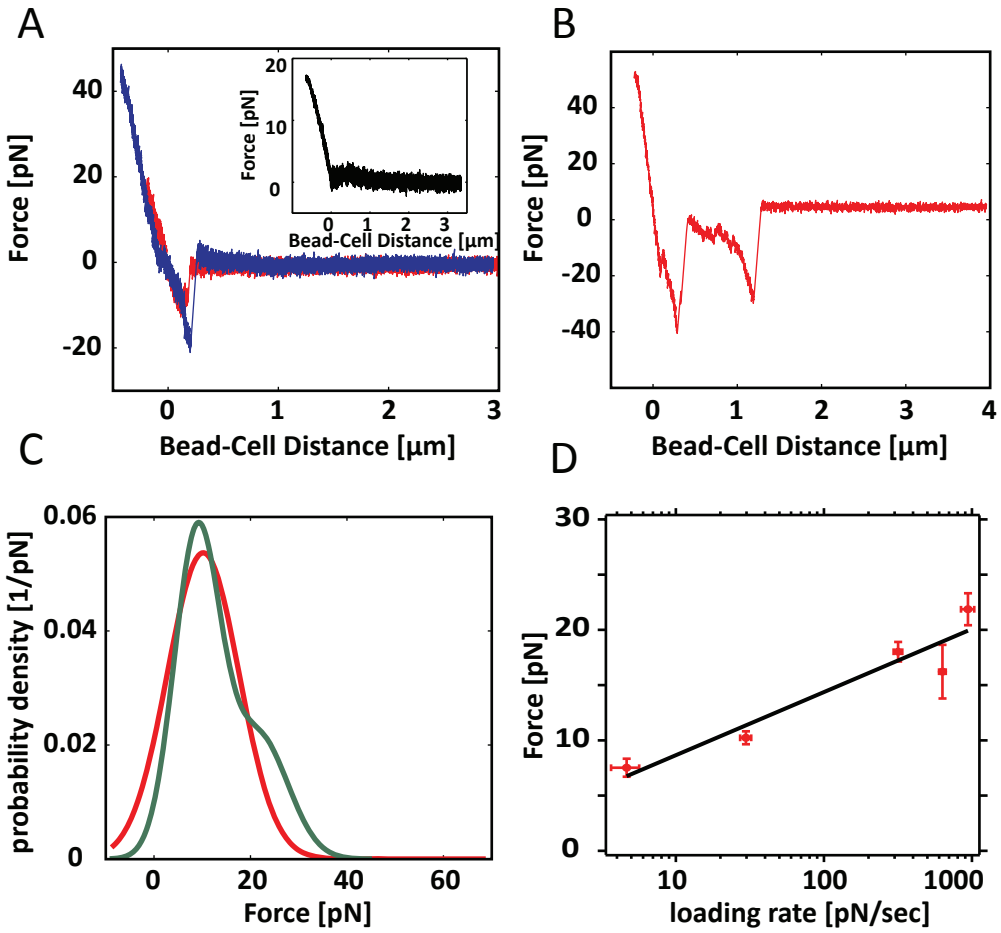

Figure 3.2: Single virus force spectroscopy using optical tweezers. Virus-coated beads were trapped and moved towards an adherent cell. The speed was set and each force-distance cycle was repeated 5-10 times. Single (A) and multiple (B) unbinding events were detected (only retract curves are shown). When the beads were blocked with BSA, no interaction was observed (A, inset). The most probable rupture force at a pulling velocity of 200 nm/sec shows a maximum at 10 pN for CHO (red) and MDCK cells (green). Remarkably, on MDCK cells a significant amount of rupture events happened at higher forces with a second maximum at 23 pN (C). Variation of the pulling velocity led to a full dynamic force spectrum with a linear dependence of the loading rate (i.e. the slope of the force curve before rupture) and the most probable rupture force. The data points were fitted to Eq. 1.1 and revealed the separation from the energy barrier x_u and the kinetic off-rate constant k_{off}. The obtained values are summarized in Table 3.1. Error bars account for the uncertainties in the determination of the spring constant and in finding the most probable rupture force.

Table 3.1.

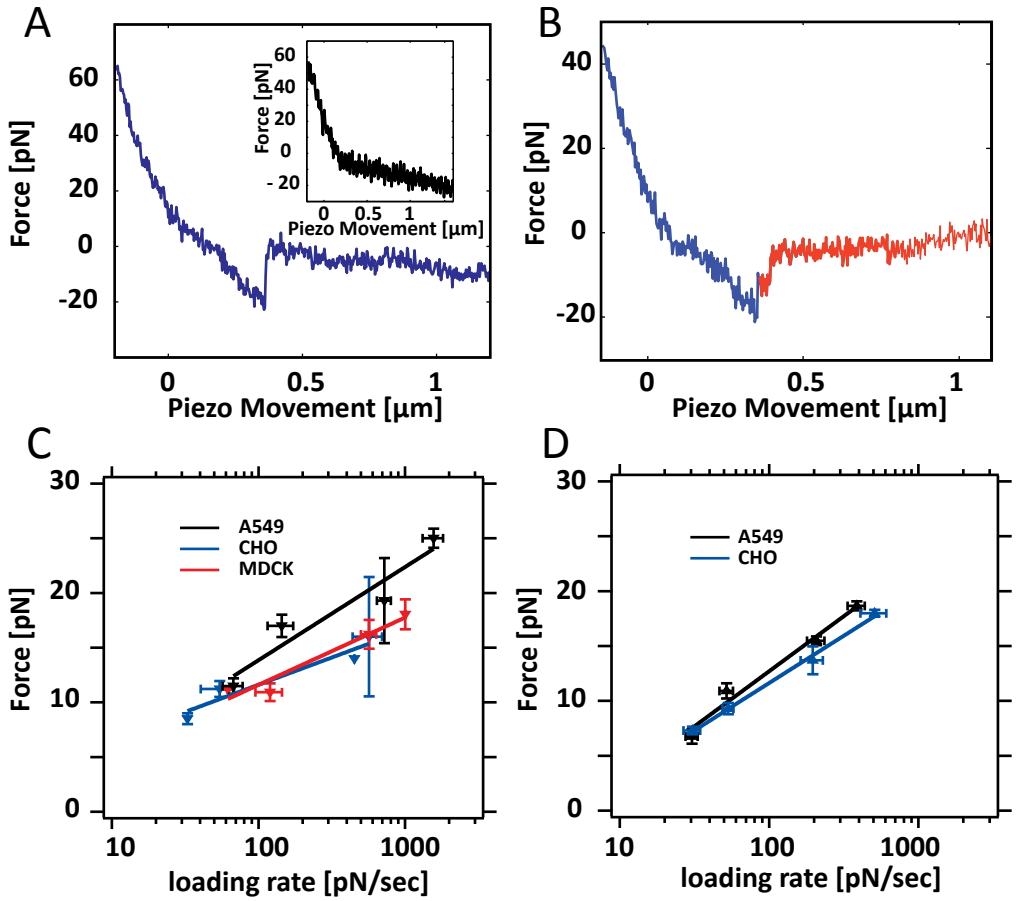

Figure 3.3: Single virus force spectroscopy using AFM. Viruses were covalently attached to AFM cantilevers as described in (Rankl et al., 2008). The cantilever was moved above a suitable cell, lowered and force distance cycles were recorded at various pulling velocities. Single and stepwise unbinding events were detected (A, B), which indicates rupture of individual bonds. Increasing the pulling velocity led to an increase of the most probable rupture force. Plotting the corresponding loading rate against the most probable rupture force revealed a linear dependence, which could be described by Eq. 1.1. Dynamic force spectroscopy was applied for influenza A/X-31 (H3N2) (C) and A/WSN (H1N1) virus strains (D) using the indicated cell lines. Error bars account for the uncertainties in the determination of the spring constant and in finding the most probable rupture force.

3.2 Whole cell-virus binding

Single virus cell binding was compared to binding on the macroscopic scale of the whole cell. Virus-cell binding was assessed using flow cytometric quantification of R18-labeled viruses. Viruses from both strains bound better to CHO cells compared to MDCK and A549 (Fig. 3.4).

Table 3.1: Results obtained by fitting SMFS data in Fig. to Eq. 1.1 k_{off}, kinetic off rate; x_u, separation between bound and unbound state; $_{off}$, bond lifetime

cell line	method	virus strain	$k_{off}(s^{-1})$		$x_u(nm)$		$_{off}(s)$
CHO	OT	H3N2	0.12	1.23	3.4	4.23	8.3
CHO	AFM	H3N2	0.18	0.17	2.6	3.11	5.5
A549	AFM	H3N2	0.64	0.52	0.42	0.41	1.6
MDCK	AFM	H3N2	0.45	0.35	0.84	0.79	2.2
A549	AFM	H1N1	1.22	0.32	0.18	0.06	0.8
CHO	AFM	H1N1	1.16	0.13	0.24	0.03	0.9

This interaction was dependent on SA and hence strongly reduced after NA treatment. Important to note is that the signal per cell was normalized to the cell surface, which was calculated from Casy counter cell diameter measurements. This allows to directly compare the three cell lines concerning virus-cell binding.

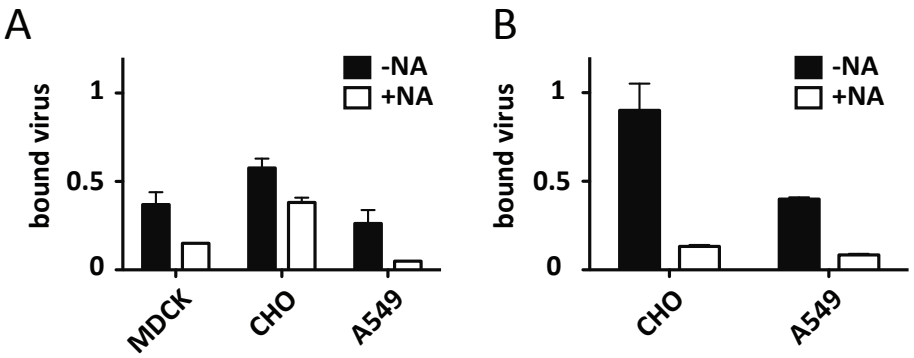

Figure 3.4: Fluorescence-based virus-cell binding assay. Influenza A/X-31 (A) and A/WSN (B) viruses were labeled with R18 and incubated with the indicated cells. Unbound viruses were removed by centrifugation and the amount of bound virus was determined by flow cytometry as the mean R18 signal per cell. The signal per cell was normalized to the cell surface, which was calculated from Casy counter cell diameter measurements. This allows to directly compare the three cell lines concerning virus-cell binding. Error bars correspond to SEM of three independent experiments.

3.3 Infection ef ciency of influenza A/X-31 viruses in A549, CHO and MDCK cells

A successfully infecting virus must enter its host cell by endocytosis, fuse with the endosomal membrane and deliver its genome. To find out if the initial virus-cell binding correlates with the infection efficiency, different cell lines where incubated with influenza A/X-31 viruses and infection was detected using anti-NP immunostaining. The NP signal per cell was visualized by confocal microscopy and quantified by flow cytometry (Fig. 3.5). At a MOI of 10-20, 5 h post-infection 90 % of MDCK cells were infected displaying strong nuclear anti-NP signal. The infection was lower in CHO cells and reached only 65 %. The lowest infection was detected in A549 cells, where only 22 % of the cells where infected.
In a competition experiment MDCK and CHO cells were mixed and seeded at 2 different ratios in the same dish and subsequently infected with influenza A/X-31. Successful infection was detected by immunostaining of NP. This was done to directly compare the infection efficiency of two cell lines with different SA-coupled receptors on their plasma membrane in the same sample. Fig.3.6 shows confocal micrographs of two cell ratios: MDCK:CHO of 2:1 (upper row) and 1:3 (lower row). In order to discriminate between the two populations, the cells were stained with the fluorescent lectin SNA-FITC, which binds -2,6-linked SA. This carbohydrate is not present on CHO cells and thus only MDCK cells were labeled and can be discriminated. Between 60 - 80 % of MDCK cells were infected in both samples. In contrast, CHO cells were infected to a much lesser extend of only about 10 - 20 %, which corresponds to less infected cells than in the experiment with only one cell line (Fig. 3.5). This experiment verifies that although CHO cells bind more viruses than MDCK cells, their infectivity is strongly reduced and that this effect is still present and even more pronounced when both cells grow side-by-side.

3.4 Cell surface topography and sialic acid composition of A549, CHO and MDCK cells

Influenza A viruses have a certain receptor specificity, which is determined by the amino acid composition of the receptor binding site (see 1.1.3). Human and avian type receptors are composed of sialic acid coupled to lactose (sialyllactose). While within the human type receptor both sugars are connected via a -2,6 glycosidic linkage, in the avian type a -2,3 glycosidic linkage is existent. To characterize the used cell lines concerning their surface SA composition, specific fluorophore-conjugated lectins were used to discriminate between -2,6 and -2,3 connected SA. The cells were labeled with fluorophore-conjugated WGA (binds all SA), SNA (-2,6) and MAA (-2,3) to quantify the overall amount of SA on the cell surface as well as to characterize

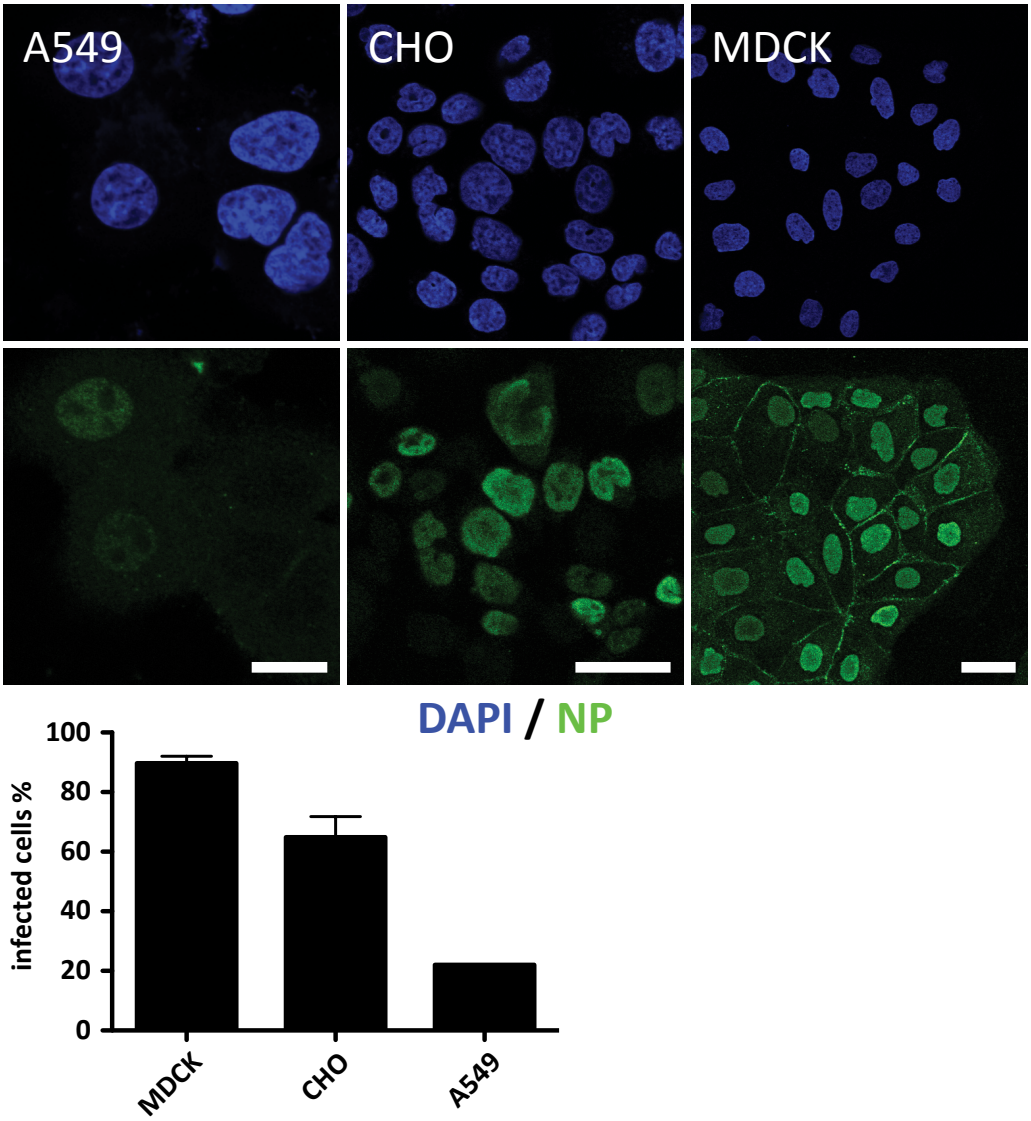

Figure 3.5: Infuenza A/X-31 infection efficiency of A549, CHO and MDCK cells. The efficiency of influenza A/X-31 virus to infect different cell lines was measured by immunostaining of the viral NP. Cells were infected at a MOI of 10-20 and stained 5 h post-infection. The production of viral NP was visualized by confocal microcopy and quantified by flow cytometry. Cells with a NP signal above the background fluorescence were considered as infected. Scale bar 10 µm. Error bars correspond to SEM of three independent experiments.

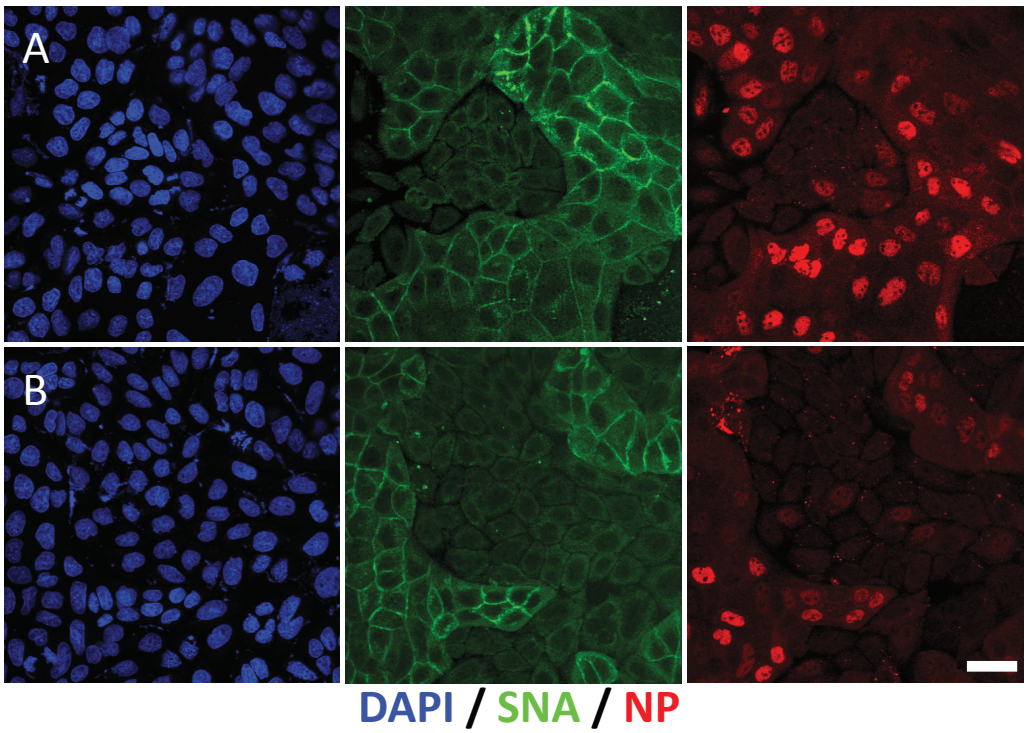

Figure 3.6: Infuenza A/X-31 infection efficiency of CHO and MDCK cells growing side-by-side. The efficiency of influenza A/X-31 virus to infect CHO and MDCK cells growing side-by-side was measured by immunostaining of the viral NP. Two different MDCK:CHO ratios of 2:1 (A) and 1:3 (B) were used. Cells were infected at an MOI of 10-20 and stained 5 h post-infection. The cells were co-stained with the fluorescent lectin SNA-FITC, which marks -2,6-linked SA. Since CHO cells do not express this particular glycan, only MDCK cells were labeled and could be discriminated. Scale bar 30 µm.

the specific SA linkage. The cells were analyzed by confocal microscopy and flow cytometry. Fig. 3.7 shows confocal micrographs of A549, CHO and MDCK cells stained with either WGA or MAA and SNA. While A549 and MDCK cells present both types of SA linkage, CHO cells only present -2,3 linked SA. The flow cytometric analysis of the WGA signal shows that all three cell lines possess equal amounts of surface sialic acid (Fig. 3.8A). Because CHO cells (diameter 13 µm) are much smaller than MDCK (diameter 19 µm) and A549 cells (diameter 20 µm), to get information about the SA surface density, the fluorescence signals were normalized to the cell surface.
Flow cytometric analysis of SNA/WGA labeling confirmed the microscopic observations that A549 and MDCK cells present both types of SA linkage while CHO cells do not present -2,6 linked SA (Fig. 3.8). The surface sialic acid content was assessed after treating the cells with neuraminidase from *Clostridium perfringens*, an enzyme which hydrolyzes -2,6 as well as -2,3 glycosidic linkages of terminal sialic acid residues. Treating the cells with NA reduced the amount of surface sialic acid by 50 - 90 % on all three cells lines. Further, NA treatment reduced both SNA and MAA signals, indicating that both types of SA linkage where cleaved (Fig. 3.8B).

The cellular topography was analyzed by scanning electron microscopy (SEM)[1]. Fig. 3.9 and 3.10 show SEM micrographs of A549, CHO and MDCK cells at 2 different confluency states. In Fig. 3.9 the cells were analyzed at low confluency of 50 - 70 %. A549 and MDCK cells appear very flat, while CHO cells have a higher curvature. All cell lines already display a high amount of cellular protrusions (microvilli), which vary in number and size. On A549 and CHO cells about 1-5 microvilli per μm^2 were counted. These have a length of 0.5-1 µm and are 100 nm in diameter. In contrast, on MDCK cells 5-10 microvilli with length of 0.2-0.5 µm and a diameter of 100 nm were detected per μm^2. The cells in Fig. 3.10 were imaged at full confluency. The size of microvilli is similar compared to low confluent cells, but the number increases for A549 and MDCK cells. On A549 cells 5-10 and on MDCK cells 10-20 microvilli are visible per μm^2. Interestingly, MDCK cells form a compact cell layer in which individual cells are hardly visible. A549 cell grow dense, but with space between individual cells. CHO cells loose shape and grow on top of each other.

3.5 Conclusions from 3.1 - 3.3

The interaction of influenza viruses with the plasma membrane of living cells was characterized on the level of single molecules as well as on the whole virus-cell level. By choosing cell lines with different SA repertoire on their surface, it was possible to study virus binding to human

[1] SEM sample preparation and image acquisition were conducted by Katharina Horst during her BA work under my supervision in the lab of Dr. Maik Lehmann.

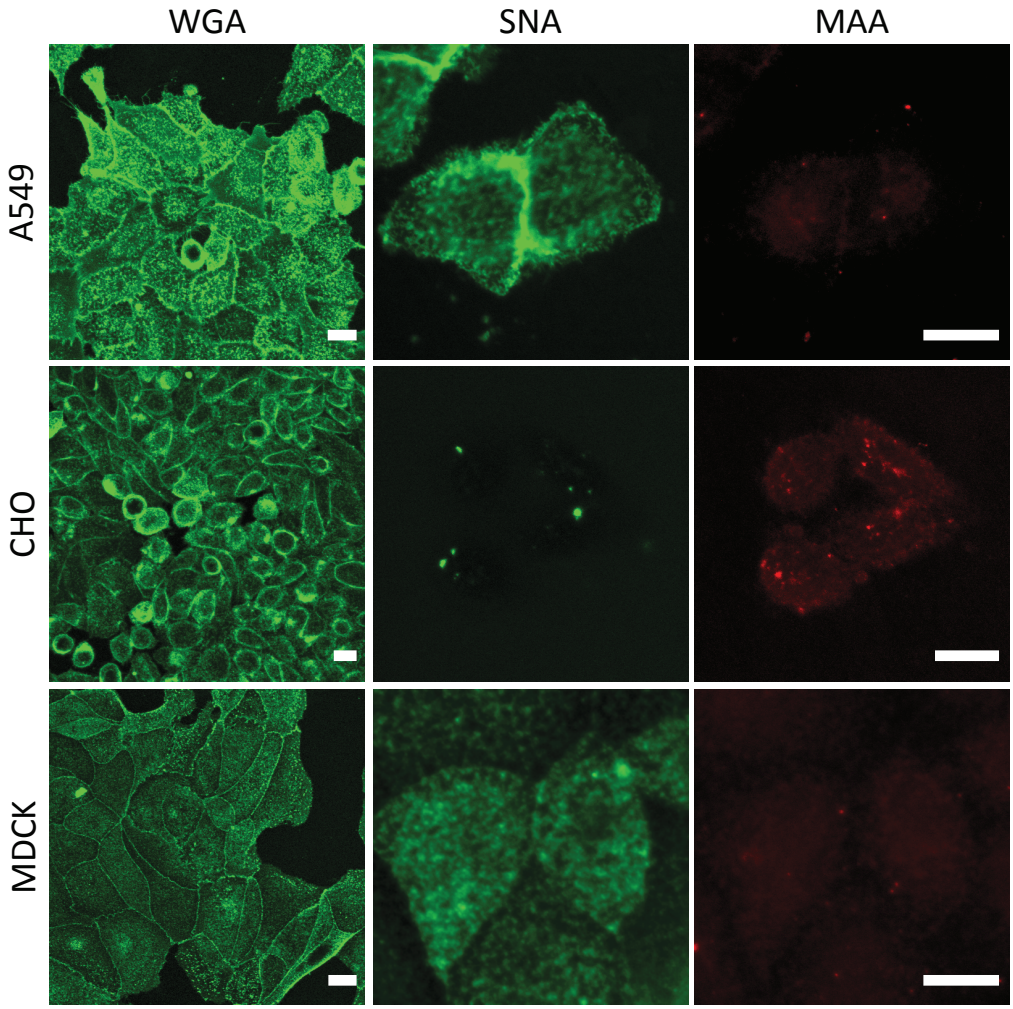

Figure 3.7: Confocal microscopy of lectin binding to A549, CHO and MDCK cells. A549, CHO and MDCK cells were washed in PBS and incubated with the fluorescent lectins FITC-WGA (40 µg/ml), Rho-MAA (50 µg/ml) or FITC-SNA (10 µg/ml) for 20 min on ice. The cells were washed with PBS and analyzed by confocal microscopy. All used cell lines present a high degree of sialic acid. A549 and MDCK cells feature -2,6 as well as -2,3-linked SA on the cell surface. In contrast CHO cells exclusively present -2,3 linked SA. Scale bar 10 µm.

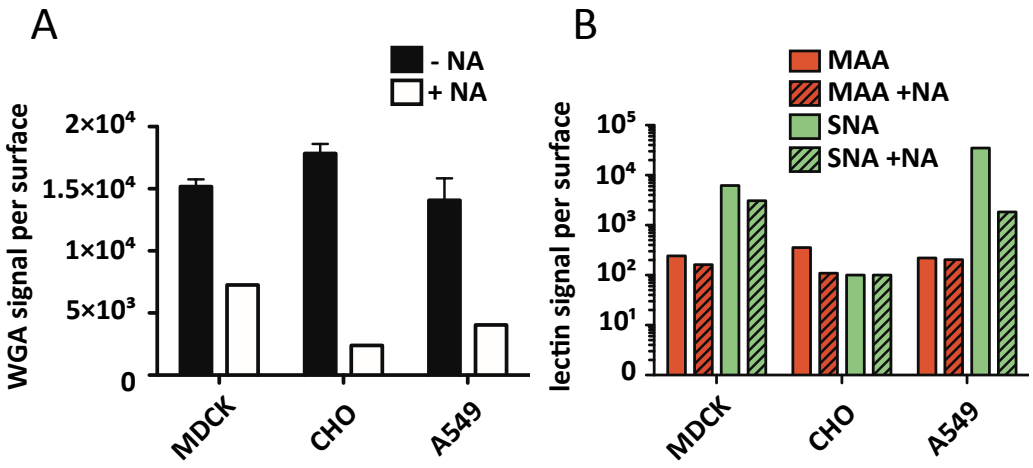

Figure 3.8: Flow cytometric quantification of lectin binding to A549, CHO and MDCK cells. A549, CHO and MDCK cells were detached from the culture flask surface using PBS -/- supplemented with 2 mM EDTA. The cells were washed in PBS and incubated with the fluorescent lectins FITC-WGA (40 µg/ml), Rho-MAA (50 µg/ml) or FITC-SNA (10 µg/ml) for 20 min on ice. The cells were washed in PBS, pelleted (2000 g, 5 min) and resuspended in 300 µl PBS buffer and immediately analyzed by flow cytometry. Error bars correspond to SEM of three independent experiments.

and avian type receptors. The used influenza virus strains A/X-31 and A/WSN did not exhibit a strong receptor specificity in SVFS, meaning they did not favor binding to either the human or avian type receptor. Further, the single SA-HA interaction was found to be very weak. Therefore, virus-cell binding probably depends on multiple simultaneous interactions. This binding mode provided the basis for the design of a variety of multivalent SA-functionalized nanoparticles made to mimic the cell surface to efficiently prevent virus-cell binding. Due to the small differences in preferential virus binding, the nanoparticles were coated with SA without additional carbohydrates. Furthermore, due to the unnatural linkage this approach has the advantage that SA can not be cleaved by viral NA. In the next section the results of influenza virus activity measurements under the influence of multivalent nanoparticles are described.

3.6 Inhibition of influenza virus activity using multivalent nanoparticles

Two species of particles were utilized as summarized in 2.1.5. Organic polyglycerol (PG) particles were used at two size ranges of 3 nm (PG 1-3) and 50-70 nm (PG 4-5) as well as varying SA surface content (see Table 2.1.5). As a second nanoparticle system, gold colloids with a diameter of 2 and 14 nm coated with SA were used. The particles were tested for their ability to bind HA and to inhibit HA-associated events during influenza virus infection. The results are

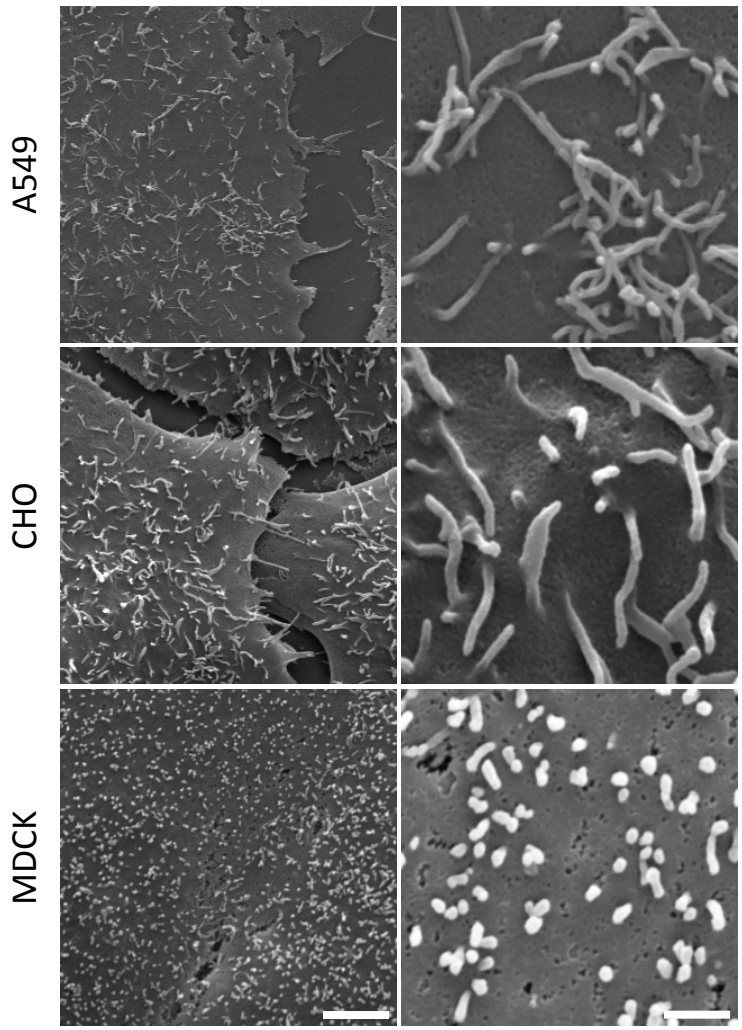

Figure 3.9: Scanning electron microscopic analysis of the cellular topography of A549, CHO and MDCK cells at low confluency. Approximately 5 10^5 A549, CHO and MDCK cells were seeded in glass bottom petri dishes. After 24 h the cells had reached 50-70 % confluency. The cells were washed three times in PBS and incubated in fixation buffer for 30 min. After another 3 washing steps in PBS the cells were prepared and analyzed by SEM. Scale bar 5 µm (left) and 1 µm (right).

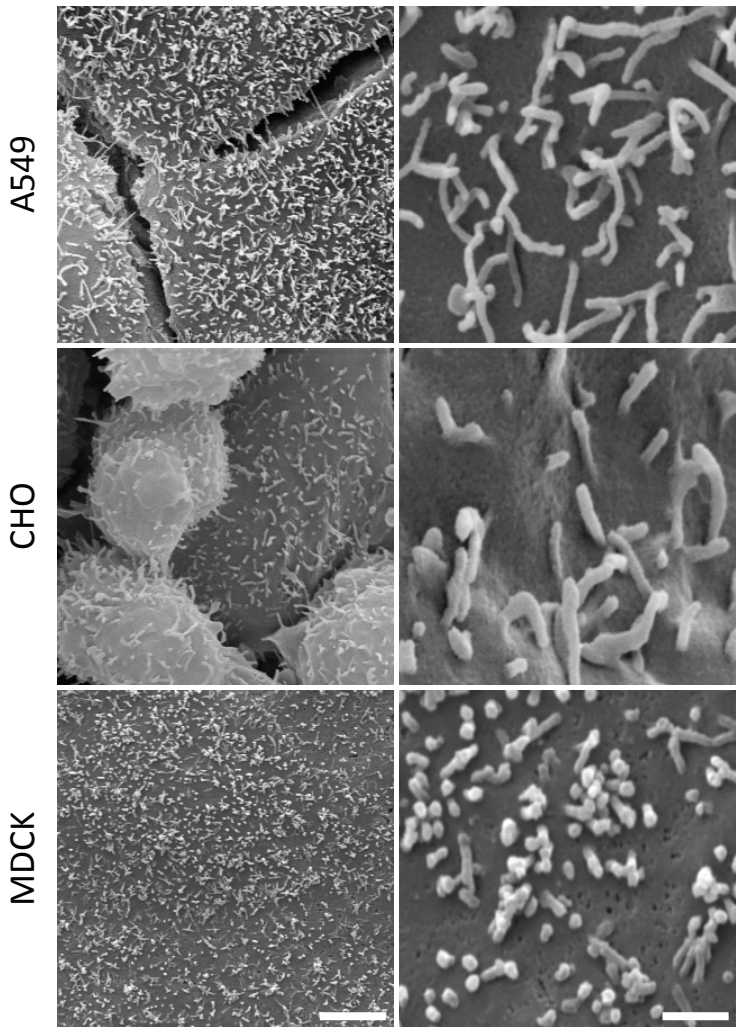

Figure 3.10: Scanning electron microscopic analysis of the cellular topography of A549, CHO and MDCK cells at full confluency. Approximately 5 10^5 A549, CHO and MDCK cells were seeded in glass bottom petri dishes. After 24 h the cells had reached full confluency The cells were washed three times in PBS and incubated in fixation buffer for 30 min. After another 3 washing steps in PBS the cells were prepared and analyzed by SEM. Scale bar 5 µm (left) and 1 µm (right).

illustrated in the next section.

3.6.1 Inhibition of influenza virus activity using multivalent polyglycerol (PG) particles

Inhibition of virus-cell binding

First, the ability of the PG constructs to act as competitive inhibitors of virus-erythrocyte binding was investigated. To this end, R18-labeled viruses and washed human erythrocytes were incubated for 30 min before unbound virus was removed by centrifugation. The amount of bound virus per erythrocyte was quantified by flow cytometry as the mean R18 intensity per cell. To study the inhibitory activity of PGs, viruses were pre-incubated with PGs 1-5 (see Table 2.1.5) in varied concentrations. Fig. 3.11A summarizes the results of binding experiments. To express the effect of multivalency, monovalent SA was used as an inhibitor reference in all experiments. Accordingly, the amount of PGs is expressed as concentration of SA equivalents. The monomeric SA had no effect on viral adhesion between 400 μM and 4 mM. In contrast, pre-incubation of influenza virus with sialic acid functionalized PGs 1-3 led to a strong reduction of the fluorescence signal per erythrocyte. Binding was inhibited to 50 % of the control level at approximately 3 mM PG but significant reductions in virus binding were only observed above 1 mM. There was no strong difference between PGs 1-3 with varied degrees of functionalization. The distribution displays a rather linear dependence of SA concentration at least in the studied range. On a per sialic acid basis, PG 4 (dF 12 %) reached 50 % inhibition already at concentrations 40-fold lower than the small PGs. This leads to a markedly exponential increase in binding strength with greater particle size and number of multivalent binding units. In comparison, PG 5 (dF 80 %) showed weaker binding and did not reach 50 % inhibition in the used concentration range. Notably, the sulfated PG had only a minor inhibitory effect at concentrations above 1 mM, emphasizing the importance of SA as a specific ligand for HA.

Inhibition of HA-mediated virus-cell fusion

The ability of influenza A/X-31 virus to undergo fusion was investigated using fluorescence de-quenching of R18 upon fusion of labeled viruses with erythrocyte ghost membranes.
Viruses were labeled with R18 at self-quenched concentration, bound to RBC ghosts and fusion was triggered by addition of citric acid (0.2 M). The results are presented in Figure 3.11 B. The monomeric form of SA had a small effect on the fluorescence de-quenching and reduced the extent of fusion by 15 % at the highest measured concentration of 4 mM. However, all tested sialic acid functionalized polymers had a more pronounced effect on virus fusion. PGs 1-3 reduced the extent of fusion to 35 % at 4 mM sugar equivalents; 50 % inhibition was achieved

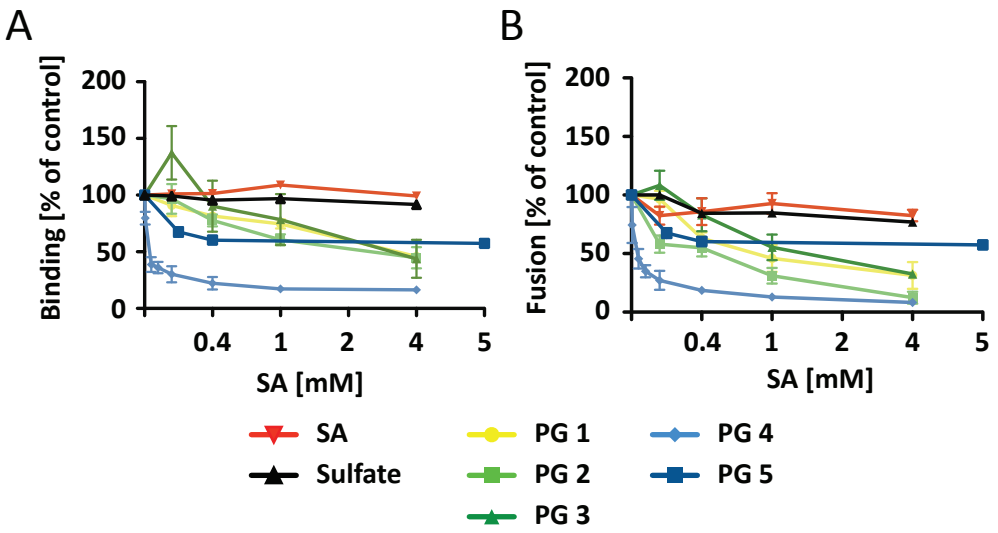

Figure 3.11: Fusion and binding efficiency of influenza A/X-31 virus after pre-incubation with multivalent PG inhibitors. Relative binding (A) and fusion (B) efficiency of X-31 virus to human red blood cells dependent on the inhibitor concentration. Viruses were pre-incubated with the indicated inhibitor concentration (SA equivalents) for 30 min at RT and subsequently used for binding and fusion quantification. Error bars correspond to SEM of three independent experiments.

at approximately 2 mM sugar equivalents. No significant differences were observed within the small PG series 1-3, which differ only by their dF. Similar to binding inhibition, PG 4 was most effective, causing almost total inhibition at 4 mM SA equivalent concentration; 50 % inhibition could be achieved below 100 µM. On a per sugar basis, PG 5 was found to be approximately 20-fold more effective than the small PG series at causing 50 % inhibition. Again, the sulfated polymer showed no effect.

Notably, the fusion assay reflects the fusion of all bound viruses whose number was also strongly reduced (Fig. 3.11 B). For instance, PG 5 reduced the binding by 40 % at 1 mM. The same concentration reduced the fusion by 20 %. This means that only 50 % of the viruses were able to bind and fuse for this particular case.

Inhibition of infection

For a successful infection, the virus has to enter via endocytosis and deliver its genomic material after fusion with the endosomal membrane. To investigate if the PG polymers have an impact on infectivity, unlabeled viruses were incubated with different amounts of polymers and exposed to MDCK cells at a multiplicity of infection (MOI) of 25. The production of viral proteins is a clear sign for a successful infection. Accordingly, the production of viral NP was assessed by immunofluorescence microscopy and flow cytometry using anti-NP antibodies. Using both

techniques, six hours post-infection NP protein signal could be detected in 80-90 % of the cells which indicates a positive infection (Fig. 3.12 A). At this stage of infection a strong nuclear and some cytoplasmic signal was observed. Compared to the background fluorescence of uninfected cells, this allowed a clear identification of infected cells. Using viruses treated with 1 mM PG 3, NP signal was detected in 20 % less cells compared to the control (Fig. 3.12 B). At a concentration of 1 mM PG 4, the amount of infected cells was even reduced to 20 % of the control level. An increase of the concentration to 4 mM led only to a small increase of inhibition (15 % of control level). The fluorescence per cell was quantified by flow cytometry and allowed to deduce the infection level (Fig. 3.12C).

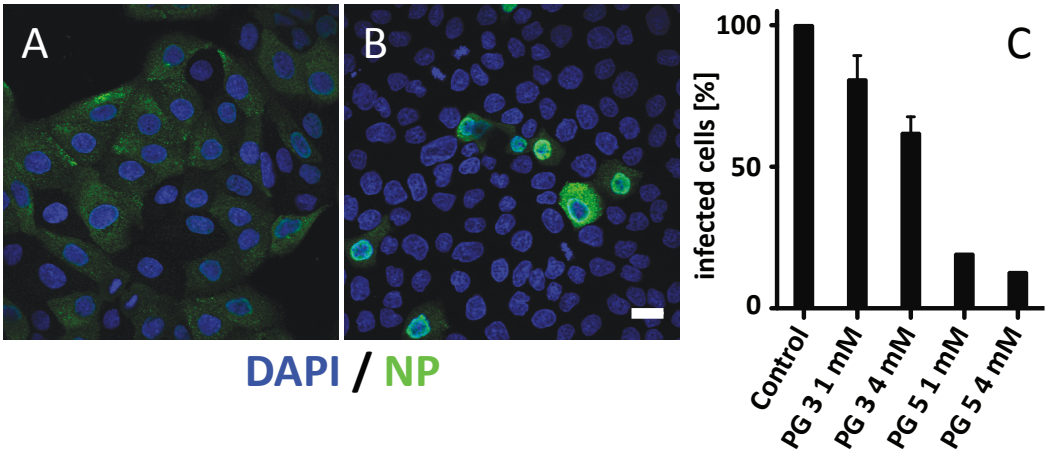

Figure 3.12: Infection efficiency of influenza A/X-31 virus after pre-incubation with multivalent PG inhibitors. MDCK cells were infected with influenza A/X-31 virus without (A) and after pre-incubation with 4 mM PG 4 (B). Positive infection was detected by immunostaining of the viral NP. The production of viral NP was visualized by confocal microcopy and quantified by flow cytometry (C). Cells with a NP signal above the background fluorescence were considered as infected. Scale bar 10 µm. Error bars correspond to SEM of three independent experiments.

Cell viability after treatment with SA-conjugated polyglycerol particles

The cell toxicity is an important parameter within the evaluation of synthetic antiviral test substances. To verify that the used polyglycerol particles are biocompatible, the cell viability was assessed after treating the cells with different concentrations of SA-conjugated polyglycerols as well as monomeric sialic acid. As shown in Fig. 3.13, the cells were treated with 4 and 1 mM PG (SA concentration) as well as monomeric SA. 4 mM PG reduced the cell viability by 20%. Interestingly, the same concentration of monomeric SA led to an increase of the signal. The lower 1 mM concentration of SA-PG, SA and the control polymer (PM OH) had only very little effects on cell viability.

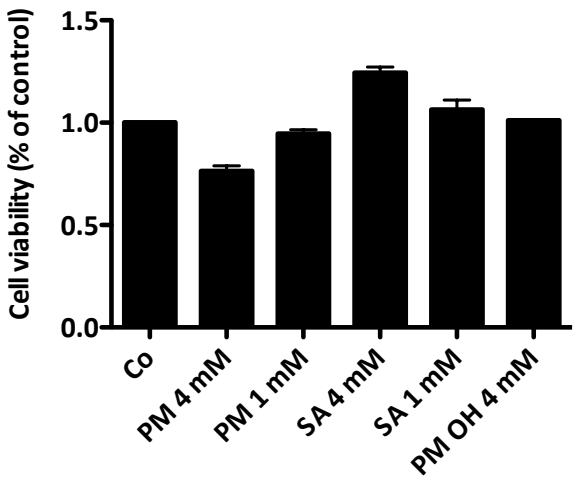

Figure 3.13: Cell viability after treatment with PGs and monovalent SA. MDCK cells were incubated with SA-conjugated polymers, OH-precursor polymer and monovalent SA. After 4 hours, the cells were treated with Celltiter Blue for an additional hour before the cell viability was fluorometrically quantified via the metabolically produced resorufin as described in 2.2.2. Error bars correspond to SEM of three independent experiments.

3.6.2 Inhibition of influenza virus activity by multivalent sialic acid functionalized gold particles (AuNP)

In a second nanoparticle-based approach, gold was used as a carrier for sialic acid, which was attached via thiol-coupling as a dendrimer with four terminal SA moieties (Papp et al., 2010).

Due to the strong interference of gold particles with organic fluorophores (Schneider et al., 2006; Hazarika et al., 2006), it was not possible to use the R18-based binding assay described before. Therefore, the ability of influenza virus to bind target membranes was tested by measuring the virus-induced agglutination of red blood cells (HAI). HAI is a widely used method to evaluate inhibitors of influenza virus binding. The assay measures the lowest concentration of inhibitor that still prevents hemagglutination which is defined as K_{HAI}.

Unlabeled influenza A/X-31 viruses were mixed with 2-fold dilutions of AuNPs and allowed to pre-incubate for 30 min at RT. RBCs were added and the system was incubated for another hour at RT. SA conjugated AuNPs inhibited hemagglutination at K_{HAI} in the nM range (Fig. 3.14). In contrast, the 2 nm particles had no effect on virus-induced agglutination of RBCs. This demonstrates that the potential of multivalent inhibitors clearly depends on the particle radii and thus on the spacial distribution of the interacting ligand/receptor pairs.

To test whether AuNPs directly bind to HA, HA coupled to a yellow fluorescent protein (HA-YFP) was expressed in CHO cells. Gold nanoparticles quench organic fluorophores by a mechanism that is not yet fully understood (Schneider et al., 2006; Hazarika et al., 2006). AuNPs

($\approx 0\ 5M$) were mixed with $5*10^5$ HA-YFP expressing cells and incubated for 30 min. The overall YFP emission was measured in a fluorescence spectrometer between 500 and 600 nm (λ_{ex} = 490 nm). Without washing the YFP emission was reduced by $\geq$ 60 % (Fig. 3.15 A). If the complex was washed once in PBS after the first incubation only 20 % reduction were achieved (Fig. 3.15 B). As a negative control, the same experiment was done using the hydroxylated control AuNP. Here, the YFP emission was reduced only by 5 and 10 % respectively, which indicates specific binding of SA-AuNP. However, since the effect was strongly reduced upon washing the cells in buffer, the binding seemed to be weak.

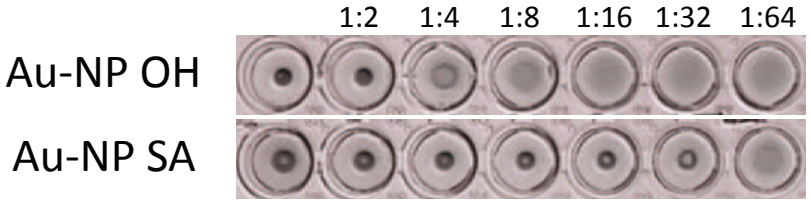

Figure 3.14: Inhibition of hemagglutination (HAI) by influenza A/X-31. The virus was pre-treated with SA- and control OH-AuNPs for 30 min before addition of RBCs. AuNPs were sequentially diluted by a factor of 2 in PBS. If agglutination was inhibited, the RBCs sedimented to the bottom of the well and formed a pellet (see Fig. 2.1). Otherwise, they were crosslinked by the virus particles and formed a gel.

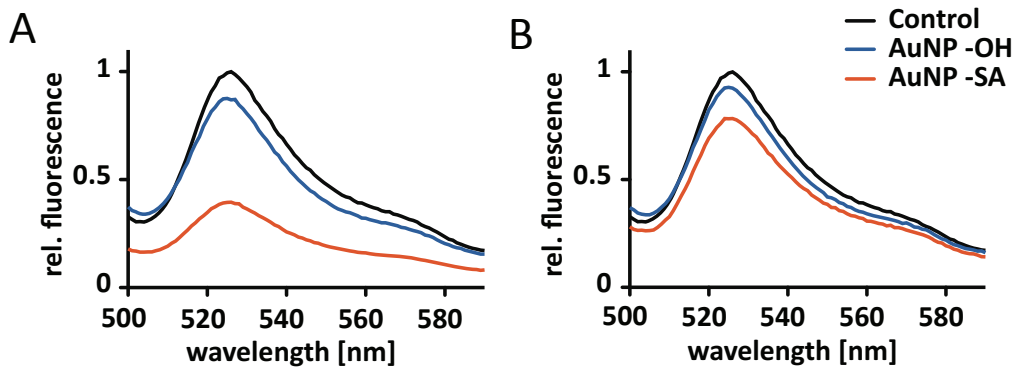

Figure 3.15: Fluorescence emission spectra of HA-YFP transiently expressed in CHO cells. Cells expressing HA-YFP in suspension were mixed with SA- and OH- conjugated AuNPs. Emission spectra were recorded directly after 30 min incubation time (A) and after an additional washing step (B) at λ_{ex} = 490 nm between 500 and 600 nm.

One advantage of using gold as a carrier is the strong contrast in transmission electron microscopy (TEM). From the size of the particles one can deduce a possible binding mode. Regarding the diameter of an HA trimer (7 nm), the 2 nm particles can only bind to one trimer. The larger 14 nm particles can presumably bind to more than one trimer. In order to test this

binding hypotheses, both SA-conjugated AuNP species were used for binding studies and subsequent TEM visualization [2]. To avoid the influence of negative staining chemicals on binding, cryogenic-TEM was used for the visualization of AuNP binding. In this approach the sample is vitrified using liquid ethane. Figure 3.16 shows influenza A/X-31 viruses incubated with 2 nm SA AuNPs. Due to the similar size of the HA trimers seen from above, the particles are only clearly detectable in the side view projection (Fig. 3.16 B, arrows). In contrast, the larger 14 nm particles can easily be identified and show binding of multiple HA trimers. This verifies the previously concluded binding architecture and might explain why 2 nm particles are not able to inhibit hemagglutination.

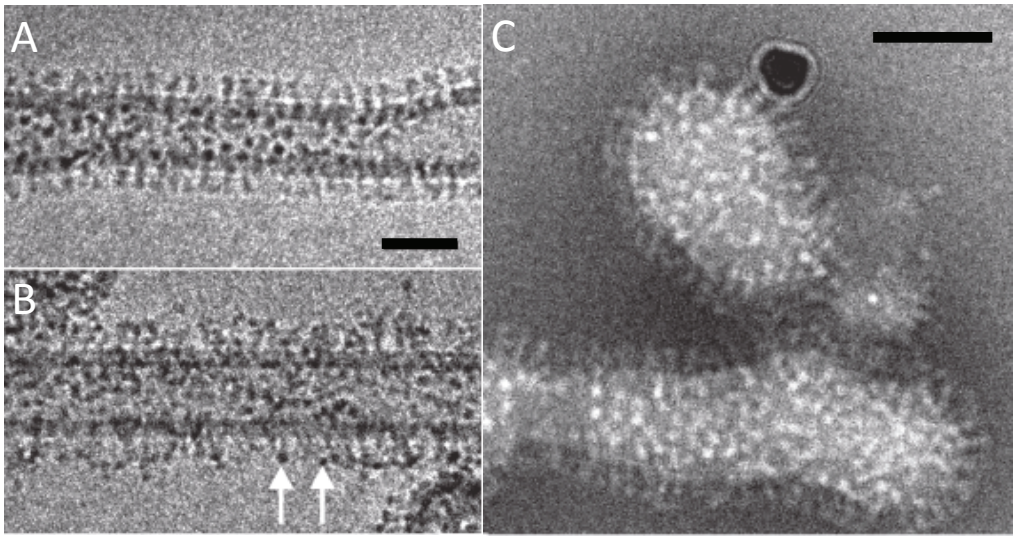

Figure 3.16: Cryo-TEM visualization of AuNP binding to influenza A/X-31. 2 and 14 nm SA-conjugated AuNPs were incubated with influenza A/X-31 virus for 60 min at RT and then prepared for cryo-TEM. The 2 nm particles are only visible in side view projections. In contrast, the 14 nm particles can be easily identified. Both particle types bind to the used influenza A/X-31 virions. Scale bar 50 µm.

Finally, the ability of AuNPs to inhibit viral infection was tested. The virus was pre-incubated with SA- and control-AuNPs for 30 min. Subsequently, the virus was exposed to adherent MDCK cells at a MOI of 10-20 at 37 C. Five hours post-infection, the cells were fixed and immunostained against viral NP to measure the extent of successful infection. The expression of viral NP was quantified by flow cytometry. 80 - 90 % of the control cells (absence of AuNPs) showed an increased NP signal indicating successful infection (Fig. 3.17). The virus incubated with SA-AuNP reduced the infection by 40 %, while the control OH-AuNP led only to a reduction of 20 %.

[2] Cryo-TEM sample preparation and image acquisition were performed by Dr. Kai Ludwig, Research Center of Electron microscopy, Freie Universität Berlin.

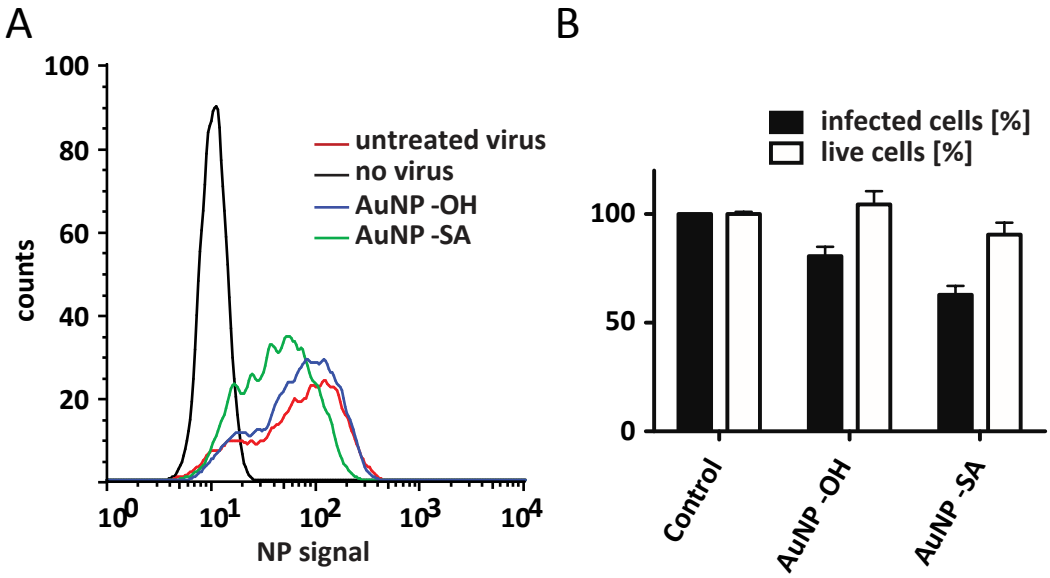

Figure 3.17: Infection efficiency of influenza A/X-31after pre-incubation with AuNPs. Cell viability in the presence of AuNPs. Influenza A/X-31 viruses were pre-incubated with SA- and OH-conjugated AuNPs and applied to MDCK cells. The cells were fixed and stained for viral NP 5 h post-infection. The NP signal per cell was quantified by flow cytometry (A). While the negative control shows the background fluorescence, the positive control includes cells infected with untreated virus. Cells with a NP signal above the background fluorescence were considered as infected (B). Cell viability was measured using PI staining (B). Error bars correspond to SEM of two independent experiments.

It was essential to examine the cell toxicity of the used AuNPs. MDCK cells were incubated in the presence of AuNPs for six hours. The cells were detached and labeled with the DNA-intercalating fluorescent dye, propidium iodide (PI) which is membrane-impermeable and hence excluded from vital cells. In contrast, injured and dead cells become efficiently stained by the probe as indicated by an intense fluorescence signal. Figure 3.17 B shows that the cell viability was maintained close to 100 % compared to the untreated control cells.

3.6.3 Conclusions from 3.6

The previous section described how synthetic particles mimicking the cell surface in terms of sialic acid presentation can efficiently prevent virus-cell interaction. Differently sized particles with diverse degrees of functionalization were tested and showed that both parameters indeed play a pivotal role in virus binding. While the degree of functionalization does not play an apparent role for small particles, it becomes much more important when the particles get in the size range of the virus. The presented PGs with sizes similar to that of the virus inhibit its activity *in vitro* by 80%. However, in the presence of inhibitory nanoparticles, viruses were still able to infect cells. In the next section the first steps of influenza A virus cell infection starting from virus entry were studied in order to characterize this fundamental phase of infection and identify possible points for targeted antiviral strategies.

3.7 Intracellular traf cking and fusion of influenza A virus in MDCK cells

3.7.1 Influenza A/X-31 virus is rapidly transported within the endo-/ lysosomal degradative pathway

Upon endocytosis, influenza A virus is rapidly transported to early endosomal compartments. To visualize the time scale of these events, MDCK cells were transfected with endosomal marker proteins. The small GTPases Rab5 and Rab7 are well characterized markers for early and late endosomes respectively (Huotari and Helenius, 2011). Early endosomes associate only with Rab5. During the endosomal maturation, Rab5 and its effectors are replaced by Rab7, which is then present on late endosomes and lysosomes. Since this is a gradual process, intermediate/maturing endosomes (ME, multivesicular bodies) carry both proteins.
MDCK cells were transfected with Rab5-GFP and Rab7-CFP 16 h prior to the experiment. To simultaneously follow the viruses, their viral envelope was labeled with R18. Figure 3.18 shows a timeline of the intracellular virus transport. Upon internalization, the virus reaches early endosomes after about 5 min. At 10 min, the virus-containing endosomes show already Rab7 signal

which indicates ME localization. The viruses co-localize with both Rab proteins until 30 min. As previously shown, a gradual decrease of Rab5 goes along with a gradual increase of Rab7 (Rink et al., 2005). In addition, a gradual increase of the endosome size was observed. After 30 min the virus-containing endosomes show only Rab7 signal. Taken together, these results show that the virus is rapidly transported after internalization and reaches late endosomes after 30 min.

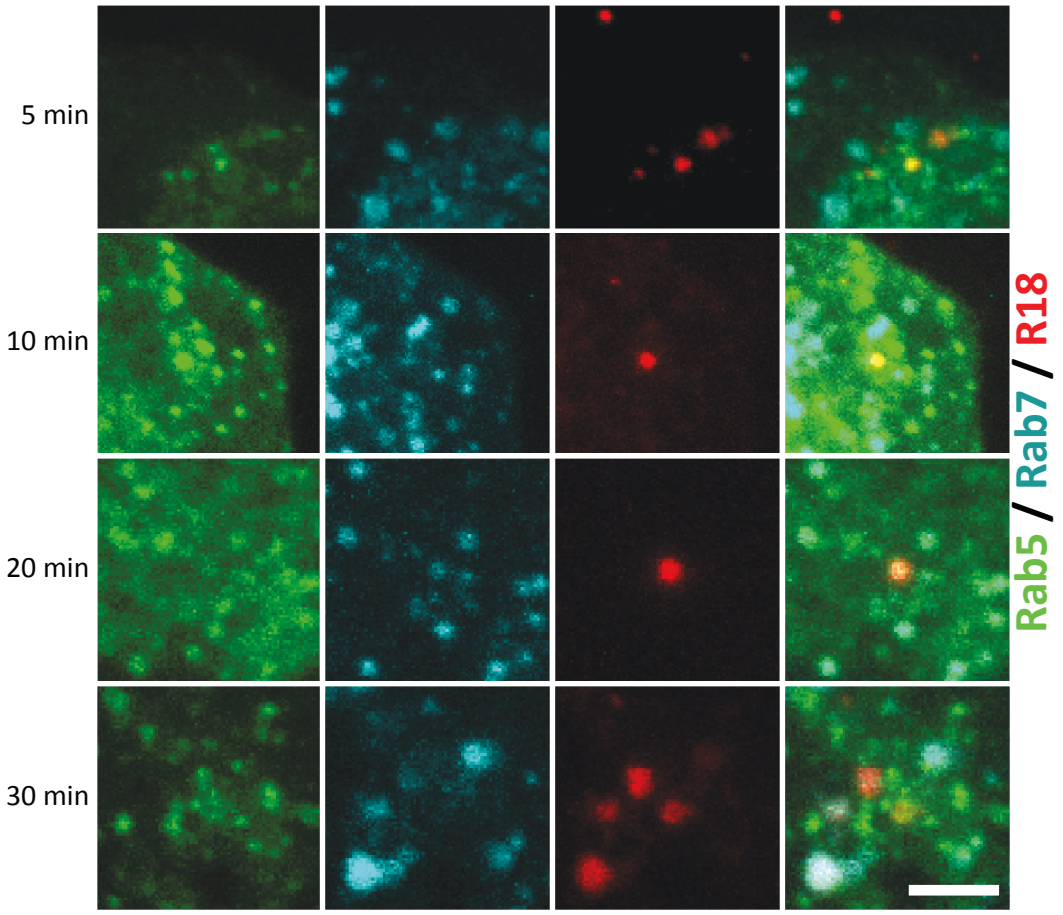

Figure 3.18: Endosomal localization of influenza A/X-31 viruses after endocytosis. MDCK cells were transfected with Rab5-GFP / Rab7-CFP and infected with R18-labeled viruses. Viruses were adsorbed on ice for 10 min, washed and transferred into pre-warmed growth medium. The cells were immediately followed by confocal microscopy at 37 C. Scale bar 10 µm.

3.7.2 Intracellular fusion of influenza A/X-31 virus detected by R18 - dequenching

R18 labeling provides an advantage, that was used before to study virus-ghost fusion. The high concentration of the fluorophore in the viral envelope leads to strong self-quenching, which will

be releaved upon fusion and dilution of the dye into the endosomal membrane. To illustrate this, Fig. 3.19 shows R18-labeled viruses (spots) at 0 (A) and 20 min (B) post-infection. Some of the R18 spots show a strong signal increase, which indicates de-quenching due to virus-endosome fusion (D). This effect was much less pronounced when the endosomal acidification was inhibited by the presence of 20 µM bafilomycin A (BafA) during the experiment. This indicates that indeed intracellular fusion of influenza A viruses can be measured using R18 labeling. Spontaneous probe exchange due to the close proximity of viral envelope and endosomal membrane was very low, as shown by BafA treatment (Fig. 3.19 C, D).

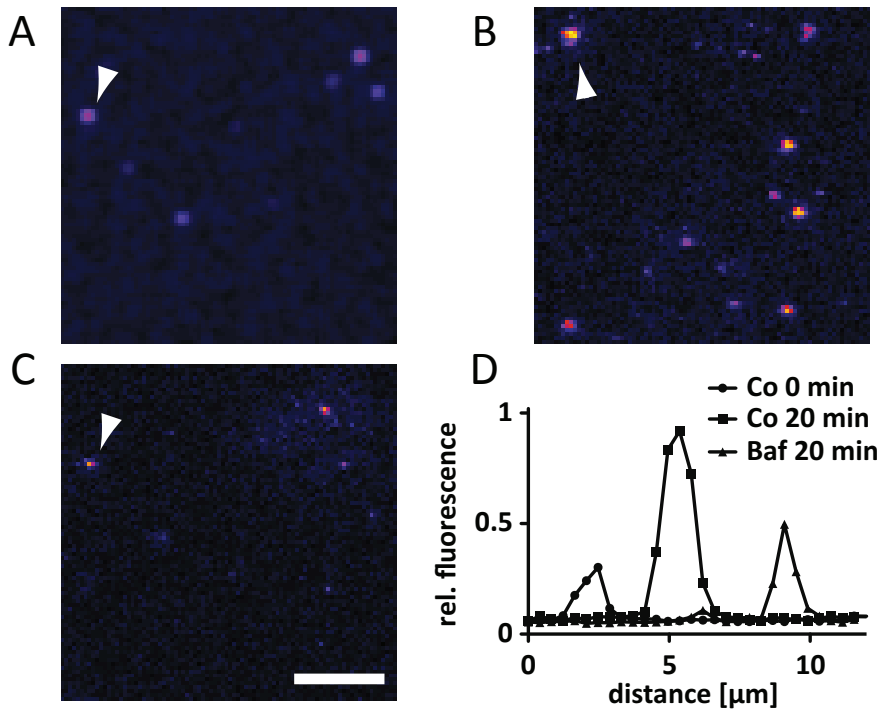

Figure 3.19: Intracellular fusion of influenza A/X-31 virus can be detected using R18 labeling. MDCK cells were infected with influenza A/X-31 viruses labeled with R18 at self-quenched concentrations. The viruses were adsorbed on ice for 10 min. The cells were washed three times with cold PBS, transferred into pre-warmed growth medium and immediately observed using a confocal microscope. The cells were kept at 37 C throughout the experiment. Stacked images of untreated cells were acquired at 0 (A) and 20 min (B) post-infection. To estimate the amount of spontaneous R18 exchange, the endosomal acidification was blocked using 20 µM BafA. Images were taken after 20 min (C). The R18 spots marked with an arrow head (A-C) were quantified using a line plot measurement (D). Scale bar 10 µm.

To gain insights into the kinetics of intracellular fusion, MDCK cells were infected with R18-labeled viruses and the fluorescence was followed over 60 min. At every time point, image stacks of the whole cell were acquired, summed and analyzed using the software Localize (Thompson et al., 2002). The software identifies and measures the size and intensity of individual R18 spots.

The results are shown in Fig. 3.20 A. Interestingly, the mean spot signal immediately increases within the first 5-10 min, suggesting early endosomal localization at the time of fusion. Infection of Rab5/Rab7 expressing cells verified this notion. Fig. 3.20 D shows an example of an R18-labeled virus with high intensity co-localizing with Rab5 without Rab7. However, these events were only rarely observed.

The reliability of the R18-based assay was further tested using a different labeling technique introduced by Sakai *et al.* (Sakai et al., 2006). This approach makes use of two fluorophores DiO and DiI with overlapping excitation and emission spectra. This allows Foerster Resonance Energy Transfer (FRET) due to the close proximity of both dyes within the viral membrane. Upon fusion, FRET as well as self-quenching will be reduced, which can be quantified by calculating the ratio between DiO and DiI. Figure 3.20 C shows double labeled viruses at different time points post-infection. On the first images, 2 min after infection, the viruses appear red due to self-quenching of DiO as well as FRET to DiI. At 15 min post-infection an increase of the DiO signal became visible, which results in a yellow appearance of the virus spots. After 25 min, the viruses became green with only a little fraction of red fluorescence. In each image the red and green signal of each visible virus spot were quantified and the ratio calculated (Fig. 3.20 A). The kinetics are very similar as measured using R18 de-quenching.

The fusion kinetics were further studied in cells treated with BafA. Treatment led to a linear increase of the R18 signal (Fig. 3.20 B), indicating a very low probe exchange in the absence of fusion.

To study if the described intracellular fusion assay is robust against variable virus concentrations, the fusion kinetics were investigated using different MOIs. The cells were treated as described and followed over 60 min (Fig. 3.21A). The kinetics of fusion were similar and were thus assumed not to depend on the MOI in the investigated regime.

It was previously shown by the group of Zhuang (Rust et al., 2004; Lakadamyali et al., 2006, 2003) that influenza viruses are rapidly transported along microtubules towards the perinuclear region (PNR) before fusion occurs. Figure 3.21 shows the kinetics of fusion in untreated cells and cells treated with the microtubule disrupting drug nocodazole. In untreated cells, the R18 signal rises immediately with = 10 min. The signal saturated already after 25 min. In nocodazole treated cells, the R18 fluorescence showed a delayed increase (Fig. 3.21 B). The time constant increased to = 32 min. The overall growth of the R18 signal which is the sum of all individual de-quenching events per cell was reduced by about 30% in nocodazole treated cells without saturation in the observed time range.

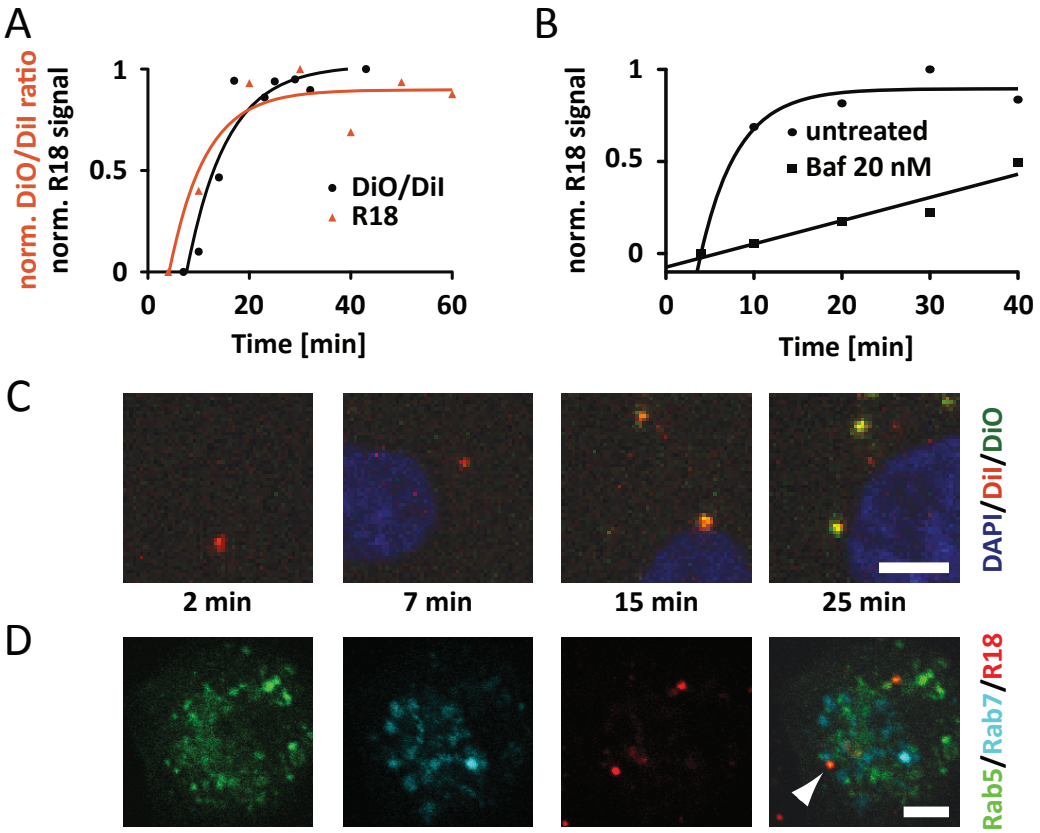

Figure 3.20: Intracellular fusion kinetics of influenza A viruses using R18-only and double-fluorophore labeling. R18-labeled viruses were adsorbed to MDCK cells on ice for 10 min. Afterwards, the cells were washed 3 times with cold PBS, transferred into pre-warmed growth medium and immediately observed using a confocal microscope. The cells were kept at 37 C throughout the experiment. Stacked images were acquired over 60 min and the fluorescence of each R18 spot was quantified using the software Localize (Thompson et al., 2002) (A). Shown are the mean R18 intensities of all detected spots of 3-5 image stacks per time point. In a second approach, viruses were labeled with DiO and DiI, which allows to detect fusion via de-quenching and FRET. Upon fusion, reduced FRET from DiI to DiO as well as de-quenching of DiI can be observed (C). This results in an increase of the DiO/DiI ratio (A). The kinetics are essentially the same, which verifies the results from R18 labeling. Further, the effect of the H^+-ATPase inhibitor bafilomycin A (BafA) was tested. BafA inhibits fusion and allows to observe spontaneous probe exchange, which had a linear time dependence and remained low compared to fusion-induced R18-dequenching. D shows a summed image stack of a Rab5/7 co-expressing cell infected with R18-labeled viruses. The arrow head marks a fusion event that co-localizes with Rab5 but not Rab7. Scale bar 5 µm.

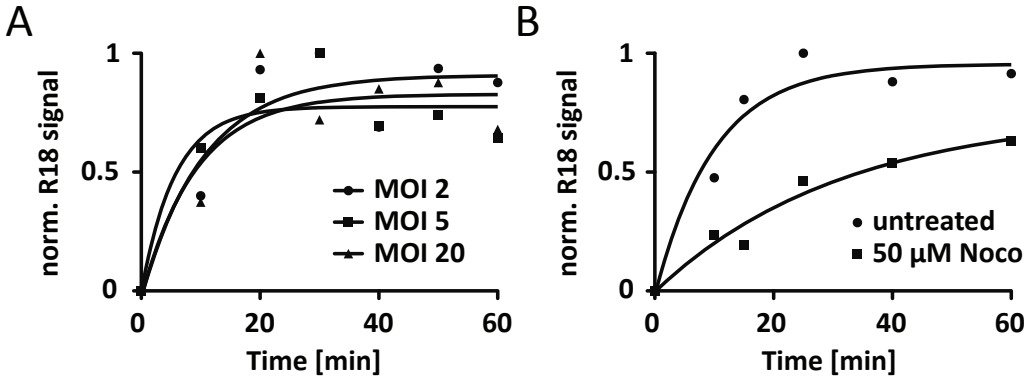

Figure 3.21: Intracellular fusion kinetics of influenza A virus in MDCK cells do not depend on the used MOI but on intact microtubules. MDCK cells were infected as described before using different amounts of viruses (A). R18-labeled viruses were adsorbed on ice for 10 min, the cells were washed and transferred into pre-warmed growth medium. The cells were immediately followed by confocal microscopy over a period of 60 min. In another experiment MDCK cells were pre-treated with 50 µM nocodazole for 30 min. The cells were infected as described, with nocodazole present throughout the experiment.

3.7.3 Virus-endosome fusion mostly occurs in the perinuclear region (PNR) and depends on an intact microtubule network

As shown in the previous section, the kinetics of fusion are influenced by the presence of the microtubule disrupting drug nocodazole leading to slower fusion and reduced R18 de-quenching. In a next step, the subcellular localization of the fusion events was analyzed. The cell nuclei were stained with Hoechst and the cell boundary was deduced from the brightfield microscopic image. The cytoplasm was divided into two parts. The area within 2 µm around the nucleus was regarded as the PNR, the rest of the cytoplasm as cell periphery. Figure 3.22 summarizes the results of the fusion localization analysis. In untreated cells, 75 % of the fusion events were localized in the PNR. This prevalence was balanced after nocodazole treatment (Fig. 3.22 C). The fusion events were randomly distributed in the cytoplasm and 55 % were found to be in the PNR. Remarkably, the total number of fusion spots per cell was only very weakly affected (Fig. 3.22 D).

In order to relate the localization of fusion events with the success of infection, cells were infected in the presence and absence of nocodazole. Infection was visualized by immunostaining of the viral NP. Figure 3.23 shows MDCK cells infected with influenza A/X-31 virus 5 h post-infection. All of the untreated cells show NP signal in the nucleus (A). In contrast, after nocodazole treatment, the NP signal was reduced by 40 - 60 % (B).

The distance to the nucleus can be maximized using an acid-mediated by-pass of endocytosis, to circumvent endosomal uptake and transport of viruses. This was achieved by adding cell

fusion buffer to cells with bound virus, thus inducing fusion of the viral envelope directly with the plasma membrane (Helenius et al., 1980). Influenza A/X-31 viruses were bound to MDCK cells on ice for 10 min. The cells were washed with cold PBS and virus fusion with the plasma membrane was triggered using cell fusion buffer. Fusion was allowed to proceed for 5 min at 37 C. Afterwards, the cells were washed and either directly fixed or incubated for the indicates times.

Figure 3.24 A and B shows MDCK cells at 0 and 20 min after acid by-pass stained with polyclonal H3N2 and NP antibodies. After zero minutes, the virus particles are well labeled, while only in very rare cases NP signal could be detected. At 20 min post-fusion, punctate NP signals are visible in the cytosol. This indicates that the viral genome was successfully released after plasma membrane fusion. At 5 h post-fusion successful vRNP nucleus-import can be detected by newly produced NP accumulation in the cell nucleus (Fig. 3.24 C). The nuclear NP signal was quantified and revealed a 50-70 % lower signal compared to untreated cells (Fig. 3.24 D).

3.7.4 Influenza A/X-31 virus delays the endosomal acidi cation to ensure optimal residence time in early and late endosomes.

The time point of virus fusion and hence its intracellular localization essentially depends on the endosomal pH. The pH threshold of influenza A/X-31virus fusion was determined using virus-ghost fusion. Additionally, in a similar set of experiments the threshold of HAs conformational change was probed using the polarity sensitive fluorophore bis-ANS (Korte and Herrmann, 1994). Figure 3.25 A shows that the fusion activity of influenza A/X-31 virus starts already at around pH 6. The bisANS signal increased earlier immediately below pH 7 (Fig. 3.25 B). This is not necessarily an indication for the conformational change of HA. Some of the bisANS signal must be attributed to other parts of the virus apart from HA since pH-inactivated virus gave a signal as well. However, still the signal starts to rise at pH above 6. Taken together, these experiments indicate that virus-endosome fusion starts already at subacidic pH, which corresponds to the pH of early endosomes (see 3.7.2) and reached its maximum at pH 5.4.

But how does the virus ensure perinuclear localization at the time point of fusion? The intra-endosomal pH was monitored in the presence and absence of an influenza virus using a combination of a pH sensitive and an insensitive fluorophore. Endosomes without virus were loaded with FITC/Rhodamine-labeled dextran and the fluorescence of both dyes was followed over 30 min. If a virus was co-internalized, the virus was labeled with DiD and mixed with FITC-dextran prior to incubation with the cells. Stacked images were recorded, summed and searched for endosomes that could be re-found between the time points (Fig. 3.26 A). Without virus, the endosomal pH drops very quickly reaching a pH around 6 after 10 min (Fig. 3.26 B, C). If a virus was co-internalized the acidification was delayed and reached pH 6 only after 30min. The intra-

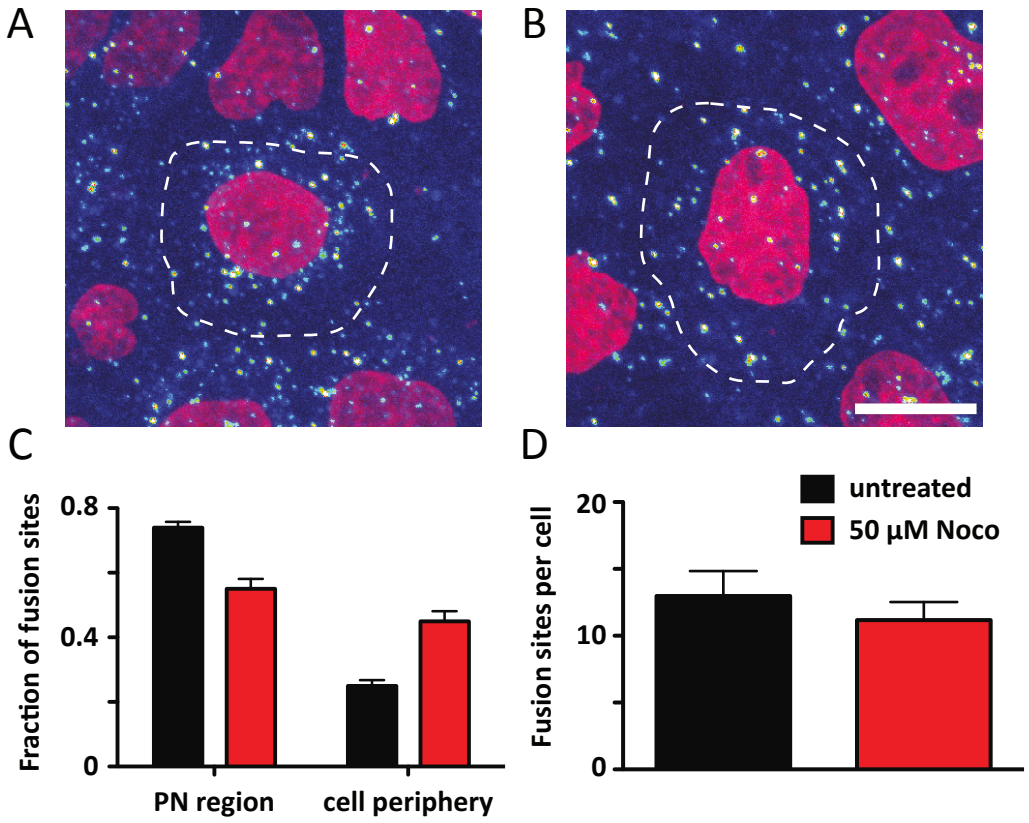

Figure 3.22: Nocodazole treatment leads to randomly localized fusion of influenza A/X-31 viruses in MDCK cells. MDCK cells were pre-treated with 50 µM nocodazole for 30 min. Viruses were adsorbed on ice for 10 min, the cells were washed and transferred into pre-warmed growth medium. The cells were immediately followed by confocal microscopy. The dashed line represents the cell boundaries, determined from the brightfield microscopic image. The DNA staining is shown in red. The fusion sites per cell were counted and classified by their location (C, D). In untreated cells, 75 % of the fusion events were localized within the PNR (A, C). In contrast, nocodazole treatment almost balanced this prevalence leaving only 55 % in the PNR (B, C). Interestingly, the number of fusion events was only very weakly affected (D). Scale bar 10 µm. Error bars correspond to SEM of 20 cells from three independent experiments.

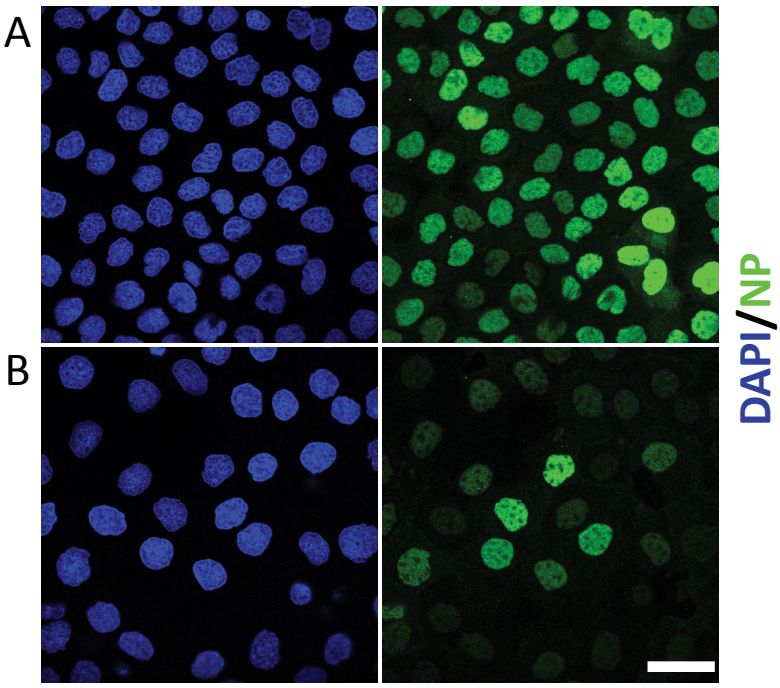

Figure 3.23: Infection efficiency of influenza A/X-31 virus in MDCK cells treated with nocodazole. MDCK cells were pre-treated with 50 µM nocodazole for 30 min. The cells were infected with influenza A/X-31 virus and immunostained using anti NP antibodies 5 h post-infection. In untreated cells (A) all nuclei show a clear NP signal. In contrast in cells treated with nocodazole (B) the nuclear signal was reduced by 40 - 60 %. Scale bar 20 µm.

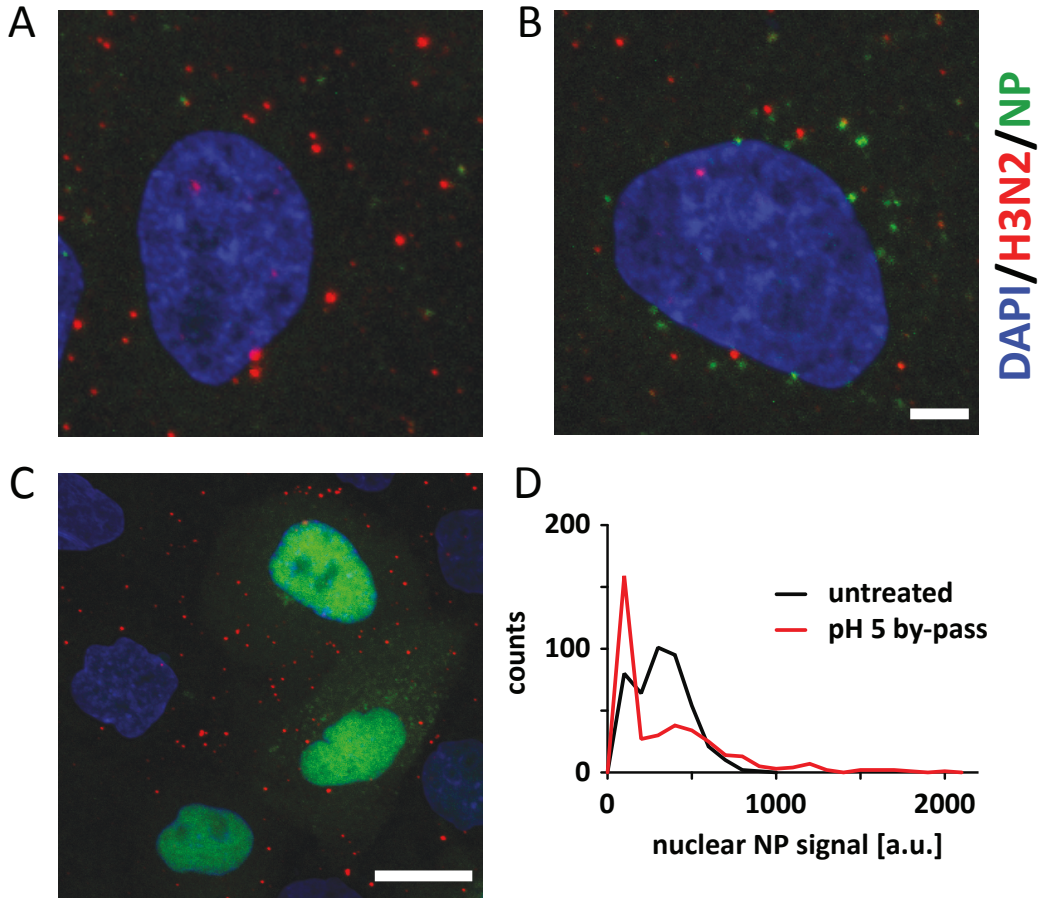

Figure 3.24: Genome release and infection after plasma membrane fusion (acid by-pass) of influenza A/X-31 virus with MDCK cells. Influenza A/X-31 virus was bound to MDCK cells on ice for 10 min. The cells were washed 3 times in cold PBS and transferred into pre-warmed cell fusion buffer. Fusion was allowed to proceed for 5 min, during which the cell dish was placed in a water bath to ensure complete temperature equilibration. The cells were washed in PBS and either directly fixed or incubated at 37 C for another 20 min. Afterwards, the cells were immunostained using anti H3N2 and NP antibodies. At zero minutes (A) almost no NP signal was visible while the H3N2 antibody detects bound viruses on the cell surface. At 20 min (B) free NP was detected in the cytosol, indicating successful fusion and uncoating. The by-pass leads to successful infection, which was visualized 5 h post-infection (C). The nuclear NP signal per cell after 5h was quantified using ImageJ based image analysis (D). Scale bar 1 µm (A, B) 10 µm (C).

endosomal pH in the absence of viruses was further determined in a whole-cell configuration where FITC and Rhodamine signals were quantified by flow cytometry (D). The acidification kinetics are very similar to the single endosome measurements without a co-internalized virus (Fig. 3.26 B). This indicates that dextran is mainly sorted into the lysosomal pathway (Baravalle et al., 2005) and thus can be used in comparison with virus-loaded endosome acidification

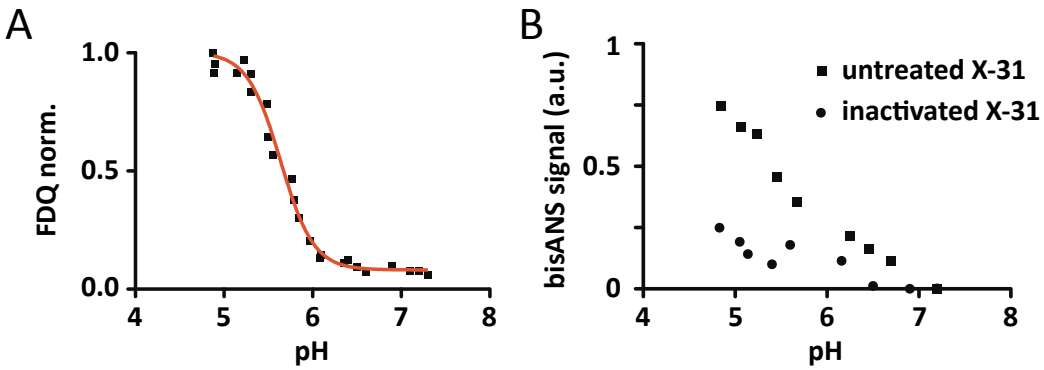

Figure 3.25: pH dependence of fusion and HA conformational change of influenza A/X-31. R18-labeled viruses were incubated with RBC ghosts for 20 min at RT. Virus-ghost suspension was transferred into 2 ml fusion buffer. The pH was lowered using 0.2 M citric acid and R18 de-quenching kinetics were recorded over 9 min. Fluorescence de-quenching (FDQ) was calculated according to Eq. 2.1 and plotted against the pH (A). This plot shows that the fusion starts around pH 6 and reaches a maximum at pH 5.4. Unlabeled virus was mixed with fusion buffer and 3 µM bisANS. The pH was adjusted as described above and the bisANS signal was followed over 5 min. The final bisANS value was plotted against the pH (B). As a control, the virus was inactivated by pre-incubation at pH 5 for 10 min, re-neutralized and used for bisANS binding.

3.7.5 Influenza A/X-31 virus must travel trough early and late endosomes to ensure successful infection.

Infection was strongly reduced after acid by-pass (see Fig. 3.24), suggesting at least two possible scenarios. First, a premature release of vRNPs in the cell periphery would increase the risk of vRNP recognition by cellular factors and trigger the cellular pathogen response. Second, direct fusion with the plasma membrane circumvents early endosomal residence. This would include a certain time at a subacidic pH before reaching more acidic late endosomal compartments. Such a hypothesis was already proposed in 1992 by Helenius (Helenius, 1992b) and suggested that the virus interior gets acidified at subacidic pH trough the envelope bound proton channel M2 before HA triggers virus-endosome fusion at more acidic pH. A process that would be necessary for virus uncoating. A set of by-pass experiments, where an early endosomal residence was simulated by a pre-incubation step was used to test this hypothesis.

To evaluate the influence of the proton channel M2, the used virus must be sensitive to the M2

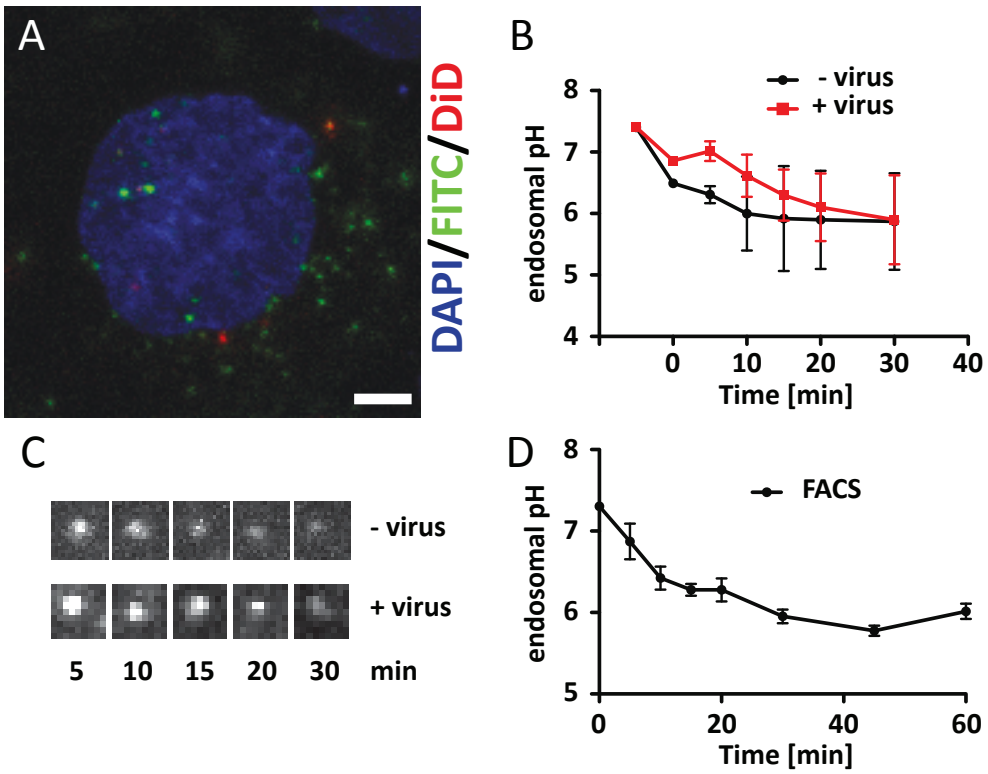

Figure 3.26: Kinetics of the intra-endosomal pH in the presence and absence of an influenza A/X-31 virus. MDCK cells were incubated with 10 mg/ml FITC-Dextran and DiD labeled influenza A/X-31 viruses for 5 min at 37 C, immediately washed and analyzed by confocal microscopy (A). If no virus was present the cells were labeled with FITC/Rho dextran. Ratio imaging of the pH sensitive FITC with a pH insensitive dye (DiD or Rhodamine) allows determination of the endosomal pH (B). At each time point, stacked images were obtained to allow tracking of individual endosomes. The presence of the virus led to a delayed acidification of the endosomal lumen, marked by a slower quenching of the pH sensitive probe (B, C). The intra-endosomal pH was further determined in a whole-cell configuration where both signals were quantified by flow cytometry (D). Scale bar 1 µm. Error bars in C correspond to SEM of 10 endosomes form three independent experiments. Error bars in D correspond to SEM of three independent experiments.

channel inhibitor amantadine. Since it was reported earlier (Scholtissek and Faulkner, 1979) that the M2 channel of A/X-31 is resistant to amantadine, a more recent strain influenza A/Panama/99 (H3N2) was tested. MDCK cells were infected with influenza A/X-31 and A/Panama/99 viruses in the presence of 10 µM amantadine, fixed and immunostained against the viral NP 5 h post-infection. Figure 3.27 shows that X-31 is resistant to the drug, leaving 90 % cells with a strong NP signal. In contrast, A/Panama was fully sensitive. Here amantadine completely blocked the infection in treated cells. Thus, influenza A/Panama/99 was used for all further by-pass experiments.

In a set of by-pass experiments influenza A/Panama was incubated at pH 7, pH 6 or pH 6 with 10 µM amantadine for 30 min at 37 C. The virus was re-neutralized by addition of 0.2 M NaOH, chilled on ice and bound to MDCK cells for 10 min on ice. Fusion with the plasma membrane was triggered as described above and the cells were incubated for 30 min, fixed and immunostained against the viral M1 and NP. Figure 3.28 shows summed image stacks representing the whole cell. If the virus was not pre-incubated and after pH 7 treatment, M1 and NP mostly co-localize in clusters in the cytosol.

After pre-incubation at pH 6, the number of aggregates decreased and both signals appear to be more diffuse within the cytoplasm. The presence of amantadine during the pre-incubation reversed the effect and the two proteins mostly appeared in clusters. The cytosolic M1 signal was quantified using ImageJ (Fig. 3.29). A region of interest (ROI) was defined in the cytoplasm of different cells (excluding clusters) and the M1 signal was quantified. Figure 3.29 A shows an example of a pixel intensity distribution of cells after the indicated treatment. The histogram in B summarizes the mean values. After pre-treatment at pH 6 the cytosolic M1 signal increased by 32 %. The presence of 10 µM amantadine led only to an increase of 16 %.

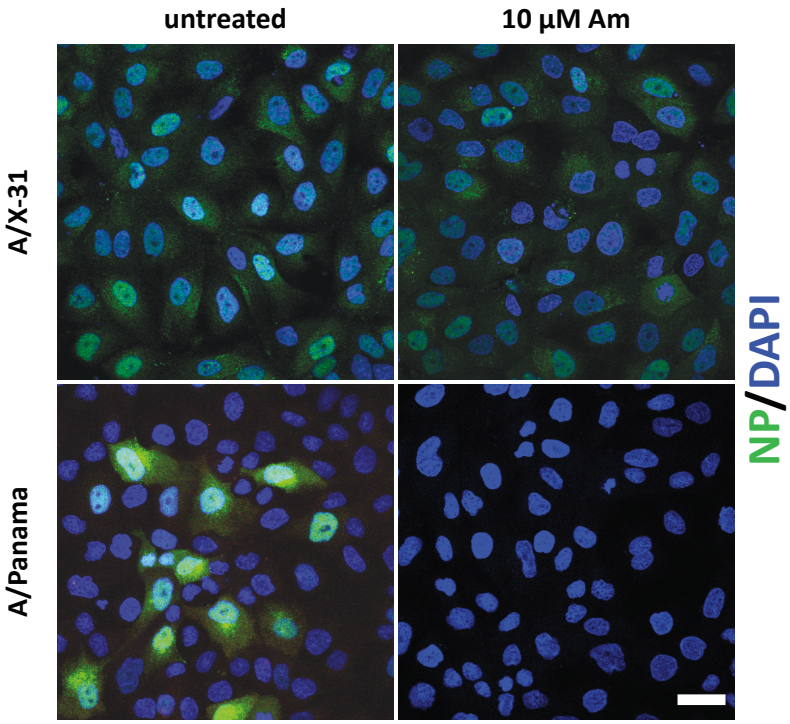

Figure 3.27: Infection by influenza A/Panama but not A/X-31 is sensitive to amantadine. MDCK cells were infected with influenza A/X-31 and A/Panama viruses at a MOI of 10-20 in the presence and absence of the M2 inhibitor amantadine. Infection by X-31 is resistant to 10 µM of the drug leaving 90 % cells infected. In contrast, A/Panama was fully sensitive and here amantadine completely blocked the infection in treated cells. Scale bar 20 µm.

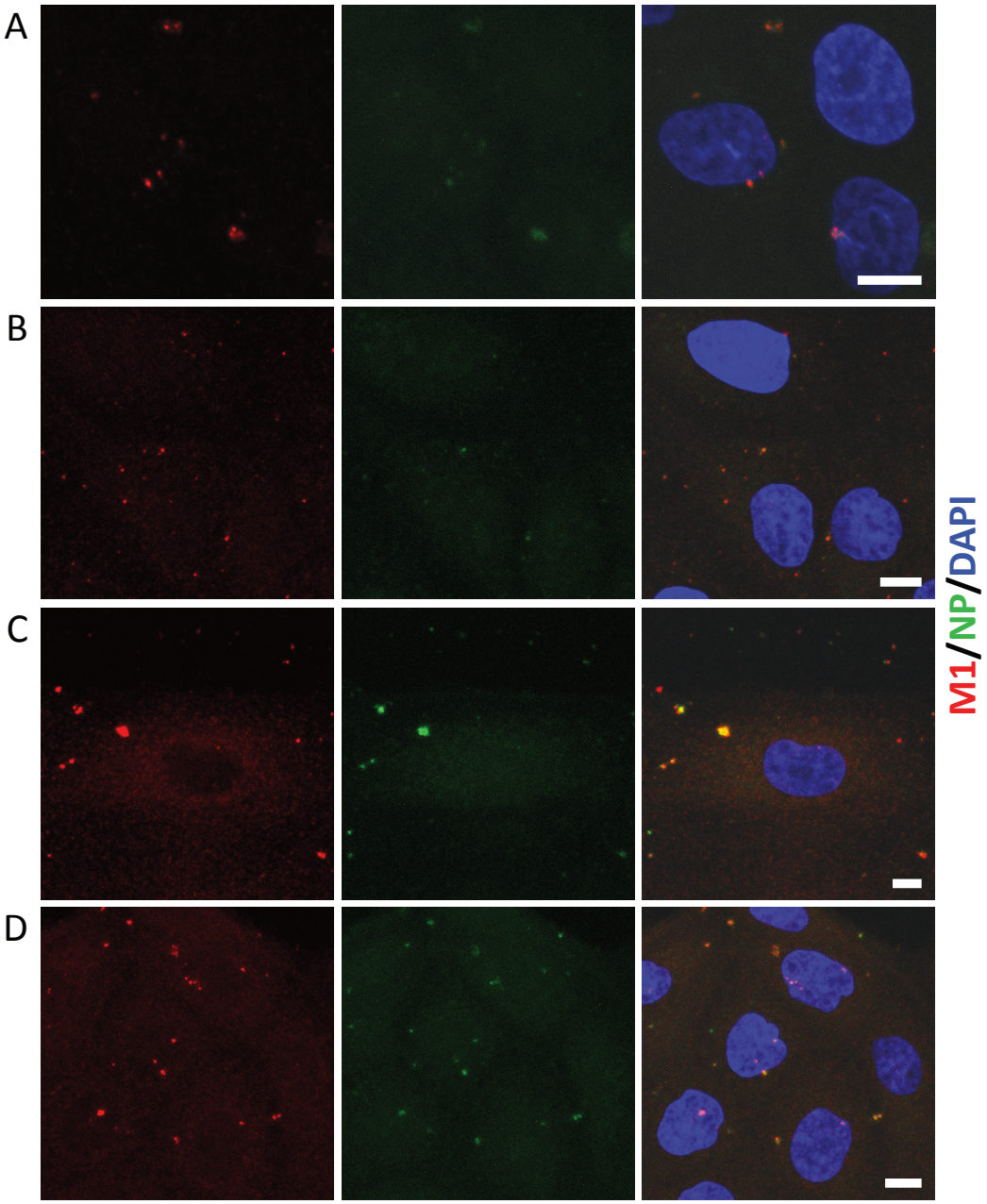

Figure 3.28: Pre-incubation at subacidic pH and an active M2 channel allow dissociation of M1 and vRNPs after acid by-pass of influenza A/Panama/99 with MDCK cells. MDCK cells were incubated with influenza A/Panama/99 viruses. The cells were either not pre-incubated (A), pre-incubated at pH 7 (B), pH 6 (C) or pH 6 with 10 µM amantadine (D). After pre-incubation, fusion was induced by addition of cell fusion buffer for 5 min at 37 C. The cells were washed and further incubating for 30 min at 37 C and subsequently immunostained for M1 and NP. Summed image stacks through the whole cell are shown. Without pre-incubation and after pre-incubation at pH 7, both NP and M1 were found to co-localize. After pre-incubation at pH 6.0, the amount of aggregates decreased. M1 and NP were found more homogeneously distributed in the cells cytoplasm. This effect was reduced by the presence of amantadine. Scale bar 5 µm.

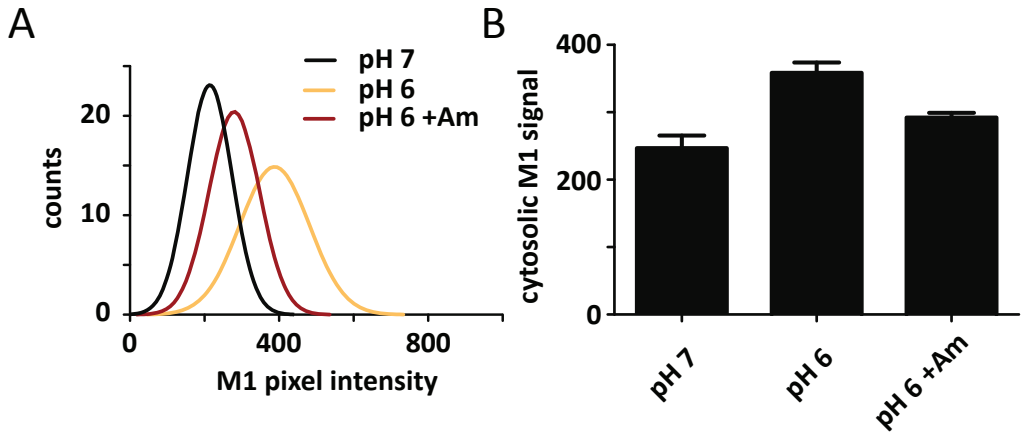

Figure 3.29: Quantification of the cytosolic M1 signal. A region of interest (ROI) was drawn in the cytoplasm of different cells and the M1 signal was quantified. Figure 3.29 A shows an example of a pixel intensity distribution of one cell after each treatment. The histogram in B summarizes mean values of 20-40 cells for each treatment. After pre-treatment at pH 6, the cytosolic M1 signal increased by 32 %. The presence of 10 µM amantadine led only to an increase of 16 %. Error bars correspond to SEM from 20 - 40 cells from two independent experiments.

4 Discussion

Influenza virus infection starts with binding of the spike protein HA to receptors on the host cell surface. This fundamental step in virus replication was characterized in the first part of this study on living cells by means of single virus force spectroscopy. Combining this method with experiments characterizing the topography and receptor configuration of three different cell lines, revealed that the unique features of a cell surface, rather than the receptor conformation itself, significantly influence virus-cell binding.
This information was then employed to design inhibitory nanoparticles that can mimic the cell surface and hence be used to prevent virus infection already at the stage of cell binding. In the second part of this study, the influence of two types of nanoparticles on virus activity was studied and revealed remarkable inhibitory capacity.
The third part of the study concentrates on entry and trafficking of influenza viruses, i.e. processes that directly follow virus-cell binding. Two important mechanisms were identified: (1) Efficient virus uncoating (i.e. vRNP release) depends on subacidic pH values apparent in early endosomes. (2) The presence of a virus inside an endosome delays acidification of the endosomal lumen. Disturbing these two processes by using specific drugs considerably decreased virus infectivity. Taken together, these findings could provide hints for future targeted antiviral approaches.

4.1 Single Virus Force Spectroscopy

Compared to optical trapping of single viruses (Fig. 3.1 and Ashkin and Dziedzic (1987)), it is much more accurate to use a larger sample carrier, which allows precise calibration of the optical trap and force measurements with single-pN accuracy. Influenza A viruses were bound to polystyrene microspheres by non-specific adsorption. This is a simple and common sample-probe attachment method in AFM and OT based force spectroscopy experiments (Rief et al., 1997; Li and Liu, 2008; Arya et al., 2005). However, the use of spherical beads also has limitations. Particularly, the contact area between bead and cell surface is very large, which decreases the probability to detect single virus-receptor interactions as observed for example on MDCK cells. Hence in this thesis, a low virus concentration per bead was used and permitted measure-

ments of single virus-receptor interactions.
Meanwhile, more specific and stable attachment protocols have been developed by other groups (Ebner et al., 2009), and thus, an AFM-based approach was utilized as an additional method. In the present study, influenza virions were covalently attached to the AFM tip by using a bifunctional crosslinker (Rankl et al., 2008). Both methods, AFM and OT, revealed unbinding forces between 7 and 25 pN in the investigated loading rate regime (Fig. 3.2 and 3.3). These forces are much lower than the adhesive forces between polystyrene and proteins (Sagvolden et al., 1999), ensuring stable attachment of viruses to the bead surface during the force measurements. The combination of two methods demonstrates the reliability of the new optical tweezers approach by confirming the measurements by AFM, which was successfully used before to measure cell adhesion forces of human rhinovirus (HRV) and HIV (Rankl et al., 2008; Dobrowsky et al., 2008).
Dynamic force spectroscopy using varying pulling velocities revealed the characteristics of the underlying interaction. For CHO cells investigated by OT, the dissociation constant k_{off} 0.12 s^{-1} corresponds to a bond lifetime of 8.3 sec without applied force (Fig. 3.2). A broad distribution of unbinding forces was observed, which led to an increased variability of the values for k_{off} and x_u. This correlates with results from *in silico* simulations (molecular dynamics) of the same interaction (Sieben et al., 2012)[1]. Molecular dynamics (MD) calculate time-dependent interactions between all atoms within a given system. Force-probe molecular dynamics simulations (FPMD) extend this method by introducing a moving harmonic potential as a "virtual spring" acting on the ligand thereby pulling it away from the protein (Grubmüller et al., 1996). Using the crystal structure of HA bound to its receptor (Eisen et al., 1997), force simulations revealed a high variety of unbinding pathways (Sieben et al., 2012). The interaction was shown to be very dynamic including spontaneous release and rebinding of the receptor to HA. Zipper-like and all-or-none unbinding events were observed and had a strong impact on the measured force resulting in high variability as it was observed in this study using experimental techniques.
The obtained values describe a notably weak interaction compared to other lectin-carbohydrate bonds (reviewed in Helenius et al. (2008)) like Concavalin A (Chen and Moy, 2000) or Helix Pomatia Lectin (Grandbois et al., 2000) with sialic acid. For comparison, other receptor-ligand interactions studied by AFM- and OT- based force spectroscopy are listed in Table 4.1. Compared to surface plasmon resonance (SPR) measurements of the interaction between HA and Fetuin (Takemoto et al., 1996a), a highly glycosylated blood plasma protein, dissociation rates of about 100 times higher were observed. Since SPR experiments are often complicated by high re-binding rates, the detected dissociation rates can be drastically decreased. This dynamic is

[1] Force simulations using single HA trimers bound to sialic acid have been done in collaboration with Dr. Christian Kappel and Prof. Helmut Grubmüller from the Max-Planck-Institute for Biophysical Chemistry in Göttingen.

apparent in the case of multivalent interactions and show the advantage of this interaction type. Such differences between molecular and cellular dissociation were observed before for HRV and HIV cell adhesion (Rankl et al., 2008; Dobrowsky et al., 2008) and underline the suitability of SVFS to investigate binding between live cells and intact virions.
AFM measurements presented here suggest stronger interaction between X-31 virus and CHO cells (-2,3-linked SA), compared to MDCK and A549 (-2,3 and 2,6-linked SA). This contradicts earlier studies showing specificity of X-31 HA to human type receptors (Sauter et al., 1989; Rogers et al., 1983). Further, the amino acid composition of the receptor binding site in X-31 HA also indicates specificity for the human type receptor. On the other hand, the receptor binding site of influenza A/WSN HA points to a rather dual specificity (Gambaryan et al., 1999), which would explain the very similar bond lifetimes found in AFM pulling experiments using influenza A/WSN with CHO and A549 cells (also see below 4.3.2).
Interestingly, at least for influenza A/X-31 neither the amino acid composition of HA nor receptor binding studies with purified ligands (Sauter et al., 1989) correlate with the binding preference obtained from SVFS measurements performed in this study. This observation suggests that the unique environment of the receptor on the cell surface strongly affects virus-cell binding. It further indicates that virus specificity is very complex and that the observed properties of a certain virus or HA strongly depend on the experimental approach as well as on the level on which it is investigated. This concept and accompanying parameters will be discussed below.

4.2 Reviewing results from SVFS regarding the cell surface

4.2.1 Receptor composition of the cell surface

The receptor composition of the used cell lines was studied utilizing the well characterized fluorescent lectins MAA and SNA. This approach is commonly applied to address receptor composition in primary lung sections (Matrosovich et al., 2004a) or in cell culture (Ito et al., 1997). MAA was reported to be specific for -2,3- (Wang and Cummings, 1988) and SNA for -2,6-linked sialic acids (Shibuya et al., 1987). However, in particular MAA has certain drawbacks that have to be considered. The protein exists in two isoforms (MAA 1 and 2) that are selective for the adjacent sugars. MAA1 binds Sia -2,3Gal 2,3GlcNAc/Glc and MAA2 preferentially binds Sia -2,3Gal 1,3 (Sia -2,6)GalNAc (Nicholls et al., 2008). Both isoforms recognize -2,3-linked SA but, depending on the isoform that was used in the experiment, the signal provides a measure for the adjacent sugars, which could bias the experimental results. SNA has three isoforms, but here only SNA-1 very specifically recognizes -2,6-linked SA (Mach et al., 1991). Another problem that could arise is likely caused by the supplier-dependent fluorescent labeling

Table 4.1: Receptor-ligand interactions studied by AFM- and OT- based force spectroscopy

interaction	k_{off} (s^{-1})	energy (k_BT)	method	reference
gp120 - CD4 (HIV)	4.1	20.9	AFM	Chang et al. (2005)
BabA - Lewis b (*Helicobacter*)	0.015	26.5	OT	Björnham et al. (2009a)
Galabiose - PapG (*E.coli*)	$2.6*10^{-3}$	28.3	OT	Björnham et al. (2009b)
HRV2 - LDLR (Rhinovirus)	$5*10^{-7}$	36.8	AFM	Rankl et al. (2008)
sLe^x - selectin (Leukocyte)	41 0.3	18.6 23.5	AFM	Zhang et al. (2004)
Steptavidin - biotin	$1.67*10^{-5}$ $2.09*10^{-5}$	33.4 31.1	AFM	Yuan et al. (2000)
Digoxigenin - anti-digoxigenin	0.015 4.6	26.5 20.8	AFM	Neuert et al. (2006)
HA - SA (X-31, CHO cells)	0.12 0.18	24.5 24	OT AFM	present study

of the lectin. As a consequence, the lectins from different suppliers show altered binding patterns when applied to the same sample (Nicholls et al., 2007). To circumvent the first problem, a mixture of both MAA isoforms sold by EY laboratories was used in this thesis.
The observed binding was generally very weak on all probed cell lines, a problem that did not occur for SNA (Fig. 3.7). It was shown before that MDCK (Ito et al., 1997) and A549 cells (Guo et al., 2009) possess both types of SA linkages and these findings were confirmed in this study (Fig. 3.7). However, the detected amount of -2,3-linked SA may vary due to the problems discussed above and thus fluorescent lectins, in particular MAA, can hardly be used to calculate relative SA abundances. Its correct to state that both SA-linkages are present, but to conclude that one or the other may be more abundant, is already critical. For CHO cells, the situation is more clear since those do not express a sialyltransferase specific for -2,6-linked SA and present only -2,3-linked SA (Xu et al., 2011). Hence, CHO cells are a good model system to study virus binding to -2,3-linked SA. MDCK and A549 cells present both linkage types and data presented here indicate that the more abundant linkage is -2,6 (Fig. 3.7). However, a precise quantitative measure of the cell glycan structure can only be obtained using mass spectrometry as demonstrated by North et al. (2010).

4.2.2 Cell surface topography

From section 3.1, it was surmised that the virus-cell interaction mediated by SA-HA binding is strongly influenced by the presentation of SA on the host cell plasma membrane. In section 3.4, the cell surface topography was studied utilizing scanning electron microscopy. The cell surface topography is strongly cell line dependent and is further influenced by the state of cell growth. In addition, the surface topography depends on the position of the cell within the colony. This phenomenon was described as cell-to-cell variability and might further influence virus infection (Snijder and Pelkmans, 2011; Snijder et al., 2009). In the present study, the cells were found to show a variety of cellular protrusions, presumably microvilli, which can dramatically increase the cell surface. This is in particular important for epithelial cells due to their polarized organization and transport function (Rodriguez-Boulan et al., 2005). While the distance between the microvilli was similar, the length was dependent on the cell line. The protrusions of A549 and CHO cells were rather long, while MDCK cells featured shorter microvilli (Fig. 3.9).
During initial binding, the virus may either attach to one or more microvilli or to rather smooth parts of the cell surface between them. Considering the high density of microvilli in a confluent cell culture (Fig. 3.10), it is more likely for the virus to bind a microvillus than directly on the smooth cell surface. Indeed, it was observed that influenza A viruses primarily associates with microvilli on MDCK cells (Matlin et al., 1981). This was also shown for semliki forest virus (SFV) on baby hamster kidney cells (Helenius et al., 1980). Microvilli are actin-stabilized and have a diameter of about 100 nm, which precludes direct virus uptake into the microvillus (Lodish et al., 2007). Thus, the virus needs to move towards the base of the microvillus to enter the cell. This mechanism was described for murine leukemia virus (MLV) (Lehmann et al., 2005) and was recently revised showing that viruses can actually move between cells exploiting cellular protrusions (Sherer et al., 2007).
In SVFS experiments, the cells were used at both low (OT) and higher confluency (AFM). At least for CHO cells, results obtained at both confluency levels can be compared and show that X-31 binds better to low confluent cells (Fig. 3.2 and Table 3.1). However, in particular for CHO cells, the microvilli presentation did not change significantly during cell growth in culture (Fig. 3.9 and 3.10) indicating that the surface topography did not account for the different bond lifetimes.
Nevertheless, the cell surface topography indeed strongly varies between the cell lines, and furthermore, the parameter of the pulling angle has to be considered in SVFS. In OT experiments, the bead approaches the cell from the side, while AFM cantilevers always operate in vertical directions. It was shown before that the angle at which a single bond is pulled influences the resulting unbinding force (Ke et al., 2007). Considering the dynamic and highly structured surface of a cell, no information can be obtained regarding the pulling geometry during SVFS exper-

iments. A variable pulling angle influences the unbinding behavior and could lead to higher variation of the resulting forces as observed by SVFS (see 3.1). One way to circumvent this in force spectroscopy is to use a flexible linker between surface and receptor as well as between cantilever and ligand. This could be accomplished by using polyethylene glycol (PEG) or DNA (Neuert et al., 2006; Cecconi et al., 2008), but is not applicable for receptors on cells due to their natural presentation on the cell surface. However, during the AFM experiments, the virus was attached to the cantilever using a PEG crosslinker, thereby providing a certain amount of flexibility.

4.2.3 Interaction complexity affects receptor speci city.

SVFS investigates binding forces of single or a few receptor-ligand complexes. A fluorescence-based binding assay was used to compare the results from SVFS with whole-cell virus binding (i.e. many simultaneous interactions). R18-labeled viruses were incubated with a defined number of cells from each cell line and the R18 signal per cell was quantified using flow cytometry. Considering multivalent binding, one would expect that small differences measured by SVFS translate into more pronounced differences when looking at multiple interactions on the whole-cell level. Influenza A/X-31 bound better to CHO than to MDCK and A549 (Fig. 3.4) as expected from SVFS. Interestingly, A/WSN bound better to CHO than to A549 cells, which contradicts the AFM results. This supports the earlier conclusion that receptor specificity and cell specificity are not necessarily connected. Receptor specificity is presumably mainly determined by HA, i.e. the structure of the receptor binding site (Imai and Kawaoka, 2012). How the cellular specificity is established, remains to be investigated.
In summary, these results point to multiple levels of complexity that have to be considered for understanding virus-cell binding. The proposed levels of complexity as well as their major determining factors are summarized in Fig. 4.1. Hence, the results obtained on virus specificity critically depend on the applied technique, since each method targets virus binding on a different complexity level. Technical aspects and the role of the mentioned dual receptor binding behavior are discussed in the next section.

4.3 Dual receptor binding behavior

4.3.1 Technical considerations

Among the first who studied the receptor specificity of HA, Rogers *et al.* (Rogers et al., 1983) used sialidase treated (asialo) erythrocytes which where specifically re-sialylated with either -2,3- or -2,6-linked SA, an elegant approach that is still used in current publications (Glaser

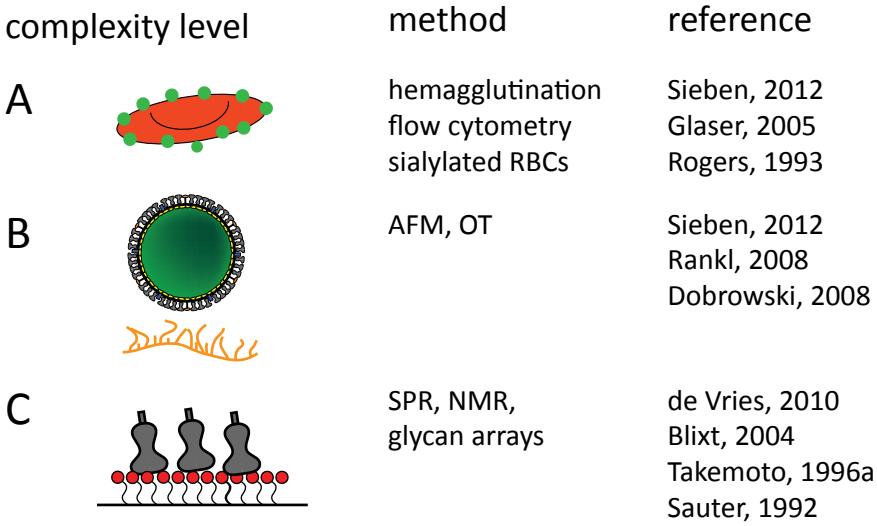

Figure 4.1: Virus receptor specificity can be measured on different complexity levels using specialized methods. Virus specificity can be measured on the whole-cell level (A) as well as on the single virus level (B). These two techniques have the advantage that viruses and cells are intact and thus represent the natural situation. Receptor specificity can further be analyzed utilizing purified binding partners, such as SA-coupled ligands or HA (C). This approach allows precise control over the studied ligands, but ligand density and orientation can barely be adjusted. AFM, atomic force microscopy; OT, optical tweezers; SPR, surface plasmon resonance; NMR, nuclear magnetic resonance

et al., 2005; Tumpey et al., 2007). However, among other methods, solid-phase binding assays or glycan arrays represent a widely used convenient way to analyze HA-receptor interactions (Blixt et al., 2004). The desired ligand is coupled to a flat surface and can either be probed with intact viruses (Imai et al., 2012) or purified HA (Stevens et al., 2006; de Vries et al., 2010), which is then detected using antibody binding. Other studies used NMR (McCullough et al., 2012; Sauter et al., 1989) or SPR (Takemoto et al., 1996b) to measure receptor binding (Fig. 4.1). These studies used purified SA receptors as binding partners for HA and certainly provide very accurate binding profiles and affinities. However, already on this level the techniques (including sample preparation) are not directly comparable. The ligand density, which likely affects binding (see 4.4 below) is not easily controllable. SPR is known to often underestimate dissociation due to high re-association rates. A problem that becomes apparent when using multivalent ligands (e.g. viruses). This might also be the case for force spectroscopy studies. Here the ligand is immobilized on a force transducer leading to an almost two-dimensional dissociation and reduced ligand entropy. Indeed, it is important to consider the described factors, but among the current techniques, SVFS is the only tool to measure virus-cell adhesion in a set-up that closely mimics the natural situation.

4.3.2 Dual receptor speci city

The above mentioned studies often report dual receptor binding, meaning HA binds both, avian and human receptors. However, HA often shows a preference for one of the two types and hence receptor specificity is to be understood as preferential binding. HA from influenza A/X-31 was shown to preferentially bind -2,6-linked SA (Takemoto et al., 1996b; Sauter et al., 1989; Rogers et al., 1983). The identified critical amino acids in H3 HA at position 226 (leucine) and 228 (serine) further indicate binding of X-31 HA to human type receptors. For H1 HA, the critical amino acids were identified at position 190 and 225 (Gambaryan et al., 1999). With glutamic acid at position 190 and aspartic acid at position 225 the HA of A/WSN shows similarities to both the avian and human consensus sequence, but preferentially binds -2,6 sialylated red blood cells (Leung et al., 2012).

As mentioned above, it is difficult to make predictions about receptor binding based on the amino acid composition of the receptor binding site. As an example, H1 from influenza A/Cal/09 (H1N1), an isolate from the recent pandemic, exhibits aspartic acid at positions 190 as well as 225 and thus should preferentially bind human type receptors. In contrast, the virus shows pronounced dual binding to both receptors, a property that is opposed to seasonal H1 viruses and might be linked to the pandemic character of A/Cal/09 (Childs et al., 2009). Indeed, H3 from A/X-31, which originates from the pandemic virus A/Aichi/2/68 (H3N2) as well shows dual binding behavior (Childs et al., 2009). This suggests that also on this level, many other factors

might play a role in determining the receptor specificity.
Regarding the virus, other critical amino acids where reported for various HAs that favour binding to a variety of different complex glycans (Stevens et al., 2006). This means that when studying cellular specificity, it is important to consider the complex glycans behind the terminal SA linkage. Another important factor is the glycosylation state of the virus itself. HA being a transmembrane protein, follows the secretory pathway and thus underlies secondary protein modifications. It is glycosylated inside the ER and Golgi apparatus (Keil et al., 1985) and the structure of the glycans critically depends on the infected host cell (see 1.4.1). The glycosylation state of HA was shown to alter the receptor specificity (de Vries et al., 2010). Apart from carbohydrate modifications, further host-cell factors where shown to be involved in virus-cell binding. Recently, blocking of fibronectin was shown to interfere with influenza A virus entry (Leung et al., 2012). Remarkably, only -2,6 specific viruses were affected. The study by Londrigan *et al.* showed that other proteinaceous receptors including DC-SIGN or L-SIGN can act as SA-independent attachment factors (Londrigan et al., 2011).
To conclude, Stray *et al.* provided evidence for influenza virus infection in the absence of sialic acid, suggesting other possible attachment factors (Stray et al., 2000). Hence, virus-cell binding is a very complex process that goes beyond HA-SA interaction. As stated above, the present study further hypothesizes different levels of complexity that influence virus binding and must be considered.

4.3.3 Relevance of the HA-SA binding for influenza virus infection

Several recent studies suggested that receptor binding might not correlate with infection *per se*. The study presented by Chu and Whittaker (Chu and Whittaker, 2004) described an important role for N-linked glycans in influenza virus infection. The study describes the infection of Lec1 cells, a mutant CHO cell line deficient of the N-acetylglucosaminyltransferase I (GnT1) gene. It was found that virus invasion is stopped at the point of entry after virus attachment. A more recent study puts these results in a different light. De Vries *et al.* (de Vries et al., 2012) investigated the dependence of N-linked glycans using other cells than the Lec1 CHO mutant. They conclude that N-linked glycans are not essentially required but that other post-attachment factors are important for virus entry, a hypothesis that was also mentioned by Chu and Whittaker (Chu and Whittaker, 2004). Indeed, the involvement of multiple entry pathways (Mercer et al., 2010), the *de novo* induction of clathrin-mediated endocytosis (Rust et al., 2004) and the use of specific adaptor proteins such as Epsin 1 (Chen and Zhuang, 2008) suggests that more specific signals than the initial HA-SA contact are necessary to trigger internalization and promote infection. These signals might be responsible for the missing link between binding and infection that was characterized in the present study. SFVS experiments of influenza A/X-31 nicely correlate with

whole cell binding studies, indicating better binding to CHO and comparable binding to MDCK and A549 cells. This binding behavior is not translated into better infection efficiency. MDCK cells showed higher NP production when infected separately and in a competition assay growing side-by-side with CHO cells. These results suggest the existence of post-attachment factors necessary for efficient infection in MDCK cells, a finding that is supported by the study of Nunes-Correira *et al.* (Nunes-Correia et al., 1999) presenting a kinetic model for virus binding to and endocytosis in MDCK cells. The study points to two kinds of binding sites: (1) low-affinity receptors responsible for binding and (2) high-affinity receptors responsible for uptake. It is also possible that the observed differences in infectivity are related to the cellular pathogen defense response. A quantitative proteomic study comparing A549 with MDCK cells detected a changed abundance of interferon induced Mx proteins (Vester et al., 2009). Mx GTPases represent a family of antiviral proteins that interfere with the viral polymerase complex (Ehrhardt et al., 2010). The innate immunity might also be directly connected to receptor binding. Interestingly, in a recently presented hypothesis, virus binding to either human or avian type receptors activates differential immune signaling pathways (Ramos and Fernandez-Sesma, 2012), a factor that is important considering preferred binding or more dual-binding behavior of influenza viruses.

4.4 Inhibition of influenza A virus activity using multivalency

As mentioned above, a cell surface without sialic acid does not protect from influenza A virus infection. However, it is well accepted that SA is the major receptor for HA, a fact that is known for more than 50 years (Gottschalk, 1959). In addition, it is well known that HA is the most abundant spike protein. The virus overcomes the problem of weak interaction between HA and SA by using multiple interactions as studied by SVFS in this study. This generates strong binding and permits agglutination of red blood cells, a property that was known before SA was identified as the receptor. For this study, the idea was to mimic this multivalent interaction and thereby prevent virus-cell binding. This concept was studied before using many different scaffolds as described in section 1.3.2. The most potent inhibitors reached effective concentrations in the pM range (Mammen et al., 1995). These inhibitors were polyacrylamide-based and tested exclusively *in vitro*. Other scaffolds such as dendritic polymers (Reuter et al., 1999) or polyamidoamine (PAMAM) dendrimers were also tested in cell culture or mouse models (Landers et al., 2002) and reached effective concentrations in the μM range. Important to consider is the cytotoxicity, which is high for polyacrylamide and much lower for the later mentioned polymers. In the present study, spherical polyglycerol (PG) particles were used. Polyglycerols are highly biocompatible and can be synthesized in different sizes ranging from 1-100 nm (Calderón

et al., 2010; Sisson et al., 2009; Reichert et al., 2011). According to the results from SVFS that the SA linkage does not play a primary role in binding, the used particles were functionalized with only SA.

4.4.1 Inhibition of influenza virus binding

Two different size regimes were tested for their effect of SA surface content (dF, see section 2.1.5). Small PGs with a diameter of about 3 nm and larger PGs of 40 - 80 nm were tested. The size relation between nanoparticles and virus is summarized in Fig. 4.2. The binding was tested using a flow cytometric approach, where binding of fluorescently labeled viruses is measured in terms of signal per cell (Fig. 3.11). Both PG variants show an evident concentration dependent effect, but with a different progression. For the small PGs, RBC binding was inhibited in a linear fashion, without an effect of the dF (Fig. 3.11). In contrast, the larger PGs bound in an exponential manner and showed a strong dF-dependence. This indicates that increase in size leads to a fundamentally different binding behavior. Due to their size, the small PGs can presumably only bind 1-3 HA trimers and consequently benefit only minimally from steric stabilization. The higher local SA concentration still leads to better binding compared to the monomeric ligand. Likely, these particles merely act as competitive binding inhibitors for SA on the cell surface. The larger PGs had a pronounced effect at small concentrations which quickly saturated, without further increase of inhibition. The inhibition curve saturated at 1 mM SA concentration and inhibited virus-cell binding by 60 % (PG 5, dF = 80%) and 80 % (PG 4, dF = 12%). The data indicates that binding at this concentration ceased to be affinity dependent. Otherwise, higher concentrations would lead to better binding and stronger inhibition.
Several conclusions can be made from this behavior. Up to 1 mM SA, both PGs bind viruses, but PG 4 binds distinctly better and shows about double the inhibition of virus-cell binding. At the same SA concentration, the effect of the small PGs is less pronounced indicating a steric contribution for the larger PGs 4-5 (Mammen et al., 1995; Choi et al., 1996). At least two reasons can account for the difference between PG 4 and 5: (1) The increase of charged SA side chains also increases repulsion of the particles, which could lead to destabilized binding (Reuter et al., 1999; Mammen et al., 1995). This may alter hydration and thereby change the form of the PG away from ideally spherical (Reuter et al., 1999; Mammen et al., 1995; Kiessling et al., 2000). More flexibility would lead to increased binding as observed for polyacrylamide polymers (Mammen et al., 1995). (2) Another aspect is the distance and flexibility of each individual ligand. A fourfold increase of ligand density on a PG of a given size (i.e. similar contact area between PG and virus) can negatively affect binding due to a higher fraction of unbound ligands.

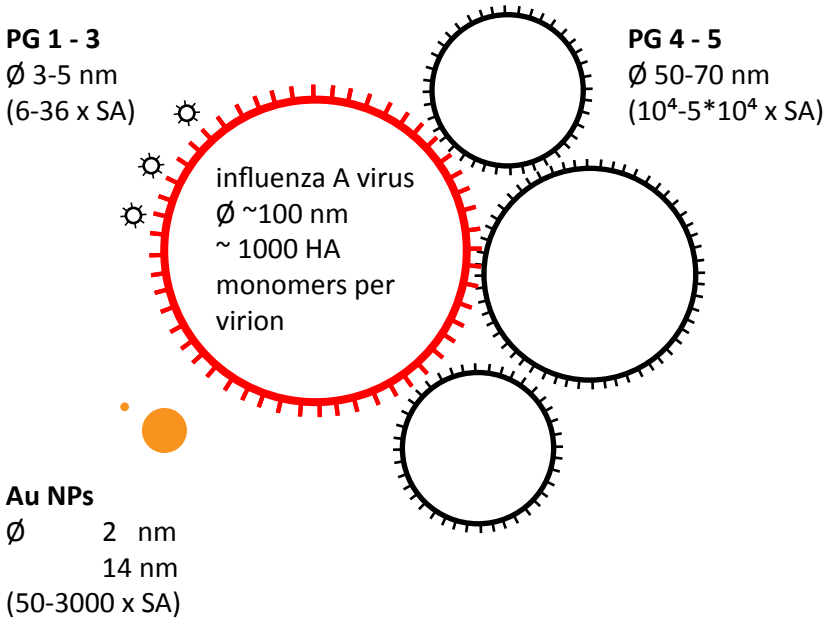

Figure 4.2: Size comparison of the used SA-conjugated nanoparticles with an influenza A virus.

4.4.2 Inhibition of influenza virus fusion and infection

Even at high concentrations of inhibitory nanoparticles, some viruses could still bind to the target cell surface. To test the functionality of HA, its ability to mediate fusion and enable infection was tested by R18 fluorescence de-quenching and anti-NP immunostaining respectively. Notably, after virus-cell binding, the RBC ghost-virus suspension was pelleted to separate unbound virus. That means that only the fusion activity of viruses that were still able to bind was detected. The overall virus activity then arises from the product of inhibition of binding and fusion.

Both PG variants inhibited fusion more prominently than binding. This is not surprising since HA-mediated fusion is supposed to be a cooperative process (Bentz, 2000; Markovic et al., 2001; Floyd et al., 2008) and virus-cell binding can be mediated by as little as one HA. However, the investigation of HA reconstituted in vesicles suggests that single HA trimers can mediate fusion as well (Imai et al., 2006). In this scenario, fusion inhibition is expected to be as strong as binding reduction. Stronger fusion inhibition, as shown in this study, indicates the presence of a minimal HA aggregate size to initiate fusion, supporting the cooperativity model. Virus binding to inhibitor nanoparticles blocks a subset of HA trimers that cannot engage in fusion.

Fusion inhibition was less pronounced for the higher dF PG 5. This supports the described hypothesis of charge repulsion leading to sparser packing of PG on the virus surface. This would allow some of the HA trimers to form functional complexes that can mediate fusion.

To successfully infect a cell, the virus needs to enter the host cell, fuse with the endosome and deliver its genomic material. The PG effect on these first steps of infection until NP production was tested for one of the small PGs and compared with the larger PG 4. The larger PG 4 inhibited infection by 80 %, while the smaller PG reduced it by 40 %. The effect was less pronounced than expected from fusion inhibition. However, it has to be considered that the fusion as observed by R18 de-quenching is the results of the fusion activity of an ensemble of viruses. In this fusion assay, 5 % remaining activity still means thousands of viruses. Genome delivery of a few viruses may suffice to render a cell infected in the immunostaining assay.

4.4.3 Gold nanoparticles as tools for imaging-activity-correlation

To study multivalency, gold nanoparticles have a crucial advantage compared to polyglycerol: their high contrast in transmission electron microscopy (TEM). The application of SA functionalized gold particles permits a new type of molecular imaging-activity correlation. Gold particles with a diameter of 2 and 14 nm were first tested for their binding capacity to HA. Gold nanoparticles quench organic fluorophores in a distance dependent manner by a mechanism that is not yet fully understood (Schneider et al., 2006; Hazarika et al., 2006). These properties were used to quench the emission of YFP tagged to HA expressed in CHO cells (Fig. 3.15). This experiment showed that the particles indeed specifically bind to HA, but that the binding was very weak as a single washing step almost eliminated the effect. However, binding was verified by hemagglutination inhibition (HAI), where the particles were found to be still effective in the low nM range (particle concentration). This corresponds to a SA concentration of 10-50 µM, a very high value compared to other studies where HAI was achieved with nM or pM SA concentrations (Spaltenstein and Whitesides, 1991; Mammen et al., 1995). This difference could be explained by the tight packing of ligands on the particle surface. Unfortunately, the ligand density could not be controlled and the gold nanoparticles were found to be constantly fully coated. This reduces flexibility and accessibility of each ligand and results in high negative surface charge, possibly reducing virus binding.
Inhibition of agglutination was achieved only by using the 14 nm particles, while the smaller 2 nm colloids had no effect (Fig. 3.14). The failure of the 2 nm particles to inhibit hemagglutination is possibly due to their binding architecture. The diameter of an HA trimer is about 7 nm and thus the smaller 2 nm particles can not bind to multiple trimers. This binding mode was verified by TEM, showing clearly that the 2 nm particles can only bind one trimer, while the larger particles can be connected to approximately 3-5 trimers.

4.4.4 Relevance and optimization of multivalent inhibitors

Due to the multivalent interaction between virus and cell surface, the virus effectively never unbinds, even if single HA-SA connections are opened and closed at high frequency. This proposed binding mechanism is based on SVFS and whole-cell measurements performed in this study. It was the idea to mimic this situation by using nanoparticles exposing multiple copies of SA on their surface. Via combined competitive binding and steric stabilization of the complex, viruses can efficiently be trapped before they can engage with cell surface receptors.
Earlier studies often faced high cytotoxicity and were limited to hemagglutination inhibition (Spaltenstein and Whitesides, 1991; Mammen et al., 1995). In the present study, it was shown that the used particles are biocompatible and efficiently inhibit infection of MDCK cells. As described in section 1.4.2, SA is involved in a variety of host interactions. The studied nanoparticles might therefore be used to inhibit other pathogens as well. Targeting Siglecs was shown before to control B-cell regulation (Courtney et al., 2009), thereby suggesting another possible application for SA-conjugated PGs. Mouse models could be used to evaluate the effect of PGs on influenza infection *in vivo* as demonstrated for PAMAM dendrimers (Landers et al., 2002). Sulfated PGs were recently shown to inhibit inflammation *in vivo* (Dernedde et al., 2010).
However, sialic acid is involved in many signaling pathways (as described in 1.4.2) and could produce unwanted side effects. Recent publications therefore suggested alternatives for SA, possibly avoiding SA-related side effects. For example, several studies used HA-targeting peptides that bind efficiently to HA and inhibit infection (Rajik et al., 2009; Nicol et al., 2012; Matsubara et al., 2010). The use of a more complex sugar such as sialyllactose could increase the affinity and thus lower the required amount of inhibitor. A disadvantage of this approach would be the susceptibility against digestion by NA, which would inactivate the inhibitor. However, this links to another concept which was introduced by Choi *et al.* (Choi et al., 1996). Here monomeric NA inhibitors were used to bind NA in addition to HA. This synergistic binding of two ligands enhanced the steric stabilization of the virus-inhibitor complex.

4.5 Intracellular traf cking of influenza A viruses

4.5.1 Spatio-temporal characterization of intracellular fusion

The initial part of influenza A virus infection was studied to identify and characterize potential targets for antiviral therapy. Some major steps of cell entry are already well described (Lakadamyali et al., 2004). It was shown that the virus is internalized predominantly via clathrin-mediated endocytosis (Rust et al., 2004), but can also infect in the absence of clathrin (Sieczkarski and Whittaker, 2002b). Moreover, macropinocytosis (de Vries et al., 2011; Rossman et al., 2012)

and also entry via caveolae (Nunes-Correia et al., 2004) were shown to mediate virus entry into the host cell.

Live cell imaging in combination with single particle tracking provided important insights into the dynamics of cell entry and trafficking. It was shown that the virus is rapidly transported along microtubules while quickly passing Rab5-positive early endosomes (after 5 min) to co-localize with Rab5 and Rab7 on maturing endosomes (multivesicular bodies), where most of the fusion events where detected (Lakadamyali et al., 2006). These findings could be confirmed in this study. The combination of intracellular fusion and co-localization confocal microscopy shows that viruses quickly progress along the endosomal system and that indeed, the majority of fusion events happen between 5 and 20 min, which corresponds to localization in maturing endosomes (see 3.7.1). Although it is technically demanding to study the first 10 min with high time resolution, it could be shown that intracellular virus fusion started almost immediately and even occurs in early endosomes (see Fig. 3.20). Early endosomes have a lumenal pH of 6.1 - 6.8 (Huotari and Helenius, 2011), which is higher than the optimal fusion pH of influenza A/X-31 (Korte et al., 1999). However, virus-ghost fusion showed a clear onset of fusion at a pH slightly above 6, which would enable fusion with early endosomes (Fig. 3.25). Notably, the R18 de-quenching assay primarily detects lipid mixing, which is the first step of membrane fusion (hemifusion, Harrison (2008); Floyd et al. (2008)). The onset of content mixing (i.e. viral genome release) happens at slightly lower pH values (Chernomordik et al., 1998). The endosomal system is highly dynamic and thus the endosomal pH also underlies some variation. The low number of fusion events within early endosomes and the low virus-ghost fusion at pH above 6 further suggest that early endosomes are not the preferred localization of fusion for the virus.

Nocodazole treatment was shown to have a strong effect on influenza virus infection. The drug interferes with microtubule polymerization, which leads to missorting (Lakadamyali et al., 2006) and inhibits intracellular virus transport (Lakadamyali et al., 2003). After nocodazole treatment, a random sorting of viruses into different types of early endosomes was observed, some of which may not progress towards the lysosomal pathway (Lakadamyali et al., 2006). This suggests a strong effect of nocodazole on virus fusion and infection.

Indeed, it could be shown that the drug strongly inhibits virus infection and this correlates with reduced fusion kinetics (Fig. 3.23). Since the fusion kinetics represent the sum of many fused viruses, there are at least two reasons explaining the inhibitory effect on virus fusion: (1) Either less viruses undergo fusion or (2) the area of endosomal membrane that is available for the dilution of viral envelope-bound R18 is smaller. To test these hypotheses, virus fusion events after nocodazole treatment were quantified. The number of fused viruses was similar in nocodazole treated and control cells (Fig. 3.22). In addition, the localization of fusion events was categorized and scored as either peripheral or perinuclear (PNR). In untreated cells, the majority

of fusion events were perinuclear as expected from Lakadamyali et al. (2003) and Sakai et al. (2006). This is in line with the observation that cargo bound for degradation (i.e. taking the lysosomal route) also travels towards the cell center (Baravalle et al., 2005; Bayer et al., 1998). Interestingly, this accumulation was lost after nocodazole treatment (Fig. 3.22). Taken together, this indicates that after nocodazole treatment the number of fusion events is not reduced but the resulting de-quenching is less pronounced. This could be explained by fusion with early endosomes, which are smaller than late endosomes (Rink et al., 2005) and thus only allow reduced de-quenching, i.e. dilution of the fluorophore R18.
Nocodazole was further shown to increase the pH in transferrin-loaded but not in dextran-loaded endosomes (Baravalle et al., 2005). In the case of transferrin, the drug prevented only the second phase of acidification happening in perinuclear recycling compartments (PNRC), leaving the first phase of acidification in early endosomes unchanged (Baravalle et al., 2005). After exiting early endosomes, influenza viruses do not travel towards perinuclear recycling compartments, but rather take the lysosomal route towards late endosomes. This suggests that the pH encountered by the virus during trafficking should not be affected by nocodazole (Bayer et al., 1998).
In summary, influenza viruses quickly travel through the endo-/lysosomal system, mostly fuse in maturing endosomes and reach the perinuclear region after 10 - 20 min. Interference with the microtubule disrupting drug nocodazole leads to randomly localized but equally numbered fusion events compared to untreated cells. Fusion kinetics show reduced de-quenching possibly due to fusion with smaller endosomes that have not yet matured to late endosomes. Nocodazole treatment further drastically decreases infection, suggesting a correlation of the localization of fusion with the success of infection. Hence, it is important for the virus to reach the perinuclear region before the pH decreases below the threshold necessary to trigger fusion.

4.5.2 Influenza virus can delay the endosomal acidi cation to optimize the localization of fusion and genome release.

Technical considerations

Due to fast endosomal transport, the localization of fusion critically depends on the acidification kinetics inside the endosome. To assess the pH on the single endosome level, fluorescent indicators were co-internalized with labeled viruses and their signal was followed over 30 min. This type of measurement has some critical aspects. The pH-sensitive spectral properties of the fluorophore must be calibrated in order to deduce the pH from the fluorescence intensity. To this end, endosomes were loaded with labeled dextran followed by an incubation step in pH standard buffers on ice. During this step the pH is equilibrated and ATP is depleted to avoid

further influence of the proton pumps. The addition of proton ionophores allows equilibration of all internal compartments. This is a widely used standard procedure to calibrate pH (in)sensitive fluorophore pairs in cells considering the intracellular pH to be equal to the extracellular standard medium (Brabec et al., 2005; Bayer et al., 1998; Baravalle et al., 2005).
However, in a live-cell measurement other factors could be involved and change the spectral properties of the fluorophore. The different amounts of endosomal loading can be deduced from intensity differences and can be explained by differently sized endosomes. In addition, components of the extracellular cell culture medium might also change the endosomal environment and could lead to changed buffering capacities of the endosome or directly interfere with the spectral properties of the fluorophore (Han and Burgess, 2010). Due to these problems, instead of co-internalization, direct coupling of the pH sensor to the virus might reduce the experimental background (Lakadamyali et al., 2006, 2003). Other fluorescent indicators like the GFP variants E^2 GFP (Bizzarri et al., 2006) or pHRed (Tantama et al., 2011) allow to asses the pH from ratiometric or fluorescence lifetime imaging and thus reduce the experimental system to only one fluorophore.
Lastly, the size of an endosome itself underlies some variability. For example, small endosomes ($d = 200nm$) have only a volume of $V = 4.2 \quad 10 \quad ^{18}l$. Consequently, at pH 6, this corresponds to 2.5 protons and to 0.5 protons at pH 7 respectively. As described by Sakai *et al.* (Sakai et al., 2006) the endosomal pH must be considered very carefully and is subjected to the described variations which were also observed in this study and resulted in significant scattering of the data (see Fig. 3.26). Considering the pH as an ensemble property, the application of this parameter to the endosomal situation remains questionable. Thus, it might be beneficial to assess only qualitative differences rather than pH values as done by Murakami *et al.* (Murakami et al., 2012). However, in the present study pH values were calculated being aware of the problems outlined above.

Influenza virus delays the endosomal acidi cation. Implications for ef cient infection.

By determining pH values of single endosomes with and without a loaded virus, it was possible to show for the first time that the presence of an influenza virus has an effect on the acidification of the surrounding endosome. During the first 15 minutes post infection, the virus leads to a retarded pH decrease compared to the uninfected control (Fig. 3.26). To correlate these results with intracellular fusion and endosomal localization, Fig. 4.3 shows a summary of the early events during influenza A virus infection characterized in this study. Measurements of fusion and pH are accompanied by accumulation kinetics of viral NP inside the nucleus [2]. It should be

[2] These data were produced during a practical course under my guidance, but represent only one measurement and where thus not presented in the results section.

noted that at this early stage of infection (30 min) the detected NP corresponds to NP brought inside the cell by the infecting virus and does not include newly produced protein.
The graph shows that fusion starts early and overlaps with early endosomal localization. Most fusion events occur between 5 and 20 min, localized in maturing endosomes. In this period, the presence of the virus has the strongest effect on the endosomal pH compared to the control. It is followed by NP accumulation inside the nucleus after 10 - 15 min. During this time, the endosomal pH drops from 7 to 6, which according to Fig. 3.25 would only allow very limited fusion. It must thus be concluded that the actual endosomal pH is lower but can not be detected with high accuracy due to technical reasons mentioned before.
One hypothesis that emerges from these results is that the virus buffers the endosomal pH by proton binding to viral components. Regarding the size of an endosome, an internalized virus represents a remarkably high protein concentration (100 mg/ml for a 200 nm endosome). Not only the dense layer of spike proteins but rather internal components such as M1, NP and RNA provide a high buffering capacity (David Holcman, Thibault Lagache personal communication). This is promoted by the simultaneous opening of the M2 proton channel (Leiding et al., 2010), allowing protons to enter the virus interior and bind to a large pool of RNA and proteins. This strategy enables the virus to reach locations close to the nucleus before the pH for efficient fusion is reached and, hence, before fusion is triggered. Accordingly, disruption of microtubule associated transport and by-pass experiments lead to strongly reduced infection.
About the reason for the observed reduction of infection in the presence of nocodazole can only be speculated. If fusion occurs more distant to the nucleus, the probability that the viral genome becomes a target of cellular defense mechanisms before reaching the nucleus may increase. An underlying mechanism could be the recognition of vRNA by the RNA helicase RIG-I, which leads to activation of transcription factors IRF3 and/or IRF7 and subsequent induction of interferon / genes (Ludwig et al., 2006). Other viral proteins including NP, M1 and HA within the cytoplasm activate nuclear factor B (NF- B) via activation of I B kinase 2 (IKK2) (Ludwig et al., 2006). This as well leads to interferon induction and apoptosis. Thus, mechanisms of the cellular innate immune response suggest that premature virus fusion negatively influences virus infection. On the other hand, if viruses fail to fuse, they reach lysosomal compartments and get degraded. In this case, endosomal Toll-Like receptors TLR3 and 7 recognize vRNA and as well induce interferon response (Diebold et al., 2004).
However, these hypotheses remain to be verified experimentally, but some recent studies support the conclusion that time and localization of fusion are important determinants for virus infection. The stability of HA controls the pH threshold of the conformational change (Rachakonda et al., 2007) and thereby could affect intracellular fusion. This suggest a correlation between HA stability and infectivity as revealed by some recent studies (Murakami et al., 2012; Imai

et al., 2012; DuBois et al., 2011). Hence, HA stability must be optimized to allow extracellular stability of the virus as well as to control the intracellular time and localization of fusion and genome release.

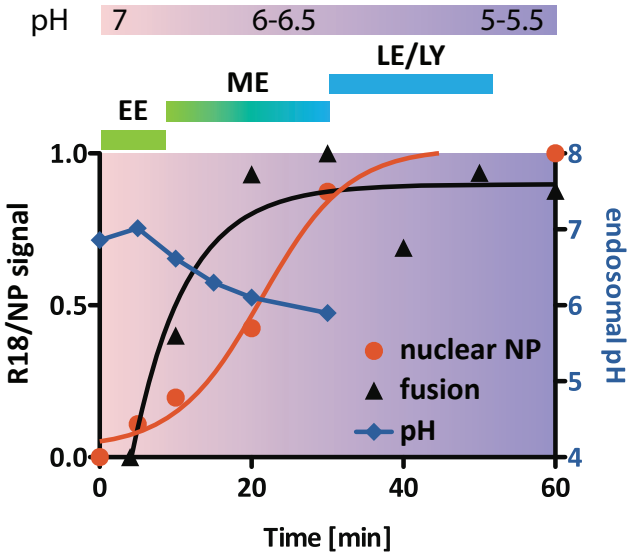

Figure 4.3: Summary of the early events during influenza A virus infection characterized in this study. The plot correlates the kinetics of pH acidification with those of fusion and nuclear NP accumulation. The graph shows that fusion starts early and overlaps with EE localization. Most fusion events occur between 5 and 20 min, localized in ME. In this period, the presence of the virus has the strongest effect on the endosomal pH compared to the control. It is followed by NP accumulation inside the nucleus after 10 - 15 min. The localization of the virus within the endo-/lysosomal system is shown above the graph. EE, early endosome; ME, maturing endosome; LE, late endosome; LY, lysosome; NP, nucleo protein

4.5.3 Influenza A/X-31 virus must travel through early and late endosomes to ensure successful infection.

Uncoating of influenza virus includes dissociation of the M1 protein layer, fusion of viral with endosomal membrane and release of the viral vRNPs into the cytoplasm. As mentioned above, the onset of fusion is preceded by opening of the viral proton channel M2 (Leiding et al., 2010). A possible uncoating mechanism was already proposed in 1992 (Helenius, 1992a) following the identification of M2 as a channel for monovalent cations (Pinto et al., 1992). The inhibitory activity of amantadine was known before and the drug was shown to inhibit an early step of influenza virus infection (Skehel et al., 1978). Ever since it has been speculated about the uncoating process and it was assumed that acidification of the viral lumen by M2 proton transport supports virus uncoating possibly by subsequent dissociation of the M1 layer (Webster et al., 1992; Whittaker, 2001). It was shown that M1 separates from vRNPs after release into the

cytoplasm and that vRNPs travel into the nucleus without M1 (Martin and Helenius, 1991a). Overexpression of M1 causes binding of M1 to vRNPs, inhibiting their nuclear transport. This can be reversed by acidification of the cytoplasm and results in rescued nuclear targeting of vRNPs (Bui et al., 1996). These results together with the reported pH-dependent dissociation of M1 (Zhang et al., 2012) resulted in the current model of influenza uncoating. However, the sequence of the uncoating events which presumably depends on virus residence in early and late endosomes (Sieczkarski and Whittaker, 2003) has not been uncovered.

The ability of the virus to delay the endosomal pH decrease raised the question whether the subacidic pH present in early endosomes is also necessary for virus uncoating. In order to study the importance of early endosomal residence, by-pass experiments were conducted in which the virus was pre-incubated at a defined pH before fusion was triggered with low pH buffer. Pre-incubation at neutral pH simulates direct late endosomal localization without transit through early endosomes. Here M1 co-localized in clusters with NP, which indicates that both proteins do not separate after release into the cytoplasm. A similar result was found in electron microscopy studies (Fontana et al., 2012; Calder et al., 2010). While at neutral pH, the M1 layer and vRNPs can be detected inside the virus, these structures are replaced by a coagulate after short incubation at pH 4.9. The coagulate is not present at pH 7 and it does not co-localize in virions with M1 and vRNPs, suggesting that the coagulate is made of vRNP and M1 (Fontana et al., 2012). In these clusters vRNPs may no longer be accessible for virus reproduction. This could be an additional explanation for the loss of infectivity after acid by-pass, described in 3.7.3 and discussed above. However, the observation was different when the virus was pre-incubated at pH 6 before fusion was triggered by low-pH treatment. In this case, the cytosolic M1 and NP signals were higher and less M1-NP clusters were observed (Fig. 3.28). This indicates that although low pH leads to dissociation of M1 and NP as shown by Zhirnov (1992) and Bui et al. (1996) subacidic pH seems to be more favorable for this process and thus renders early endosomes residence essential for efficient virus infection. Quantification of cytosolic M1 showed that the signal was indeed higher when the virus was pre-treated with subacidic pH buffer simulating early endosomes (Fig. 3.29). Accordingly, when the acidification of the virus lumen was blocked by amantadine the effect was reduced and acid by-pass resulted in M1/NP clusters (Fig. 3.28).

4.5.4 Model for the stepwise uncoating of influenza A virus

From these results, a sequential model for the uncoating of influenza virus can be concluded. The model is summarized in Fig. 4.4. Following entry, the virus quickly reaches early endosomes with subacidic pH, which leads to opening of M2 (Leiding et al., 2010) and acidification of the viral lumen. Viral components inside the virus such as vRNA and proteins bind a signif-

icant amount of protons, leading to a delayed endosomal acidification. M1-M1 and M1-vRNP contacts are loosened during this step (Zhirnov, 1992; Ye et al., 1999). The dissociation and eventual collapse of M1 must be controlled. The virus has to make sure that vRNPs detach from M1, before both coagulate at acidic pH (Li and Sieben *et al.*, submitted). This might be a slow process and benefit from the delayed endosomal acidification. Another positive consequence of this delay is that viruses are further transported towards the nucleus before fusion is triggered, thereby decreasing the distance for the vRNPs to travel. Endosome by-pass experiments presented here show that fusion close to the nucleus leads to increased infection efficiency. Subsequently at acidic pH, HA initiates fusion, reaching a maximum at pH 5 - 5.5, corresponding to the pH of late endosomes. At this stage M1 appears monomeric and fully separated from vRNP. The released vRNPs immediately travel into the nucleus (Bui et al., 1996).

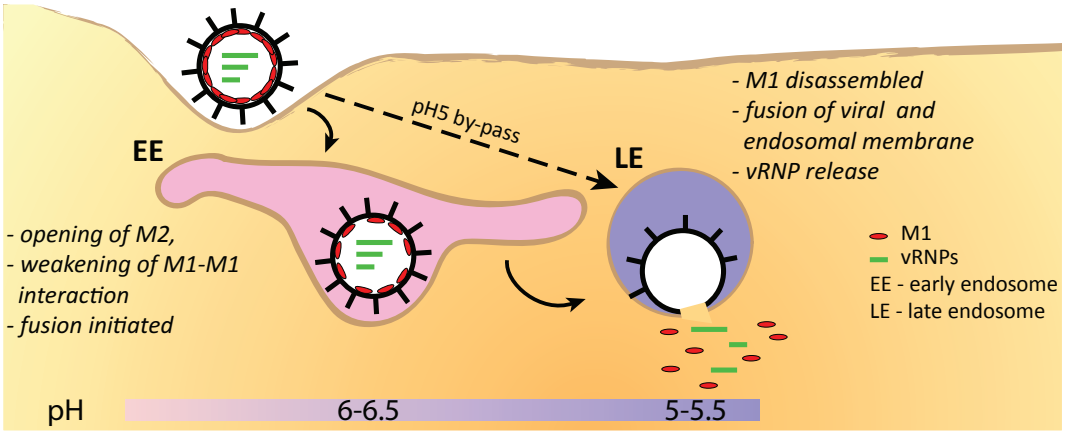

Figure 4.4: Model for the stepwise uncoating of influenza A virus (adapted from Li and Sieben *et al.*, submitted.)

4.6 Conclusion and Outlook

The binding of influenza virus to red blood cells and of HA to sialic acid is known for a long time. However, only recently many studies showed that virus-cell binding and subsequent entry is not well understood (see section 4.3.2). It was the aim of this thesis to characterize influenza virus-cell binding and entry in order to understand these important steps of virus infection as well as to provide the basis for the design of virus inhibitors. Virus-cell binding was studied using OT- and AFM-based single virus force spectroscopy (SVFS). It could be shown that the structure of the cell surface rather than the receptor itself strongly influences receptor and cell binding. The results reveal a new concept of virus specificity. According to this concept, virus specificity can be investigated on different complexity levels. By choosing a specialized technique in combination with the corresponding sample preparation, receptor and cell specificities can be studied with very high accuracy. However, as discussed above the results may not be directly comparable. Only SVFS allows to study single virus-cell binding directly on the living cell surface. For SVFS, it will be a future goal to use primary human lung explants or primary cell cultures as previously shown by Weinheimer et al. (2012). In this way, different regions and cells of the respiratory tract can be directly compared, without using model cell systems.

The obtained results were translated into the design of multivalent inhibitory nanoparticles. These were evaluated using assays to study HA-related virus activity, such as virus-cell binding and fusion. The inhibitory nanoparticles were shown to reduce virus activity by 80 %, leaving only a small fraction of infective viruses. The particles were designed to mimic the host cell surface and provide a multivalent high avidity alternative for the virus to bind. Inhibition was shown to depend on the size of the particle and the density of functional SA residues that can engage in virus binding. This implies that in order to find the optimal arrangement of SA on an inhibitory particle one first has to understand the binding architecture on the host cell surface. Atomic force in combination with super-resolution microscopy techniques can provide the basis to characterize the ultrastructure of the cells glycocalyx. Receptor microdomains as suggested by Nunes-Correia et al. (1999) could be identified and help to understand the signals necessary for the virus to trigger endocytosis after binding.
The inhibitory activity of the particles could further be improved by using ligands that bind other parts of influenza HA. Peptides or aptamers targeting the stem region could work as functional inhibitors and prevent HAs conformational change. These ligands are also promising alternatives due to their high biocompatibility without side effects as potentially produced by sialic acid. Heterofunctionalized nanoparticles could provide increased inhibitory activity by targeting both influenza virus spike proteins, HA and NA. Recently, a multivalent presentation of the

influenza NA inhibitor zanamivir was shown to block influenza virus infection in early as well as in late stages of infection (Lee et al., 2012).

Upon Endocytosis, the virus quickly travels through the endosomal system to eventually fuse in the perinuclear region. During this endosomal transport, the virus stabilizes the lumenal pH of the endosome in order to delay its own fusion. Only fusion close to the nucleus allows efficient infection. This could be shown by using specific drugs and an acid-induced by-pass of endocytosis. If the viruses fail to fuse in the perinuclear region, infection is strongly reduced. The reason for this observation remains to be investigated. One hypothesis is that premature fusion and vRNP release lead to degradation of the viral genome and attraction of the cellular innate immune response. Single virus tracking in combination with fluorescent labeling of NP would allow to investigate this hypothesis by studying the lifetime of vRNPs in the cytoplasm after fusion. In parallel, elements of the cellular immune response such as interferon induction could be studied. In addition, the consequences of early and late fusion could be nicely investigated using pH-stability variants of HA (Rachakonda et al., 2007) in combination with an intracellular fusion assay and infection markers. In this case the pH stability of HA can be increased or decreased to force early or late fusion respectively.

It was further found that the virus must travel through early and late endosomes to efficiently uncoat and deliver its genomic material. The requirement of early and late endosomal residence was known before (Sieczkarski and Whittaker, 2003), but the sequence of the uncoating events was only hypothesized. Here it could be shown that the direct late endosomal localization would render the virus inactive, presumably due to aggregation of M1 with vRNPs. Hence, the virus must travel through subacidic compartments (early endosomes). From these results a sequential model for the uncoating of influenza virus was concluded. The model offers some possible targets for future antiviral approaches. For example, it was shown in the present study that time and localization of fusion are critical for the success of virus infection. Hence, interference with endosomal acidification or transport could impede virus infection. Further, the relevance of early endosomal compartments will be studied by using siRNA silencing of the endosomal regulator proteins Mon1a/b. These proteins were shown to control the maturation from early to late endosomes (Poteryaev et al., 2010) and their knock-down would allow to study early endosomes decoupled from maturation.

Appendix

Abbreviations

AA	amino acids
AFM	atomic force microscopy
AFS	atomic force spectroscopy
AuNP	gold nanoparticle
BCA	bicinchoninic acid
BD	Becton Dickinson
CCP	clathrin coated pit
CHO	chinese hamster ovary
CME	clathrin-mediated endocytosis
cryo-TEM	cryogenic transmission electron microscopy
DC-SIGN	dendritic cell-specific intercellular adhesion molecule-3-grabbing non-integrin
DF	degree of functionalization
DIC	differential interference contrast
DMEM	Dulbecco s modified eagle medium
DMSO	Dimethyl sulfoxide
DPBS	Dulbecco s phosphate buffered saline
EDTA	Ethylenediaminetetraacetic acid
EE	early endosomes
EGF	epidermal growth factor
ER	endoplasmic reticulum
FITC	Fluoresceinisothiocyanat
FRET	Foerster resonance energy transfer
GISRS	Global Influenza Surveillance and Response System
HA	hemagglutinin
HAI	Hemagglutination inhibition assay
HEPES	4-(2-hydroxyethyl)-1-piperazineethanesulfonic acid
HIV	human immonodeficiency virus
HRV	human rhinovirus
IFN	interferon

IKK2	I B kinase 2
kDa	kilo Dalton
L-SIGN	Liver/lymph node-specific intercellular adhesion molecule-3-grabbing non-integrin
LE	Late endosomes
MAA	*Maachia amurensis* agglutinin
MDCK	madin darby canine kidney
MES	morpholineethanesulfonic acid
MVB	Multivesicular bodies
MW	molecular weight
NaCl	natrium chloride
NF- B	nuclear factor B
NIH	National Institutes of Health
nm	nano meter
NP	nucleo protein
OT	optical tweezers
PBS -/-	phosphate buffered saline without CaCl and MgCl
PBS +/+	phosphate buffered saline with CaCl and MgCl
PG	polyglycerol
PI	Propidium iodide
pN	pico newton
PNR	perinuclear region
PNRC	perinuclear recycling compartments
PS	polystyrene
QPD	quadrant photo diode
R18	octadecylrhodamine B
RBC	red blood cell
RBS	receptor binding site
RBS	receptor binding site
Rho	Rhodamine
RKI	Robert Koch Institute
RT	room temperature
SA	sialic acid

SDS	sodium dodecyl sulfate
SDS-PAGE	sodium dodecyl sulfate polyacrylamide gel electrophoresis
SEM	scanning electron microscopy
SL	sialyllactose
SMFS	single molecule force spectroscopy
SNA	*Sambucus nigra* agglutinin
SVFS	single virus force spectroscopy
TEM	transmission electron microscopy
TLR	Toll-like receptor
WGA	wheat germ agglutinin
WHO	World Health Organization
YFP	yellow fluorescent protein

Bibliography

A. Ali, R. T. Avalos, E. Ponimaskin, and D. P. Nayak. Influenza virus assembly: effect of influenza virus glycoproteins on the membrane association of m1 protein. *J Virol*, 74(18): 8709–19, Sep 2000.

M. J. Amorim, E. A. Bruce, E. K. C. Read, A. Foeglein, R. Mahen, A. D. Stuart, and P. Digard. A rab11- and microtubule-dependent mechanism for cytoplasmic transport of influenza a virus viral rna. *J Virol*, 85(9):4143–56, May 2011. doi: 10.1128/JVI.02606-10.

M. Arya, A. B. Kolomeisky, G. M. Romo, M. A. Cruz, J. A. López, and B. Anvari. Dynamic force spectroscopy of glycoprotein ib-ix and von willebrand factor. *Biophys J*, 88(6):4391–401, Jun 2005. doi: 10.1529/biophysj.104.046318.

A. Ashkin. Acceleration and Trapping of Particles by Radiation Pressure. *Physical Review Letters*, 24(4):156–159, 1970.

A. Ashkin and J. M. Dziedzic. Optical trapping and manipulation of viruses and bacteria. *Science*, 235(4795):1517–20, Mar 1987.

H. P. Babcock, C. Chen, and X. Zhuang. Using single-particle tracking to study nuclear trafficking of viral genes. *Biophys J*, 87(4):2749–58, Oct 2004. doi: 10.1529/biophysj.104.042234.

Y. Balabanova, A. Gilsdorf, S. Buda, R. Burger, T. Eckmanns, B. Gärtner, U. Groß, W. Haas, O. Hamouda, J. Hübner, T. Jänisch, M. Kist, M. H. Kramer, T. Ledig, M. Mielke, M. Pulz, K. Stark, N. Suttorp, U. Ulbrich, O. Wichmann, and G. Krause. Communicable Diseases Prioritized for Surveillance and Epidemiological Research: Results of a Standardized Prioritization Procedure in Germany, 2011. *PLoS ONE*, 6(10):e25691, Oct. 2011.

G. Baravalle, D. Schober, M. Huber, N. Bayer, R. F. Murphy, and R. Fuchs. Transferrin recycling and dextran transport to lysosomes is differentially affected by bafilomycin, nocodazole, and low temperature. *Cell and tissue research*, 320(1):99–113, Apr. 2005.

N. Bayer, D. Schober, E. Prchla, R. F. Murphy, D. Blaas, and R. Fuchs. Effect of bafilomycin A1 and nocodazole on endocytic transport in HeLa cells: implications for viral uncoating and infection. *Journal of Virology*, 72(12):9645–9655, Dec. 1998.

J. Beigel and M. Bray. Current and future antiviral therapy of severe seasonal and avian influenza. *Antiviral Res*, 78(1):91–102, Apr 2008. doi: 10.1016/j.antiviral.2008.01.003.

G. I. Bell. Models for the specific adhesion of cells to cells. *Science (New York, NY)*, 200(4342): 618–627, May 1978.

J. Bentz. Minimal aggregate size and minimal fusion unit for the first fusion pore of influenza hemagglutinin-mediated membrane fusion. *Biophysical Journal*, 78(1):227–245, 2000.

R. Bizzarri, C. Arcangeli, D. Arosio, F. Ricci, P. Faraci, F. Cardarelli, and F. Beltram. Development of a novel GFP-based ratiometric excitation and emission pH indicator for intracellular studies. *Biophysical Journal*, 90(9):3300–3314, May 2006.

O. Björnham, J. Bugaytsova, T. Borén, and S. Schedin. Dynamic force spectroscopy of the Helicobacter pylori BabA-Lewis b Binding. *Biophysical chemistry*, Mar. 2009a.

O. Björnham, H. Nilsson, M. Andersson, and S. Schedin. Physical properties of the specific papg-galabiose binding in e. coli p pili-mediated adhesion. *Eur Biophys J*, 38(2):245–54, Feb 2009b. doi: 10.1007/s00249-008-0376-y.

O. Blixt, S. Head, T. Mondala, C. Scanlan, M. E. Huflejt, R. Alvarez, M. C. Bryan, F. Fazio, D. Calarese, J. Stevens, N. Razi, D. J. Stevens, J. J. Skehel, I. van Die, D. R. Burton, I. A. Wilson, R. Cummings, N. Bovin, C.-H. Wong, and J. C. Paulson. Printed covalent glycan array for ligand profiling of diverse glycan binding proteins. *Proc Natl Acad Sci U S A*, 101 (49):17033–8, Dec 2004. doi: 10.1073/pnas.0407902101.

C. Böttcher, K. Ludwig, A. Herrmann, M. van Heel, and H. Stark. Structure of influenza haemagglutinin at neutral and at fusogenic ph by electron cryo-microscopy. *FEBS Lett*, 463 (3):255–9, Dec 1999.

N. M. Bouvier and P. Palese. The biology of influenza viruses. *Vaccine*, 26 Suppl 4:D49–53, Sep 2008.

M. Brabec, D. Schober, E. Wagner, N. Bayer, R. Murphy, D. Blaas, and R. Fuchs. Opening of size-selective pores in endosomes during human rhinovirus serotype 2 in vivo uncoating monitored by single-organelle flow analysis. *Journal of Virology*, 79(2):1008, 2005.

M. Bui, G. Whittaker, and A. Helenius. Effect of M1 protein and low pH on nuclear transport of influenza virus ribonucleoproteins. *Journal of Virology*, 70(12):8391–8401, Dec. 1996.

L. J. Calder, S. Wasilewski, J. A. Berriman, and P. B. Rosenthal. Structural organization of a filamentous influenza A virus. *Proceedings of the National Academy of Sciences of the United States of America*, May 2010.

M. Calderón, M. A. Quadir, S. K. Sharma, and R. Haag. Dendritic polyglycerols for biomedical applications. *Advanced materials (Deer eld Beach, Fla.)*, 22(2):190–218, Jan. 2010.

I. Carlescu, D. Scutaru, M. Popa, and C. V. Uglea. Synthetic sialic-acid-containing polyvalent antiviral inhibitors. *Medicinal Chemistry Research*, 18(6):477–494, July 2009.

A. F. Carlin, S. Uchiyama, Y.-C. Chang, A. L. Lewis, V. Nizet, and A. Varki. Molecular mimicry of host sialylated glycans allows a bacterial pathogen to engage neutrophil siglec-9 and dampen the innate immune response. *Blood*, 113(14):3333–6, Apr 2009. doi: 10.1182/blood-2008-11-187302.

C. M. Carr and P. S. Kim. A spring-loaded mechanism for the conformational change of influenza hemagglutinin. *Cell*, 73(4):823–32, May 1993.

C. M. Carr, C. Chaudhry, and P. S. Kim. Influenza hemagglutinin is spring-loaded by a metastable native conformation. *Proc Natl Acad Sci U S A*, 94(26):14306–13, Dec 1997.

C. Cecconi, E. A. Shank, F. W. Dahlquist, S. Marqusee, and C. Bustamante. Protein-DNA chimeras for single molecule mechanical folding studies with the optical tweezers. *European biophysics journal : EBJ*, 37(6):729–738, July 2008.

M. I. Chang, P. Panorchan, T. M. Dobrowsky, Y. Tseng, and D. Wirtz. Single-molecule analysis of human immunodeficiency virus type 1 gp120-receptor interactions in living cells. *Journal of Virology*, 79(23):14748–14755, Dec. 2005.

A. Chen and V. T. Moy. Cross-linking of cell surface receptors enhances cooperativity of molecular adhesion. *Biophys J*, 78(6):2814–20, Jun 2000. doi: 10.1016/S0006-3495(00)76824-X.

C. Chen and X. Zhuang. Epsin 1 is a cargo-specific adaptor for the clathrin-mediated endocytosis of the influenza virus. *Proceedings of the National Academy of Sciences of the United States of America*, 105(33):11790–11795, Aug. 2008.

J. Chen, S. A. Wharton, W. Weissenhorn, L. J. Calder, F. M. Hughson, J. J. Skehel, and D. C. Wiley. A soluble domain of the membrane-anchoring chain of influenza virus hemagglutinin (ha2) folds in escherichia coli into the low-ph-induced conformation. *Proc Natl Acad Sci U S A*, 92(26):12205–9, Dec 1995.

L. V. Chernomordik, V. A. Frolov, E. Leikina, P. Bronk, and J. Zimmerberg. The pathway of membrane fusion catalyzed by influenza hemagglutinin: restriction of lipids, hemifusion, and lipidic fusion pore formation. *The Journal of cell biology*, 140(6):1369–1382, Mar. 1998.

R. A. Childs, A. S. Palma, S. Wharton, T. Matrosovich, Y. Liu, W. Chai, M. A. Campanero-Rhodes, Y. Zhang, M. Eickmann, M. Kiso, A. Hay, M. Matrosovich, and T. Feizi. Receptor-binding specificity of pandemic influenza a (h1n1) 2009 virus determined by carbohydrate microarray. *Nat Biotechnol*, 27(9):797–9, Sep 2009. doi: 10.1038/nbt0909-797.

S. K. Choi, M. Mammen, and G. M. Whitesides. Monomeric inhibitors of influenza neuraminidase enhance the hemagglutination inhibition activities of polyacrylamides presenting multiple C-sialoside groups. *Chemistry & biology*, 3(2):97–104, Feb. 1996.

V. C. Chu and G. R. Whittaker. Influenza virus entry and infection require host cell n-linked glycoprotein. *Proc Natl Acad Sci U S A*, 101(52):18153–8, Dec 2004. doi: 10.1073/pnas.0405172102.

B. E. Collins and J. C. Paulson. Cell surface biology mediated by low affinity multivalent protein–glycan interactions. *Current Opinion in Chemical Biology*, 8(6):617–625, Dec. 2004.

C. S. Copeland, R. W. Doms, E. M. Bolzau, R. G. Webster, and A. Helenius. Assembly of influenza hemagglutinin trimers and its role in intracellular transport. *J Cell Biol*, 103(4):1179–91, Oct 1986.

C. S. Copeland, K. P. Zimmer, K. R. Wagner, G. A. Healey, I. Mellman, and A. Helenius. Folding, trimerization, and transport are sequential events in the biogenesis of influenza virus hemagglutinin. *Cell*, 53(2):197–209, Apr 1988.

D. Corti, J. Voss, S. J. Gamblin, G. Codoni, A. Macagno, D. Jarrossay, S. G. Vachieri, D. Pinna, A. Minola, F. Vanzetta, C. Silacci, B. M. Fernandez-Rodriguez, G. Agatic, S. Bianchi, I. Giacchetto-Sasselli, L. Calder, F. Sallusto, P. Collins, L. F. Haire, N. Temperton, J. P. M. Langedijk, J. J. Skehel, and A. Lanzavecchia. A Neutralizing Antibody Selected from Plasma Cells That Binds to Group 1 and Group 2 Influenza A Hemagglutinins. *Science (New York, NY)*, 333(6044):850–856, Aug. 2011.

A. H. Courtney, E. B. Puffer, J. K. Pontrello, Z.-Q. Yang, and L. L. Kiessling. Sialylated multivalent antigens engage cd22 in trans and inhibit b cell activation. *Proc Natl Acad Sci U S A*, 106(8):2500–5, Feb 2009. doi: 10.1073/pnas.0807207106.

P. R. Crocker. Siglecs: sialic-acid-binding immunoglobulin-like lectins in cell-cell interactions and signalling. *Current opinion in structural biology*, 12(5):609–615, Oct. 2002.

P. R. Crocker, J. C. Paulson, and A. Varki. Siglecs and their roles in the immune system. *Nature reviews Immunology*, 7(4):255–266, Apr. 2007.

W. L. Davies, R. R. Grunert, R. F. Haff, J. W. McGrahen, E. M. Neumayer, M. Paulshock, J. C. Watts, T. R. Wood, E. C. Hermann, and C. E. Hoffmann. Antiviral activity of 1-adamantamine (amanatadine). *Science*, 144(3620):862–3, May 1964.

E. De Clercq. Antiviral agents active against influenza a viruses. *Nat Rev Drug Discov*, 5(12): 1015–25, Dec 2006. doi: 10.1038/nrd2175.

E. de Vries, D. M. Tscherne, M. J. Wienholts, V. Cobos-Jiménez, F. Scholte, A. García-Sastre, P. J. M. Rottier, and C. A. M. de Haan. Dissection of the influenza a virus endocytic routes reveals macropinocytosis as an alternative entry pathway. *PLoS Pathog*, 7(3):e1001329, Mar 2011. doi: 10.1371/journal.ppat.1001329.

E. de Vries, R. P. de Vries, M. J. Wienholts, C. E. Floris, M.-S. Jacobs, A. van den Heuvel, P. J. M. Rottier, and C. A. M. de Haan. Influenza a virus entry into cells lacking sialylated n-glycans. *Proc Natl Acad Sci U S A*, 109(19):7457–62, May 2012. doi: 10.1073/pnas.1200987109.

R. P. de Vries, E. de Vries, B. J. Bosch, R. J. de Groot, P. J. M. Rottier, and C. A. M. de Haan. The influenza A virus hemagglutinin glycosylation state affects receptor-binding specificity. *Virology*, 403(1):17–25, July 2010.

P. L. Delputte, S. Costers, and H. J. Nauwynck. Analysis of porcine reproductive and respiratory syndrome virus attachment and internalization: distinctive roles for heparan sulphate and sialoadhesin. *The Journal of general virology*, 86(Pt 5):1441–1445, May 2005.

J. Dernedde, A. Rausch, M. Weinhart, S. Enders, R. Tauber, K. Licha, M. Schirner, U. Zügel, A. von Bonin, and R. Haag. Dendritic polyglycerol sulfates as multivalent inhibitors of inflammation. *Proceedings of the National Academy of Sciences of the United States of America*, 107(46):19679–19684, Nov. 2010.

S. S. Diebold, T. Kaisho, H. Hemmi, S. Akira, and C. Reis e Sousa. Innate antiviral responses by means of TLR7-mediated recognition of single-stranded RNA. *Science (New York, NY)*, 303(5663):1529–1531, Mar. 2004.

T. M. Dobrowsky, Y. Zhou, S. X. Sun, R. F. Siliciano, and D. Wirtz. Monitoring Early Fusion Dynamics of Human Immunodeficiency Virus Type 1 at Single-Molecule Resolution. *Journal of Virology*, 82(14):7022–7033, July 2008.

R. M. DuBois, H. Zaraket, M. Reddivari, R. J. Heath, S. W. White, and C. J. Russell. Acid stability of the hemagglutinin protein regulates H5N1 influenza virus pathogenicity. *PLoS Pathogens*, 7(12):e1002398, Dec. 2011.

A. Ebner, L. Chtcheglova, J. Tang, D. Alsteens, V. Dupres, Y. F. Dufrene, and P. Hinterdorfer. Recognition imaging using atomic force microscopy. In P. Hinterdorfer and A. Oijen, editors, *Handbook of Single-Molecule Biophysics*, pages 525–554. Springer US, 2009. ISBN 978-0-387-76497-9.

C. Ehrhardt, R. Seyer, E. R. Hrincius, T. Eierhoff, T. Wolff, and S. Ludwig. Interplay between influenza A virus and the innate immune signaling. *Microbes and infection / Institut Pasteur*, 12(1):81–87, 2010.

T. Eierhoff, E. R. Hrincius, U. Rescher, S. Ludwig, and C. Ehrhardt. The epidermal growth factor receptor (egfr) promotes uptake of influenza a viruses (iav) into host cells. *PLoS Pathog*, 6 (9):e1001099, 2010. doi: 10.1371/journal.ppat.1001099.

M. B. Eisen, S. Sabesan, J. J. Skehel, and D. C. Wiley. Binding of the influenza a virus to cell-surface receptors: structures of five hemagglutinin-sialyloligosaccharide complexes determined by x-ray crystallography. *Virology*, 232(1):19–31, May 1997. doi: 10.1006/viro.1997.8526.

D. C. Ekiert, A. K. Kashyap, J. Steel, A. Rubrum, G. Bhabha, R. Khayat, J. H. Lee, M. A. Dillon, R. E. O Neil, A. M. Faynboym, M. Horowitz, L. Horowitz, A. B. Ward, P. Palese, R. Webby, R. A. Lerner, R. R. Bhatt, and I. A. Wilson. Cross-neutralization of influenza A viruses mediated by a single antibody loop. *Nature*, pages 1–10, Sept. 2012.

S. Engel, S. Scolari, B. Thaa, N. Krebs, T. Korte, A. Herrmann, and M. Veit. Flim-fret and frap reveal association of influenza virus haemagglutinin with membrane rafts. *Biochem J*, 425(3): 567–73, Feb 2010. doi: 10.1042/BJ20091388.

E. Evans. Looking inside molecular bonds at biological interfaces with dynamic force spectroscopy. *Biophysical chemistry*, 82(2-3):83–97, Dec. 1999.

E. Evans and K. Ritchie. Dynamic strength of molecular adhesion bonds. *Biophysical Journal*, 72(4):1541–1555, Apr. 1997.

H. Ewers, W. Römer, A. E. Smith, K. Bacia, S. Dmitrieff, W. Chai, R. Mancini, J. Kartenbeck, V. Chambon, L. Berland, A. Oppenheim, G. Schwarzmann, T. Feizi, P. Schwille, P. Sens, A. Helenius, and L. Johannes. GM1 structure determines SV40-induced membrane invagination and infection. *Nature Cell Biology*, 12(1):11–8– sup pp 1–12, Jan. 2010.

C. Fasting, C. A. Schalley, M. Weber, O. Seitz, S. Hecht, B. Koksch, J. Dernedde, C. Graf, E.-W. Knapp, and R. Haag. Multivalency as a chemical organization and action principle. *Angew Chem Int Ed Engl*, Sep 2012. doi: 10.1002/anie.201201114.

F. M. Fazal and S. M. Block. Optical tweezers study life under tension. *Nature photonics*, 5: 318–321, May 2011.

D. Floyd, J. Ragains, J. Skehel, S. Harrison, and A. van Oijen. Single-particle kinetics of influenza virus membrane fusion. *Proceedings of the National Academy of Sciences of the United States of America*, Sept. 2008.

J. Fontana, G. Cardone, J. B. Heymann, D. C. Winkler, and A. C. Steven. Structural changes in influenza virus at low ph characterized by cryo-electron tomography. *J Virol*, 86(6):2919–29, Mar 2012. doi: 10.1128/JVI.06698-11.

D. Fotiadis, Y. Liang, S. Filipek, D. A. Saperstein, A. Engel, and K. Palczewski. Atomic-force microscopy: Rhodopsin dimers in native disc membranes. *Nature*, 421(6919):127–8, Jan 2003. doi: 10.1038/421127a.

R. A. M. Fouchier, A. García-Sastre, and Y. Kawaoka. Pause on avian flu transmission studies. *Nature*, 481(7382):443, Jan 2012. doi: 10.1038/481443a.

A. S. Gambaryan, J. S. Robertson, and M. N. Matrosovich. Effects of egg-adaptation on the receptor-binding properties of human influenza a and b viruses. *Virology*, 258(2):232–9, Jun 1999. doi: 10.1006/viro.1999.9732.

L. Glaser, J. Stevens, D. Zamarin, I. A. Wilson, A. García-Sastre, T. M. Tumpey, C. F. Basler, J. K. Taubenberger, and P. Palese. A single amino acid substitution in 1918 influenza virus hemagglutinin changes receptor binding specificity. *Journal of Virology*, 79(17):11533–11536, Sept. 2005.

A. Gottschalk. Chemistry of virus receptors. In F. M. Burnet and W. M. Stanley, editors, *The Viruses*, volume 3. Academic Press, 1959.

M. Grandbois, W. Dettmann, M. Benoit, and H. E. Gaub. Affinity imaging of red blood cells using an atomic force microscope. *J Histochem Cytochem*, 48(5):719–24, May 2000.

H. Grubmüller, B. Heymann, and P. Tavan. Ligand binding: molecular mechanics calculation of the streptavidin-biotin rupture force. *Science (New York, NY)*, 271(5251):997–999, Feb. 1996.

Y. Guo, E. Rumschlag-Booms, J. Wang, H. Xiao, J. Yu, J. Wang, L. Guo, G. F. Gao, Y. Cao, M. Caffrey, and L. Rong. Analysis of hemagglutinin-mediated entry tropism of H5N1 avian influenza. *Virology Journal*, 6:39, 2009.

J. Han and K. Burgess. Fluorescent indicators for intracellular pH. *Chemical reviews*, 110(5): 2709–2728, May 2010.

S. C. Harrison. Viral membrane fusion. *Nat Struct Mol Biol*, 15(7):690–8, Jul 2008. doi: 10.1038/nsmb.1456.

P. Hazarika, F. Kukolka, and C. M. Niemeyer. Reversible binding of fluorescent proteins at DNA-gold nanoparticles. *Angewandte Chemie (International ed in English)*, 45(41):6827–6830, Oct. 2006.

A. Helenius. Unpacking the incoming influenza virus. *Cell*, 69(4):577–8, May 1992a.

A. Helenius. Unpacking the incoming influenza virus. *Cell*, 69(4):577–578, May 1992b.

A. Helenius, J. Kartenbeck, K. Simons, and E. Fries. On the entry of semliki forest virus into bhk-21 cells. *J Cell Biol*, 84(2):404–20, Feb 1980.

J. Helenius, C.-P. Heisenberg, H. E. Gaub, and D. J. Muller. Single-cell force spectroscopy. *J Cell Sci*, 121(Pt 11):1785–91, Jun 2008. doi: 10.1242/jcs.030999.

S. Herfst, E. J. A. Schrauwen, M. Linster, S. Chutinimitkul, E. de Wit, V. J. Munster, E. M. Sorrell, T. M. Bestebroer, D. F. Burke, D. J. Smith, G. F. Rimmelzwaan, A. D. M. E. Osterhaus, and R. A. M. Fouchier. Airborne transmission of influenza A/H5N1 virus between ferrets. *Science (New York, NY)*, 336(6088):1534–1541, June 2012.

P. Hinterdorfer and Y. F. Dufrêne. Detection and localization of single molecular recognition events using atomic force microscopy. *Nature Methods*, 3(5):347–355, May 2006.

T. Horimoto and Y. Kawaoka. Influenza: lessons from past pandemics, warnings from current incidents. *Nat Rev Microbiol*, 3(8):591–600, Aug 2005. doi: 10.1038/nrmicro1208.

Q. Huang, R. P. Sivaramakrishna, K. Ludwig, T. Korte, C. Böttcher, and A. Herrmann. Early steps of the conformational change of influenza virus hemagglutinin to a fusion active state: stability and energetics of the hemagglutinin. *Biochim Biophys Acta*, 1614(1):3–13, Jul 2003.

J. Huotari and A. Helenius. Endosome maturation. *EMBO J*, 30(17):3481–500, Aug 2011. doi: 10.1038/emboj.2011.286.

M. Imai and Y. Kawaoka. The role of receptor binding specificity in interspecies transmission of influenza viruses. *Curr Opin Virol*, 2(2):160–7, Apr 2012. doi: 10.1016/j.coviro.2012.03.003.

M. Imai, T. Mizuno, and K. Kawasaki. Membrane fusion by single influenza hemagglutinin trimers. Kinetic evidence from image analysis of hemagglutinin-reconstituted vesicles. *The Journal of biological chemistry*, 281(18):12729–12735, May 2006.

M. Imai, T. Watanabe, M. Hatta, S. C. Das, M. Ozawa, K. Shinya, G. Zhong, A. Hanson, H. Katsura, S. Watanabe, C. Li, E. Kawakami, S. Yamada, M. Kiso, Y. Suzuki, E. A. Maher, G. Neumann, and Y. Kawaoka. Experimental adaptation of an influenza H5 HA confers respiratory droplet transmission to a reassortant H5 HA/H1N1 virus in ferrets. *Nature*, pages 1–11, May 2012.

T. Ito, Y. Suzuki, A. Takada, A. Kawamoto, K. Otsuki, H. Masuda, M. Yamada, T. Suzuki, H. Kida, and Y. Kawaoka. Differences in sialic acid-galactose linkages in the chicken egg amnion and allantois influence human influenza virus receptor specificity and variant selection. *Journal of Virology*, 71(4):3357–3362, Apr. 1997.

R. Y. Kao, D. Yang, L.-S. Lau, W. H. W. Tsui, L. Hu, J. Dai, M.-P. Chan, C.-M. Chan, P. Wang, B.-J. Zheng, J. Sun, J.-D. Huang, J. Madar, G. Chen, H. Chen, Y. Guan, and K.-Y. Yuen. Identification of influenza A nucleoprotein as an antiviral target. *Nature Biotechnology*, 28 (6):600–605, June 2010.

G. B. Karlsson Hedestam, R. A. M. Fouchier, S. Phogat, D. R. Burton, J. Sodroski, and R. T. Wyatt. The challenges of eliciting neutralizing antibodies to HIV-1 and to influenza virus. *Nature Reviews Microbiology*, 6(2):143–155, Feb. 2008.

C. Ke, Y. Jiang, M. Rivera, R. L. Clark, and P. E. Marszalek. Pulling geometry-induced errors in single molecule force spectroscopy measurements. *Biophysical Journal*, 92(9):L76–8, May 2007.

W. Keil, R. Geyer, J. Dabrowski, U. Dabrowski, H. Niemann, S. Stirm, and H. D. Klenk. Carbohydrates of influenza virus. Structural elucidation of the individual glycans of the FPV hemagglutinin by two-dimensional 1H n.m.r. and methylation analysis. *The EMBO journal*, 4(10):2711–2720, Oct. 1985.

D. J. Kelleher and R. Gilmore. An evolving view of the eukaryotic oligosaccharyltransferase. *Glycobiology*, 16(4):47R–62R, Apr 2006. doi: 10.1093/glycob/cwj066.

M. S. Kellermayer, S. B. Smith, H. L. Granzier, and C. Bustamante. Folding-unfolding transitions in single titin molecules characterized with laser tweezers. *Science*, 276(5315):1112–6, May 1997.

S. M. Kerfoot, K. McRae, F. Lam, E. F. McAvoy, S. Clark, M. Brain, P. F. Lalor, D. H. Adams, and P. Kubes. A novel mechanism of erythrocyte capture from circulation in humans. *Exp Hematol*, 36(2):111–8, Feb 2008. doi: 10.1016/j.exphem.2007.08.029.

L. L. Kiessling, J. E. Gestwicki, and L. E. Strong. Synthetic multivalent ligands in the exploration of cell-surface interactions. *Current opinion in chemical biology*, 4(6):696–703, Dec. 2000.

P. I. Kitov, J. M. Sadowska, G. Mulvey, G. D. Armstrong, H. Ling, N. S. Pannu, R. J. Read, and D. R. Bundle. Shiga-like toxins are neutralized by tailored multivalent carbohydrate ligands. *Nature*, 403(6770):669–672, Feb. 2000.

T. Korte and A. Herrmann. ph-dependent binding of the fluorophore bis-ans to influenza virus reflects the conformational change of hemagglutinin. *Eur Biophys J*, 23(2):105–13, 1994.

T. Korte, K. Ludwig, F. P. Booy, R. Blumenthal, and A. Herrmann. Conformational intermediates and fusion activity of influenza virus hemagglutinin. *Journal of Virology*, 73(6): 4567–4574, June 1999.

V. M. Krishnamurthy, L. A. Estroff, and G. M. Whitesides. Multivalency in ligand design. In D. A. E. Wolfgang Jahnke, editor, *Fragment-based Approaches in Drug Discovery*, pages 11–53. Wiley-VCH Verlag GmbH Co. KGaA, 2006.

M. Krumbiegel, A. Herrmann, and R. Blumenthal. Kinetics of the low pH-induced conformational changes and fusogenic activity of influenza hemagglutinin. *Biophysical Journal*, 67(6): 2355–2360, Dec. 1994.

A. Kundu, R. T. Avalos, C. M. Sanderson, and D. P. Nayak. Transmembrane domain of influenza virus neuraminidase, a type ii protein, possesses an apical sorting signal in polarized mdck cells. *J Virol*, 70(9):6508–15, Sep 1996.

M. Lakadamyali, M. J. Rust, H. P. Babcock, and X. Zhuang. Visualizing infection of individual influenza viruses. *Proc Natl Acad Sci U S A*, 100(16):9280–5, Aug 2003. doi: 10.1073/pnas.0832269100.

M. Lakadamyali, M. J. Rust, and X. Zhuang. Endocytosis of influenza viruses. *Microbes and infection / Institut Pasteur*, 6(10):929–936, Aug. 2004.

M. Lakadamyali, M. J. Rust, and X. Zhuang. Ligands for clathrin-mediated endocytosis are differentially sorted into distinct populations of early endosomes. *Cell*, 124(5):997–1009, Mar 2006. doi: 10.1016/j.cell.2005.12.038.

R. Lamb and R. Krug. Orthomyxoviridae: The viruses and replication. In D. Knipe, P. Howley, and D. Griffin, editors, *Fields Virology*. Lippincott Wiliams and Wilkins, 4th edition, 1996.

J. J. Landers, Z. Cao, I. Lee, L. T. Piehler, P. P. Myc, A. Myc, T. Hamouda, A. T. Galecki, and J. R. Baker. Prevention of influenza pneumonitis by sialic Acid-conjugated dendritic polymers. *The Journal of infectious diseases*, 186(9):1222–1230, Nov. 2002.

C. M. Lee, A. K. Weight, J. Haldar, L. Wang, A. M. Klibanov, and J. Chen. Polymer-attached zanamivir inhibits synergistically both early and late stages of influenza virus infection. *Proc Natl Acad Sci U S A*, Nov 2012. doi: 10.1073/pnas.1219155109.

F. Lehmann, E. Tiralongo, and J. Tiralongo. Sialic acid-specific lectins: occurrence, specificity and function. *Cell Mol Life Sci*, 63(12):1331–54, Jun 2006. doi: 10.1007/s00018-005-5589-y.

M. J. Lehmann, N. M. Sherer, C. B. Marks, M. Pypaert, and W. Mothes. Actin- and myosin-driven movement of viruses along filopodia precedes their entry into cells. *J Cell Biol*, 170 (2):317–25, Jul 2005. doi: 10.1083/jcb.200503059.

T. Leiding, J. Wang, J. Martinsson, W. F. DeGrado, and S. P. Arsköld. Proton and cation transport activity of the M2 proton channel from influenza A virus. *Proceedings of the National Academy of Sciences of the United States of America*, 107(35):15409–15414, Aug. 2010.

H. S. Y. Leung, O. T. W. Li, R. W. Y. Chan, M. C. W. Chan, J. M. Nicholls, and L. L. M. Poon. Entry of influenza a virus with a 2,6-linked sialic acid binding preference requires host fibronectin. *J Virol*, 86(19):10704–13, Oct 2012. doi: 10.1128/JVI.01166-12.

K. Ley, C. Laudanna, M. I. Cybulsky, and S. Nourshargh. Getting to the site of inflammation: the leukocyte adhesion cascade updated. *Nat Rev Immunol*, 7(9):678–89, Sep 2007. doi: 10.1038/nri2156.

C. Li and K. K. Liu. Nanomechanical characterization of red blood cells using optical tweezers. *J Mater Sci Mater Med*, 19(4):1529–35, Apr 2008. doi: 10.1007/s10856-008-3382-9.

X. Li, P. Wu, G. F. Gao, and S. Cheng. Carbohydrate-Functionalized Chitosan Fiber for Influenza Virus Capture. *Biomacromolecules*, 12(11):3962–3969, Nov. 2011.

C. Lizak, S. Gerber, S. Numao, M. Aebi, and K. P. Locher. X-ray structure of a bacterial oligosaccharyltransferase. *Nature*, 474(7351):350–5, Jun 2011. doi: 10.1038/nature10151.

H. Lodish, A. Berk, C. A. Kaiser, M. Krieger, M. P. Scott, A. Bretscher, H. Ploegh, and P. Matsudaira. *Molecular Cell Biology (Lodish, Molecular Cell Biology)*. W. H. Freeman, 6th edition, June 2007. ISBN 0716776014. URL `http://www.amazon.com/exec/obidos/redirect?tag=citeulike07-20&path=ASIN/0716776014`.

S. L. Londrigan, S. G. Turville, M. D. Tate, Y.-M. Deng, A. G. Brooks, and P. C. Reading. N-linked glycosylation facilitates sialic acid-independent attachment and entry of influenza A viruses into cells expressing DC-SIGN or L-SIGN. *Journal of Virology*, 85(6):2990–3000, Mar. 2011.

P.-Y. Lozach, J. Huotari, and A. Helenius. Late-penetrating viruses. *Curr Opin Virol*, 1(1): 35–43, Jul 2011. doi: 10.1016/j.coviro.2011.05.004.

S. Ludwig, S. Pleschka, O. Planz, and T. Wolff. Ringing the alarm bells: signalling and apoptosis in influenza virus infected cells. *Cellular Microbiology*, 8(3):375–386, Mar. 2006.

L. Mach, W. Scherf, M. Ammann, J. Poetsch, W. Bertsch, L. März, and J. Glössl. Purification and partial characterization of a novel lectin from elder (Sambucus nigra L.) fruit. *The Biochemical journal*, 278 (Pt 3):667–671, Sept. 1991.

J. Mameren, G. J. Wuite, and I. Heller. Introduction to optical tweezers: Background, system designs, and commercial solutions. In G. J. L. W. Erwin J. G. Peterman, editor, *Single Molecule Analysis*, volume 783 of *Methods in Molecular Biology*, pages 1–20. Springer Protocols, 2011. doi: 10.1007/978-1-61779-282-3_1. URL `http://www.springerprotocols.com/Abstract/doi/10.1007/978-1-61779-282-3_1`.

M. Mammen, G. Dahmann, and G. M. Whitesides. Effective inhibitors of hemagglutination by influenza virus synthesized from polymers having active ester groups. insight into mechanism of inhibition. *J Med Chem*, 38(21):4179–90, Oct 1995.

M. Mammen, S. K. Choi, and G. M. Whitesides. Polyvalent interactions in biological systems: implications for design and use of multivalent ligands and inhibitors. *Angewandte Chemie (International ed in English)*, 37(20):2754–2794, 1998.

I. Markovic, E. Leikina, M. Zhukovsky, J. Zimmerberg, and L. V. Chernomordik. Synchronized activation and refolding of influenza hemagglutinin in multimeric fusion machines. *The Journal of cell biology*, 155(5):833–844, Nov. 2001.

M. Marsh and A. Helenius. Virus entry: open sesame. *Cell*, 124(4):729–40, Feb 2006. doi: 10.1016/j.cell.2006.02.007.

K. Martin and A. Helenius. Transport of incoming influenza virus nucleocapsids into the nucleus. *J Virol*, 65(1):232–44, Jan 1991a.

K. Martin and A. Helenius. Nuclear transport of influenza virus ribonucleoproteins: the viral matrix protein (m1) promotes export and inhibits import. *Cell*, 67(1):117–30, Oct 1991b.

K. S. Matlin, H. Reggio, A. Helenius, and K. Simons. Infectious entry pathway of influenza virus in a canine kidney cell line. *J Cell Biol*, 91(3 Pt 1):601–13, Dec 1981.

M. N. Matrosovich, A. S. Gambaryan, S. Teneberg, V. E. Piskarev, S. S. Yamnikova, D. K. Lvov, J. S. Robertson, and K. A. Karlsson. Avian influenza a viruses differ from human viruses by recognition of sialyloligosaccharides and gangliosides and by a higher conservation of the ha receptor-binding site. *Virology*, 233(1):224–34, Jun 1997. doi: 10.1006/viro.1997.8580.

M. N. Matrosovich, T. Y. Matrosovich, T. Gray, N. A. Roberts, and H.-D. Klenk. Human and avian influenza viruses target different cell types in cultures of human airway epithelium. *Proc Natl Acad Sci U S A*, 101(13):4620–4, Mar 2004a. doi: 10.1073/pnas.0308001101.

M. N. Matrosovich, T. Y. Matrosovich, T. Gray, N. A. Roberts, and H.-D. Klenk. Neuraminidase is important for the initiation of influenza virus infection in human airway epithelium. *J Virol*, 78(22):12665–7, Nov 2004b. doi: 10.1128/JVI.78.22.12665-12667.2004.

T. Matsubara, A. Onishi, T. Saito, A. Shimada, H. Inoue, T. Taki, K. Nagata, Y. Okahata, and T. Sato. Sialic Acid-Mimic Peptides As Hemagglutinin Inhibitors for Anti-Influenza Therapy. *Journal of medicinal chemistry*, May 2010.

C. McCullough, M. Wang, L. Rong, and M. Caffrey. Characterization of Influenza Hemagglutinin Interactions with Receptor by NMR. *PLoS ONE*, 7(7):e33958, July 2012.

H. T. McMahon and E. Boucrot. Molecular mechanism and physiological functions of clathrin-mediated endocytosis. *Nat Rev Mol Cell Biol*, 12(8):517–33, Aug 2011. doi: 10.1038/nrm3151.

R. A. Medina and A. García-Sastre. Influenza a viruses: new research developments. *Nat Rev Microbiol*, 9(8):590–603, Aug 2011. doi: 10.1038/nrmicro2613.

J. Mercer, M. Schelhaas, and A. Helenius. Virus entry by endocytosis. *Annu Rev Biochem*, 79: 803–33, 2010. doi: 10.1146/annurev-biochem-060208-104626.

K. W. Moremen, M. Tiemeyer, and A. V. Nairn. Vertebrate protein glycosylation: diversity, synthesis and function. *Nature reviews Molecular cell biology*, 13(7):448–462, July 2012.

D. J. Muller. Afm: a nanotool in membrane biology. *Biochemistry*, 47(31):7986–98, Aug 2008. doi: 10.1021/bi800753x.

D. J. Müller, G. M. Hand, A. Engel, and G. E. Sosinsky. Conformational changes in surface structures of isolated connexin 26 gap junctions. *EMBO J*, 21(14):3598–607, Jul 2002. doi: 10.1093/emboj/cdf365.

D. J. Müller, J. Helenius, D. Alsteens, and Y. F. Dufrêne. Force probing surfaces of living cells to molecular resolution. *Nature Chemical Biology*, 5(6):383–390, June 2009.

S. Murakami, T. Horimoto, M. Ito, R. Takano, H. Katsura, M. Shimojima, and Y. Kawaoka. Enhanced growth of influenza vaccine seed viruses in vero cells mediated by broadening the optimal pH range for virus membrane fusion. *Journal of Virology*, 86(3):1405–1410, Feb. 2012.

G. Muratore, L. Goracci, B. Mercorelli, A. Foeglein, P. Digard, G. Cruciani, G. Palù, and A. Loregian. Small molecule inhibitors of influenza A and B viruses that act by disrupting subunit interactions of the viral polymerase. *Proceedings of the National Academy of Sciences*, Apr. 2012.

D. P. Nayak, E. K.-W. Hui, and S. Barman. Assembly and budding of influenza virus. *Virus Res*, 106(2):147–65, Dec 2004. doi: 10.1016/j.virusres.2004.08.012.

G. Neuert, C. Albrecht, E. Pamir, and H. E. Gaub. Dynamic force spectroscopy of the digoxigenin–antibody complex. *FEBS letters*, 580(2):505–509, Jan. 2006.

K. C. Neuman and A. Nagy. Single-molecule force spectroscopy: optical tweezers, magnetic tweezers and atomic force microscopy. *Nature Methods*, 5(6):491–505, June 2008.

G. Neumann, T. Noda, and Y. Kawaoka. Emergence and pandemic potential of swine-origin h1n1 influenza virus. *Nature*, 459(7249):931–9, Jun 2009. doi: 10.1038/nature08157.

J. M. Nicholls, A. J. Bourne, H. Chen, Y. Guan, and J. S. M. Peiris. Sialic acid receptor detection in the human respiratory tract: evidence for widespread distribution of potential binding sites for human and avian influenza viruses. *Respir Res*, 8:73, 2007. doi: 10.1186/1465-9921-8-73.

J. M. Nicholls, R. W. Y. Chan, R. J. Russell, G. M. Air, and J. S. M. Peiris. Evolving complexities of influenza virus and its receptors. *Trends Microbiol*, 16(4):149–57, Apr 2008. doi: 10.1016/j.tim.2008.01.008.

M. Q. Nicol, Y. Ligertwood, M. N. Bacon, B. M. Dutia, and A. A. Nash. A novel family of peptides with potent activity against influenza A viruses. *The Journal of general virology*, 93 (Pt 5):980–986, May 2012.

S. J. North, H.-H. Huang, S. Sundaram, J. Jang-Lee, A. T. Etienne, A. Trollope, S. Chalabi, A. Dell, P. Stanley, and S. M. Haslam. Glycomics profiling of Chinese hamster ovary cell glycosylation mutants reveals N-glycans of a novel size and complexity. *Journal of Biological Chemistry*, 285(8):5759–5775, Feb. 2010.

I. Nunes-Correia, J. Ramalho-Santos, S. Nir, and M. C. Pedroso de Lima. Interactions of influenza virus with cultured cells: detailed kinetic modeling of binding and endocytosis. *Biochemistry*, 38(3):1095–101, Jan 1999. doi: 10.1021/bi9812524.

I. Nunes-Correia, A. Eulálio, S. Nir, and M. C. Pedroso De Lima. Caveolae as an additional route for influenza virus endocytosis in MDCK cells. *Cellular & molecular biology letters*, 9 (1):47–60, 2004.

F. Oesterhelt, D. Oesterhelt, M. Pfeiffer, A. Engel, H. E. Gaub, and D. J. Müller. Unfolding pathways of individual bacteriorhodopsins. *Science (New York, NY)*, 288(5463):143–146, Apr. 2000.

M. Ohuchi, N. Asaoka, T. Sakai, and R. Ohuchi. Roles of neuraminidase in the initial stage of influenza virus infection. *Microbes and infection / Institut Pasteur*, 8(5):1287–1293, Apr. 2006.

M. K. O Reilly and J. C. Paulson. Siglecs as targets for therapy in immune-cell-mediated disease. *Trends in pharmacological sciences*, 30(5):240–248, May 2009.

I. Papp, C. Sieben, K. Ludwig, M. Roskamp, C. Böttcher, S. Schlecht, A. Herrmann, and R. Haag. Inhibition of influenza virus infection by multivalent sialic-acid-functionalized gold nanoparticles. *Small*, 6(24):2900–6, Dec 2010. doi: 10.1002/smll.201001349.

J. T. Perez, A. Varble, R. Sachidanandam, I. Zlatev, M. Manoharan, A. García-Sastre, and B. R. tenOever. Influenza a virus-generated small rnas regulate the switch from transcription to replication. *Proc Natl Acad Sci U S A*, 107(25):11525–30, Jun 2010. doi: 10.1073/pnas.1001984107.

L. H. Pinto, L. J. Holsinger, and R. A. Lamb. Influenza virus m2 protein has ion channel activity. *Cell*, 69(3):517–28, May 1992.

A. Portela and P. Digard. The influenza virus nucleoprotein: a multifunctional rna-binding protein pivotal to virus replication. *J Gen Virol*, 83(Pt 4):723–34, Apr 2002.

D. Poteryaev, S. Datta, K. Ackema, M. Zerial, and A. Spang. Identification of the switch in early-to-late endosome transition. *Cell*, 141(3):497–508, Apr. 2010.

T. J. Pritchett and J. C. Paulson. Basis for the potent inhibition of influenza virus infection by equine and guinea pig alpha 2-macroglobulin. *The Journal of biological chemistry*, 264(17): 9850–9858, June 1989.

C. Rabouille, N. Hui, F. Hunte, R. Kieckbusch, E. G. Berger, G. Warren, and T. Nilsson. Mapping the distribution of golgi enzymes involved in the construction of complex oligosaccharides. *J Cell Sci*, 108 (Pt 4):1617–27, Apr 1995.

P. S. Rachakonda, M. Veit, T. Korte, K. Ludwig, C. Böttcher, Q. Huang, M. F. G. Schmidt, and A. Herrmann. The relevance of salt bridges for the stability of the influenza virus hemagglutinin. *The FASEB Journal*, 21(4):995–1002, Apr. 2007.

M. Rajik, A. R. Omar, A. Ideris, S. S. Hassan, and K. Yusoff. A novel peptide inhibits the influenza virus replication by preventing the viral attachment to the host cells. *International journal of biological sciences*, 5(6):543–548, 2009.

I. Ramos and A. Fernandez-Sesma. Cell receptors for influenza a viruses and the innate immune response. *Frontiers in microbiology*, 3:117, 2012.

C. Rankl, F. Kienberger, L. Wildling, J. Wruss, H. J. Gruber, D. Blaas, and P. Hinterdorfer. Multiple receptors involved in human rhinovirus attachment to live cells. *Proc Natl Acad Sci U S A*, 105(46):17778–83, Nov 2008. doi: 10.1073/pnas.0806451105.

S. Reichert, P. Welker, M. Calderón, J. Khandare, D. Mangoldt, K. Licha, R. K. Kainthan, D. E. Brooks, and R. Haag. Size-dependant cellular uptake of dendritic polyglycerol. *Small (Weinheim an der Bergstrasse, Germany)*, 7(6):820–829, Mar. 2011.

J. D. Reuter, A. Myc, M. M. Hayes, Z. Gan, R. Roy, D. Qin, R. Yin, L. T. Piehler, R. Esfand, D. A. Tomalia, and J. R. Baker. Inhibition of viral adhesion and infection by sialic-acid-conjugated dendritic polymers. *Bioconjugate Chemistry*, 10(2):271–278, 1999.

M. Rief and H. Grubmüller. Force spectroscopy of single biomolecules. *Chemphyschem : a European journal of chemical physics and physical chemistry*, 3(3):255–261, Mar. 2002.

M. Rief, M. Gautel, F. Oesterhelt, J. M. Fernandez, and H. E. Gaub. Reversible unfolding of individual titin immunoglobulin domains by afm. *Science*, 276(5315):1109–12, May 1997.

J. Rink, E. Ghigo, Y. Kalaidzidis, and M. Zerial. Rab conversion as a mechanism of progression from early to late endosomes. *Cell*, 122(5):735–49, Sep 2005. doi: 10.1016/j.cell.2005.06.043.

E. Rodriguez-Boulan, G. Kreitzer, and A. Müsch. Organization of vesicular trafficking in epithelia. *Nat Rev Mol Cell Biol*, 6(3):233–47, Mar 2005. doi: 10.1038/nrm1593.

G. N. Rogers, T. J. Pritchett, J. L. Lane, and J. C. Paulson. Differential sensitivity of human, avian, and equine influenza a viruses to a glycoprotein inhibitor of infection: selection of receptor specific variants. *Virology*, 131(2):394–408, Dec 1983.

J. S. Rossman and R. A. Lamb. Influenza virus assembly and budding. *Virology*, 411(2):229–236, Mar. 2011.

J. S. Rossman, G. P. Leser, and R. A. Lamb. Filamentous influenza virus enters cells via macropinocytosis. *J Virol*, 86(20):10950–60, Oct 2012. doi: 10.1128/JVI.05992-11.

M. J. Rust, M. Lakadamyali, F. Zhang, and X. Zhuang. Assembly of endocytic machinery around individual influenza viruses during viral entry. *Nat Struct Mol Biol*, 11(6):567–73, Jun 2004. doi: 10.1038/nsmb769.

G. Sagvolden, I. Giaever, E. O. Pettersen, and J. Feder. Cell adhesion force microscopy. *Proc Natl Acad Sci U S A*, 96(2):471–6, Jan 1999.

T. Sakai, M. Ohuchi, M. Imai, T. Mizuno, K. Kawasaki, K. Kuroda, and S. Yamashina. Dual wavelength imaging allows analysis of membrane fusion of influenza virus inside cells. *J Virol*, 80(4):2013–8, Feb 2006. doi: 10.1128/JVI.80.4.2013-2018.2006.

N. K. Sauter, M. D. Bednarski, B. A. Wurzburg, J. E. Hanson, G. M. Whitesides, J. J. Skehel, and D. C. Wiley. Hemagglutinins from two influenza virus variants bind to sialic acid derivatives with millimolar dissociation constants: a 500-MHz proton nuclear magnetic resonance study. *Biochemistry*, 28(21):8388–8396, Oct. 1989.

N. K. Sauter, J. E. Hanson, G. D. Glick, J. H. Brown, R. L. Crowther, S. J. Park, J. J. Skehel, and D. C. Wiley. Binding of influenza virus hemagglutinin to analogs of its cell-surface receptor, sialic acid: analysis by proton nuclear magnetic resonance spectroscopy and x-ray crystallography. *Biochemistry*, 31(40):9609–9621, Oct. 1992.

R. Schauer. Achievements and challenges of sialic acid research. *Glycoconjugate Journal*, 17:485–499, 2000. ISSN 0282-0080. URL `http://dx.doi.org/10.1023/A:1011062223612`. 10.1023/A:1011062223612.

R. Schauer. Sialic acids as regulators of molecular and cellular interactions. *Current opinion in structural biology*, 19(5):507–514, Oct. 2009.

G. Schneider, G. Decher, N. Nerambourg, R. Praho, M. H. V. Werts, and M. Blanchard-Desce. Distance-Dependent Fluorescence Quenching on Gold Nanoparticles Ensheathed with Layer-by-Layer Assembled Polyelectrolytes. *Nano letters*, 6(3):530–536, Mar. 2006.

C. Scholtissek and G. P. Faulkner. Amantadine-resistant and -sensitive influenza A strains and recombinants. *The Journal of general virology*, 44(3):807–815, Sept. 1979.

S. Scolari, S. Engel, N. Krebs, A. P. Plazzo, R. F. M. De Almeida, M. Prieto, M. Veit, and A. Herrmann. Lateral distribution of the transmembrane domain of influenza virus hemagglutinin revealed by time-resolved fluorescence imaging. *J Biol Chem*, 284(23):15708–16, Jun 2009. doi: 10.1074/jbc.M900437200.

G. I. Shapiro, T. Gurney, and R. M. Krug. Influenza virus gene expression: control mechanisms at early and late times of infection and nuclear-cytoplasmic transport of virus-specific RNAs. *Journal of Virology*, 61(3):764–773, Mar. 1987.

N. M. Sherer, M. J. Lehmann, L. F. Jimenez-Soto, C. Horensavitz, M. Pypaert, and W. Mothes. Retroviruses can establish filopodial bridges for efficient cell-to-cell transmission. *Nat Cell Biol*, 9(3):310–5, Mar 2007. doi: 10.1038/ncb1544.

N. Shibuya, I. J. Goldstein, W. F. Broekaert, M. Nsimba-Lubaki, B. Peeters, and W. J. Peumans. The elderberry (sambucus nigra l.) bark lectin recognizes the neu5ac(alpha 2-6)gal/galnac sequence. *J Biol Chem*, 262(4):1596–601, Feb 1987.

C. Sieben, C. Kappel, R. Zhu, A. Wozniak, C. Rankl, P. Hinterdorfer, H. Grubmüller, and A. Herrmann. Influenza virus binds its host cell using multiple dynamic interactions. *Proc Natl Acad Sci U S A*, 109(34):13626–31, Aug 2012. doi: 10.1073/pnas.1120265109.

S. B. Sieczkarski and G. R. Whittaker. Influenza virus can enter and infect cells in the absence of clathrin-mediated endocytosis. *J Virol*, 76(20):10455–64, Oct 2002a.

S. B. Sieczkarski and G. R. Whittaker. Influenza virus can enter and infect cells in the absence of clathrin-mediated endocytosis. *Journal of Virology*, 76(20):10455–10464, Oct. 2002b.

S. B. Sieczkarski and G. R. Whittaker. Differential requirements of Rab5 and Rab7 for endocytosis of influenza and other enveloped viruses. *Traf c (Copenhagen, Denmark)*, 4(5): 333–343, May 2003.

G. B. Sigal, M. Mammen, G. Dahmann, and G. M. Whitesides. Polyacrylamides bearing pendant -sialoside groups strongly inhibit agglutination of erythrocytes by influenza virus: the strong inhibition reflects enhanced binding through cooperative polyvalent interactions. *Journal of the American Chemical Society*, 118(16):3789–3800, 1996.

A. L. Sisson, D. Steinhilber, T. Rossow, P. Welker, K. Licha, and R. Haag. Biocompatible functionalized polyglycerol microgels with cell penetrating properties. *Angewandte Chemie (International ed in English)*, 48(41):7540–7545, 2009.

J. J. Skehel and D. C. Wiley. Receptor binding and membrane fusion in virus entry: the influenza hemagglutinin. *Annu Rev Biochem*, 69:531–69, 2000. doi: 10.1146/annurev.biochem.69.1.531.

J. J. Skehel and D. C. Wiley. Influenza haemagglutinin. *Vaccine*, 20 Suppl 2:S51–4, May 2002.

J. J. Skehel, A. J. Hay, and J. A. Armstrong. On the mechanism of inhibition of influenza virus replication by amantadine hydrochloride. *J Gen Virol*, 38(1):97–110, Jan 1978.

B. Snijder and L. Pelkmans. Origins of regulated cell-to-cell variability. *Nat Rev Mol Cell Biol*, 12(2):119–25, Feb 2011. doi: 10.1038/nrm3044.

B. Snijder, R. Sacher, P. Rämö, E.-M. Damm, P. Liberali, and L. Pelkmans. Population context determines cell-to-cell variability in endocytosis and virus infection. *Nature*, 461(7263):520–3, Sep 2009. doi: 10.1038/nature08282.

A. Spaltenstein and G. M. Whitesides. Polyacrylamides bearing pendant -sialoside groups strongly inhibit agglutination of erythrocytes by influenza virus. *Journal of the American Chemical Society*, 113(2):686–687, 1991.

W. Spevak, J. O. Nagy, D. H. Charych, M. E. Schaefer, J. H. Gilbert, and M. D. Bednarski. Polymerized liposomes containing C-glycosides of sialic acid: potent inhibitors of influenza virus in vitro infectivity. *Biochemistry*, 115(3):1146–1147, Feb. 1993.

J. C. Stachowiak, E. M. Schmid, C. J. Ryan, H. S. Ann, D. Y. Sasaki, M. B. Sherman, P. L. Geissler, D. A. Fletcher, and C. C. Hayden. Membrane bending by protein–protein crowding. *Nature Cell Biology*, 14(9):944–949, Aug. 2012.

D. A. Steinhauer and J. J. Skehel. Genetics of influenza viruses. *Annu Rev Genet*, 36:305–32, 2002. doi: 10.1146/annurev.genet.36.052402.152757.

J. Stevens, O. BLIXT, L. Glaser, J. TAUBENBERGER, P. Palese, J. PAULSON, and I. WILSON. Glycan Microarray Analysis of the Hemagglutinins from Modern and Pandemic Influenza Viruses Reveals Different Receptor Specificities. *Journal of Molecular Biology*, 355(5):1143–1155, Feb. 2006.

S. J. Stray, R. D. Cummings, and G. M. Air. Influenza virus infection of desialylated cells. *Glycobiology*, 10(7):649–658, July 2000.

B. Strilić, J. Eglinger, M. Krieg, M. Zeeb, J. Axnick, P. Babál, D. J. Müller, and E. Lammert. Electrostatic Cell-Surface Repulsion Initiates Lumen Formation in Developing Blood Vessels. *Current Biology*, 20(22):2003–2009, Jan. 2010.

K. Subbarao and T. Joseph. Scientific barriers to developing vaccines against avian influenza viruses. *Nature reviews Immunology*, 7(4):267–278, Apr. 2007.

J. Sui, W. C. Hwang, S. Perez, G. Wei, D. Aird, L.-M. Chen, E. Santelli, B. Stec, G. Cadwell, M. Ali, H. Wan, A. Murakami, A. Yammanuru, T. Han, N. J. Cox, L. A. Bankston, R. O. Donis, R. C. Liddington, and W. A. Marasco. Structural and functional bases for broad-spectrum neutralization of avian and human influenza A viruses. *Nature Structural & Molecular Biology*, pages 1–9, Feb. 2009.

D. K. Takemoto, J. J. Skehel, and D. C. Wiley. A surface plasmon resonance assay for the binding of influenza virus hemagglutinin to its sialic acid receptor. *Virology*, 217(2):452–8, Mar 1996a. doi: 10.1006/viro.1996.0139.

D. K. Takemoto, J. J. Skehel, and D. C. Wiley. A surface plasmon resonance assay for the binding of influenza virus hemagglutinin to its sialic acid receptor. *Virology*, 217(2):452–458, Mar. 1996b.

M. Tantama, Y. P. Hung, and G. Yellen. Imaging Intracellular pH in Live Cells with a Genetically Encoded Red Fluorescent Protein Sensor. *Journal of the American Chemical Society*, 133(26): 10034–10037, July 2011.

J. K. Taubenberger, J. V. Hultin, and D. M. Morens. Discovery and characterization of the 1918 pandemic influenza virus in historical context. *Antivir Ther*, 12(4 Pt B):581–91, 2007.

B. Thaa, K. P. Hofmann, and M. Veit. Viruses as vesicular carriers of the viral genome: a functional module perspective. *Biochim Biophys Acta*, 1803(4):507–19, Apr 2010. doi: 10.1016/j.bbamcr.2010.01.011.

R. E. Thompson, D. R. Larson, and W. W. Webb. Precise nanometer localization analysis for individual fluorescent probes. *Biophys J*, 82(5):2775–83, May 2002. doi: 10.1016/S0006-3495(02)75618-X.

S. Tong, Y. Li, P. Rivailler, C. Conrardy, D. A. A. Castillo, L.-M. Chen, S. Recuenco, J. A. Ellison, C. T. Davis, I. A. York, A. S. Turmelle, D. Moran, S. Rogers, M. Shi, Y. Tao, M. R. Weil, K. Tang, L. A. Rowe, S. Sammons, X. Xu, M. Frace, K. A. Lindblade, N. J. Cox, L. J. Anderson, C. E. Rupprecht, and R. O. Donis. A distinct lineage of influenza a virus from bats. *Proc Natl Acad Sci U S A*, 109(11):4269–74, Mar 2012. doi: 10.1073/pnas.1116200109.

K. Totani. Chemoenzymatic synthesis and application of glycopolymers containing multivalent sialyloligosaccharides with a poly(L-glutamic acid) backbone for inhibition of infection by influenza viruses. *Glycobiology*, 13(5):315–326, May 2003.

T. M. Tumpey, T. R. Maines, N. Van Hoeven, L. Glaser, A. Solórzano, C. Pappas, N. J. Cox, D. E. Swayne, P. Palese, J. M. Katz, and A. García-Sastre. A two-amino acid change in the hemagglutinin of the 1918 influenza virus abolishes transmission. *Science (New York, NY)*, 315(5812):655–659, Feb. 2007.

M. Umemura, M. Itoh, Y. Makimura, K. Yamazaki, M. Umekawa, A. Masui, Y. Matahira, M. Shibata, H. Ashida, and K. Yamamoto. Design of a Sialylglycopolymer with a Chitosan Backbone Having Efficient Inhibitory Activity against Influenza Virus Infection. *Journal of medicinal chemistry*, July 2008.

C. Unverzagt, S. Kelm, and J. C. Paulson. Chemical and enzymatic synthesis of multivalent sialoglycopeptides. *Carbohydrate research*, 251:285–301, Jan. 1994.

A. Varki and R. Schauer. Sialic acids. In *Essentials of Glycobiology, Second Edition*, chapter 14. Cold Spring Harbor Laboratory Press, 2009. ISBN 9780879697709.

N. M. Varki and A. Varki. Diversity in cell surface sialic acid presentations: implications for biology and disease. *Laboratory investigation; a journal of technical methods and pathology*, 87(9):851–857, Sept. 2007.

C. Veigel and C. F. Schmidt. Moving into the cell: single-molecule studies of molecular motors in complex environments. *Nature reviews Molecular cell biology*, 12(3):163–176, Mar. 2011.

D. Vester, E. Rapp, D. Gade, Y. Genzel, and U. Reichl. Quantitative analysis of cellular proteome alterations in human influenza A virus-infected mammalian cell lines. *Proteomics*, 9(12):3316–3327, June 2009.

M. von Itzstein. The war against influenza: discovery and development of sialidase inhibitors. *Nature Reviews Drug Discovery*, 6(12):967–974, Dec. 2007.

A. Vonderheit and A. Helenius. Rab7 associates with early endosomes to mediate sorting and transport of semliki forest virus to late endosomes. *PLoS Biol*, 3(7):e233, Jul 2005. doi: 10.1371/journal.pbio.0030233.

W. C. Wang and R. D. Cummings. The immobilized leukoagglutinin from the seeds of maackia amurensis binds with high affinity to complex-type asn-linked oligosaccharides containing terminal sialic acid-linked alpha-2,3 to penultimate galactose residues. *J Biol Chem*, 263(10): 4576–85, Apr 1988.

Y. Watanabe, M. S. Ibrahim, Y. Suzuki, and K. Ikuta. The changing nature of avian influenza A virus (H5N1). *Trends in microbiology*, 20(1):11–20, Jan. 2012.

R. G. Webster, W. J. Bean, O. T. Gorman, T. M. Chambers, and Y. Kawaoka. Evolution and ecology of influenza a viruses. *Microbiol Rev*, 56(1):152–79, Mar 1992.

V. K. Weinheimer, A. Becher, M. Tönnies, G. Holland, J. Knepper, T. T. Bauer, P. Schneider, J. Neudecker, J. C. Rückert, K. Szymanski, B. Temmesfeld-Wollbrueck, A. D. Gruber, N. Bannert, N. Suttorp, S. Hippenstiel, T. Wolff, and A. C. Hocke. Influenza A viruses target type II pneumocytes in the human lung. *The Journal of infectious diseases*, July 2012.

W. Weis, J. H. Brown, S. Cusack, J. C. Paulson, J. J. Skehel, and D. C. Wiley. Structure of the influenza virus haemagglutinin complexed with its receptor, sialic acid. *Nature*, 333(6172): 426–31, Jun 1988. doi: 10.1038/333426a0.

G. R. Whittaker. Intracellular trafficking of influenza virus: clinical implications for molecular medicine. *Expert reviews in molecular medicine*, 2001:1–13, Feb. 2001.

I. A. Wilson, J. J. Skehel, and D. C. Wiley. Structure of the haemagglutinin membrane glycoprotein of influenza virus at 3 a resolution. *Nature*, 289(5796):366–73, Jan 1981.

M. C. Wolf, A. N. Freiberg, T. Zhang, Z. Akyol-Ataman, A. Grock, P. W. Hong, J. Li, N. F. Watson, A. Q. Fang, H. C. Aguilar, M. Porotto, A. N. Honko, R. Damoiseaux, J. P. Miller, S. E. Woodson, S. Chantasirivisal, V. Fontanes, O. A. Negrete, P. Krogstad, A. Dasgupta, A. Moscona, L. E. Hensley, S. P. Whelan, K. F. Faull, M. R. Holbrook, M. E. Jung, and B. Lee. A broad-spectrum antiviral targeting entry of enveloped viruses. *Proceedings of the National Academy of Sciences*, 107(7):3157–3162, Feb. 2010.

A. Wozniak, J. van Mameren, and S. Ragona. Single-molecule force spectroscopy using the nanotracker optical tweezers platform: from design to application. *Curr Pharm Biotechnol*, 10(5):467–73, Aug 2009.

X. Xu, H. Nagarajan, N. E. Lewis, S. Pan, Z. Cai, X. Liu, W. Chen, M. Xie, W. Wang, S. Hammond, M. R. Andersen, N. Neff, B. Passarelli, W. Koh, H. C. Fan, J. Wang, Y. Gui, K. H. Lee, M. J. Betenbaugh, S. R. Quake, I. Famili, B. O. Palsson, and J. Wang. The genomic sequence of the Chinese hamster ovary (CHO)-K1 cell line. *Nature Biotechnology*, pages 1–8, July 2011.

Z. Ye, T. Liu, D. P. Offringa, J. McInnis, and R. A. Levandowski. Association of influenza virus matrix protein with ribonucleoproteins. *J Virol*, 73(9):7467–73, Sep 1999.

C. Yuan, A. Chen, P. Kolb, and V. T. Moy. Energy landscape of streptavidin-biotin complexes measured by atomic force microscopy. *Biochemistry*, 39(33):10219–10223, Aug. 2000.

A. Zeigerer, J. Gilleron, R. L. Bogorad, G. Marsico, H. Nonaka, S. Seifert, H. Epstein-Barash, S. Kuchimanchi, C. G. Peng, V. M. Ruda, P. Del Conte-Zerial, J. G. Hengstler, Y. Kalaidzidis, V. Koteliansky, and M. Zerial. Rab5 is necessary for the biogenesis of the endolysosomal system in vivo. *Nature*, 485(7399):465–70, May 2012. doi: 10.1038/nature11133.

S. Zevgiti, J. G. Zabala, A. Darji, U. Dietrich, E. Panou-Pomonis, and M. Sakarellos-Daitsiotis. Sialic acid and sialyl-lactose glyco-conjugates: design, synthesis and binding assays to lectins and swine influenza H1N1 virus. *Journal of Peptide Science*, 18(1):52–58, Nov. 2011.

K. Zhang, Z. Wang, X. Liu, C. Yin, Z. Basit, B. Xia, and W. Liu. Dissection of Influenza A Virus M1 Protein: pH-Dependent Oligomerization of N-Terminal Domain and Dimerization of C-Terminal Domain. *PLoS ONE*, 7(5):e37786, May 2012.

X. Zhang, D. F. Bogorin, and V. T. Moy. Molecular basis of the dynamic strength of the sialyl Lewis X–selectin interaction. *Chemphyschem : a European journal of chemical physics and physical chemistry*, 5(2):175–182, Feb. 2004.

O. P. Zhirnov. Isolation of matrix protein m1 from influenza viruses by acid-dependent extraction with nonionic detergent. *Virology*, 186(1):324–30, Jan 1992.

List of Figures

List of Tables

Publications

Articles and manuscripts

1. Sutter J U, Sieben C, Hartel A, Eisenach C, Thiel G, and Blatt M R (2007) Abscisic acid triggers the endocytosis of the Arabidopsis KAT1 K^+-channel and its recycling to the plasma membrane. *Current Biology* 17:1396-1402.

2. Elter A, Hartel A, Sieben C, Hertel B, Fischer-Schliebs E, Lüttge E, Moroni A, and Thiel G (2007) A plant homolog of animal chloride intracellular channels (CLICs) generates an ion conductance in heterologous systems. *J Biol Chem* 282:8786-8792.

3. Sieben C , Mikosch M , Brandizzi F, Homann U (2008) Interaction of the K^+-channel KAT1 with the coat protein complex II coat component Sec24 depends on a di-acidic endoplasmic reticulum export motif. *Plant J* 56:997-1006.
equal contribution

4. Papp I, Sieben C, Ludwig K, Roskamp M, Böttcher C, Schlecht S, Herrmann A, Haag R (2010) Inhibition of influenza virus infection by multivalent sialic-acid-functionalized gold nanoparticles. *Small* 6(24):2900-2906

5. Papp I , Sieben C , Sisson A L, Kostka J, Böttcher C, Ludwig K, Herrmann A, Haag R (2011) Inhibition of influenza virus activity by multivalent glycoarchitectures with matched sizes. *ChemBioChem* 12(6):887-895.
equal contribution

6. Li S, Eghiaian F, Sieben C, Herrmann A, Schaap IAT (2011) Bending and puncturing the influenza lipid envelope. *Biophys J* 100:637-645.

7. Sieben C , Kappel C , Zhu R, Wozniak A, Rankl C, Hinterdorfer P, Grubmüller H, Herrmann A (2012) Influenza virus binds its host cell using multiple dynamic interactions.

Proc Natl Acad Sci U S A 109(34):13626-13631
equal contribution

8. Hoze N, Nair D, Hosy E, Sieben C, Manley S, Herrmann A, Sibarita JB, Choquet D, Holcman D (2012) Heterogeneity of AMPA receptor trafficking and molecular interactions revealed by superresolution analysis of live cell imaging. *Proc Natl Acad Sci U S A* 109:17052-17057

9. Li S , Sieben C , Ludwig K, Herrmann A, Eghiaian F, Schaap I A T (2012) pH-controlled two-step uncoating of influenza virus. submitted
equal contribution

Oral Presentations

Measuring Adhesion Forces between Influenza Virus and living Cells
First Regular Meeting EC marie Curie ITN Network
Berlin 2010

Influenza virus adhesion to living cells measured by single virus force spectroscopy (SVFS) and Force Probe MD simulations
Biophysical Society 55rd Annual Meeting
Baltimore 2011

Influenza virus adhesion to living cells measured by single virus force spectroscopy (SVFS) and molecular dynamics simulations
Young Scientists Workshop - Methods to study in uenza virus
Berlin 2011

Inhibition of influenza virus A activity by using sialic-acid conjugated multivalent nanoparticles
2nd External Workshop, Graduate School SFB 765
Rheinsberg 2011

How strong is a virus? - Measuring single virus cell adhesion forces
Annual Meeting EC Marie Curie ITN Network
Stockholm 2011

Inhibition of influenza A virus activity using multivalent nanoparticles
Mesa+/ SFB 765 Mini Symposium
Berlin 2012

Poster Presentations

Inhibition of Influenza Virus Activity by Sialic-Acid Conjugated Polymers
Christian Sieben, Ilona Papp, Thomas Korte, Kai Ludwig, Christoph Böttcher, Andreas Herrmann
Biophysical Society 53rd Annual Meeting
Boston 2009

Measuring Influenza Virus adhesion to living cells
Christian Sieben, Anna Wozniak, Rong Zhu, Christian Rankl, Peter Hinterdorfer, Andreas Herrmann
Membranes and Modules
Berlin 2009

Measuring Influenza Virus adhesion to living cells
Christian Sieben, Anna Wozniak, Rong Zhu, Christian Rankl, Peter Hinterdorfer, Andreas Herrmann
BioNanoViews (JPK conference
Berlin 2009

Measuring Adhesion Forces between Influenza Virus and living Cells
Christian Sieben, Anna Wozniak, Rong Zhu, Christian Rankl, Peter Hinterdorfer, Andreas Herrmann
Biophysical Society 54rd Annual Meeting
San Fransisco 2010

Influenza virus binds its host cell using multiple dynamic interactions revealed by Single Virus Force Spectroscopy and Force Probe MD
Christian Sieben, Christian Kappel, Anna Wozniak, Rong Zhu, Christian Rankl, Peter Hinterdorfer, Helmut Grubmüller, Andreas Herrmann
3rd international In uenza Meeting
Münster 2012

Acknowledgments

I owe thanks to the following people who helped during the creation of this thesis:

Prof. Dr. Andreas Herrmann for the opportunity to work in a fantastic lab on an exciting project. I deeply acknowledge his constant support and motivation in all circumstances. He is a great mentor and teacher. Discussing and developing the various ideas and projects with him was a constant inspiration for me.

PD Dr. Michael Veit, **Dr. Bastian Thaa** and **Chris Höfer** for many fruitful discussions.

Dr. Kai Ludwig and **PD. Dr. Christoph Böttcher** for a very good collaboration and many inspiring conversations.

Dr. Rong Zhu and **Prof. Dr. Peter Hinterdorfer** for introducing me into AFM force spectroscopy and for being great hosts during my time in Linz.

Dr. Christian Kappel and **Prof. Dr. Helmut Grubmüller** for an exciting collaboration and for jumping into a running project with impressive MD simulations.

Dr. Frédéric Eghiaian and **Dr. Salvatore Chiantia** for helpful discussions and commenting on this thesis.

I am indebted to our collaborators within the different projects. Special thanks goes to **JPK Instruments AG, Dr. Anna Wozniak, Dr. Ilona Papp, Prof. Dr. Rainer Haag, Dr. Meike Roskamp, Prof. Dr. Sabine Schlecht, Dr. Iwan A.T. Schaap, Dr. Sai Li, Dr. David Holcman, Dr. Thibault Lagache**.

I acknowledge not only experimental support from **Christopher Wolff, Katrina Meyer, Johanna Kostka, Katharina Horst, Elisa Merklinger** and **Matthias Bock**.

Sabine Schiller for all the help in the every day lab life and **Gudrun Habermann** for introducing me into virological methods.

I would like to thank all members of the molecular biophysics lab for their experimental help and for always keeping a warm and friendly atmosphere. I enjoyed every day. In particular, I

want to thank **Andrea, Anja, Aouefa, Caro, Joanna** and **Roland** for the inspiring, funny and motivating time we had inside and outside of the office.

Meinen Eltern für ihre Unterstützung und ihr Vertrauen.

Julia für alles.

Financial support for this work was provided by the DFG (SFB 765).

Selbständigkeitserklärung

Ich erkläre, dass ich die vorliegende Arbeit selbständig und nur unter Verwendung der angegebenen Literatur und Hilfsmittel angefertigt habe. Wurden Ergebnisse in Kooperation produziert, ist dies entsprechend angegeben.
Ich besitze keinen entsprechenden Doktorgrad und habe mich anderwärts nicht um einen Doktorgrad beworben.
Die dem Promotionsverfahren zugrunde liegende Promotionsordnung ist mir bekannt.

Berlin, den 23. Mai 2013 Christian Sieben